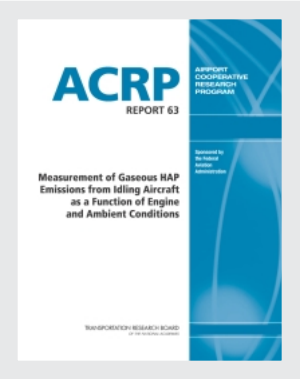

Measurement of Gaseous HAP Emissions from Idling Aircraft as a Function of Engine and Ambient Conditions

DETAILS

101 pages | 8.5 x 11 | PAPERBACK
ISBN 978-0-309-21401-8 | DOI 10.17226/13655

AUTHORS

Herndon, Scott ;Wood, Ezra ;Franklin, Jon ;Miake-Lye, Richard ;Knighton, W. Berk ;Babb, Mark ;Nakahara, Alex ;Reynolds, Tom ; and Balakrishnan, Hamsa

AIRPORT COOPERATIVE RESEARCH PROGRAM

ACRP REPORT 63

Measurement of Gaseous HAP Emissions from Idling Aircraft as a Function of Engine and Ambient Conditions

Scott Herndon
Ezra Wood
Jon Franklin
Richard Miake-Lye
AERODYNE RESEARCH, INC.
Billerica, MA

W. Berk Knighton
MONTANA STATE UNIVERSITY
Bozeman, MT

Mark Babb
SOUTHWEST AIRLINES
Dallas, TX

Alex Nakahara
Tom Reynolds
Hamsa Balakrishnan
MASSACHUSETTS INSTITUTE OF TECHNOLOGY
Cambridge, MA

Subscriber Categories
Aviation • Energy • Environment

Research sponsored by the Federal Aviation Administration

TRANSPORTATION RESEARCH BOARD

WASHINGTON, D.C.
2012
www.TRB.org

AIRPORT COOPERATIVE RESEARCH PROGRAM

Airports are vital national resources. They serve a key role in transportation of people and goods and in regional, national, and international commerce. They are where the nation's aviation system connects with other modes of transportation and where federal responsibility for managing and regulating air traffic operations intersects with the role of state and local governments that own and operate most airports. Research is necessary to solve common operating problems, to adapt appropriate new technologies from other industries, and to introduce innovations into the airport industry. The Airport Cooperative Research Program (ACRP) serves as one of the principal means by which the airport industry can develop innovative near-term solutions to meet demands placed on it.

The need for ACRP was identified in *TRB Special Report 272: Airport Research Needs: Cooperative Solutions* in 2003, based on a study sponsored by the Federal Aviation Administration (FAA). The ACRP carries out applied research on problems that are shared by airport operating agencies and are not being adequately addressed by existing federal research programs. It is modeled after the successful National Cooperative Highway Research Program and Transit Cooperative Research Program. The ACRP undertakes research and other technical activities in a variety of airport subject areas, including design, construction, maintenance, operations, safety, security, policy, planning, human resources, and administration. The ACRP provides a forum where airport operators can cooperatively address common operational problems.

The ACRP was authorized in December 2003 as part of the Vision 100-Century of Aviation Reauthorization Act. The primary participants in the ACRP are (1) an independent governing board, the ACRP Oversight Committee (AOC), appointed by the Secretary of the U.S. Department of Transportation with representation from airport operating agencies, other stakeholders, and relevant industry organizations such as the Airports Council International-North America (ACI-NA), the American Association of Airport Executives (AAAE), the National Association of State Aviation Officials (NASAO), Airlines for America (A4A), and the Airport Consultants Council (ACC) as vital links to the airport community; (2) the TRB as program manager and secretariat for the governing board; and (3) the FAA as program sponsor. In October 2005, the FAA executed a contract with the National Academies formally initiating the program.

The ACRP benefits from the cooperation and participation of airport professionals, air carriers, shippers, state and local government officials, equipment and service suppliers, other airport users, and research organizations. Each of these participants has different interests and responsibilities, and each is an integral part of this cooperative research effort.

Research problem statements for the ACRP are solicited periodically but may be submitted to the TRB by anyone at any time. It is the responsibility of the AOC to formulate the research program by identifying the highest priority projects and defining funding levels and expected products.

Once selected, each ACRP project is assigned to an expert panel, appointed by the TRB. Panels include experienced practitioners and research specialists; heavy emphasis is placed on including airport professionals, the intended users of the research products. The panels prepare project statements (requests for proposals), select contractors, and provide technical guidance and counsel throughout the life of the project. The process for developing research problem statements and selecting research agencies has been used by TRB in managing cooperative research programs since 1962. As in other TRB activities, ACRP project panels serve voluntarily without compensation.

Primary emphasis is placed on disseminating ACRP results to the intended end-users of the research: airport operating agencies, service providers, and suppliers. The ACRP produces a series of research reports for use by airport operators, local agencies, the FAA, and other interested parties, and industry associations may arrange for workshops, training aids, field visits, and other activities to ensure that results are implemented by airport-industry practitioners.

ACRP REPORT 63

Project 02-03A
ISSN 1935-9802
ISBN 978-0-309-21401-8
Library of Congress Control Number 2012935705

COPYRIGHT INFORMATION

NOTICE

The project that is the subject of this report was a part of the Airport Cooperative Research Program, conducted by the Transportation Research Board with the approval of the Governing Board of the National Research Council.

The members of the technical panel selected to monitor this project and to review this report were chosen for their special competencies and with regard for appropriate balance. The report was reviewed by the technical panel and accepted for publication according to procedures established and overseen by the Transportation Research Board and approved by the Governing Board of the National Research Council.

The opinions and conclusions expressed or implied in this report are those of the researchers who performed the research and are not necessarily those of the Transportation Research Board, the National Research Council, or the program sponsors.

The Transportation Research Board of the National Academies, the National Research Council, and the sponsors of the Airport Cooperative Research Program do not endorse products or manufacturers. Trade or manufacturers' names appear herein solely because they are considered essential to the object of the report.

Published reports of the

AIRPORT COOPERATIVE RESEARCH PROGRAM

are available from:

Transportation Research Board
Business Office
500 Fifth Street, NW
Washington, DC 20001

and can be ordered through the Internet at

http://www.national-academies.org/trb/bookstore

Printed in the United States of America

THE NATIONAL ACADEMIES

Advisers to the Nation on Science, Engineering, and Medicine

The **National Academy of Sciences** is a private, nonprofit, self-perpetuating society of distinguished scholars engaged in scientific and engineering research, dedicated to the furtherance of science and technology and to their use for the general welfare. On the authority of the charter granted to it by the Congress in 1863, the Academy has a mandate that requires it to advise the federal government on scientific and technical matters. Dr. Ralph J. Cicerone is president of the National Academy of Sciences.

The **National Academy of Engineering** was established in 1964, under the charter of the National Academy of Sciences, as a parallel organization of outstanding engineers. It is autonomous in its administration and in the selection of its members, sharing with the National Academy of Sciences the responsibility for advising the federal government. The National Academy of Engineering also sponsors engineering programs aimed at meeting national needs, encourages education and research, and recognizes the superior achievements of engineers. Dr. Charles M. Vest is president of the National Academy of Engineering.

The **Institute of Medicine** was established in 1970 by the National Academy of Sciences to secure the services of eminent members of appropriate professions in the examination of policy matters pertaining to the health of the public. The Institute acts under the responsibility given to the National Academy of Sciences by its congressional charter to be an adviser to the federal government and, on its own initiative, to identify issues of medical care, research, and education. Dr. Harvey V. Fineberg is president of the Institute of Medicine.

The **National Research Council** was organized by the National Academy of Sciences in 1916 to associate the broad community of science and technology with the Academy's purposes of furthering knowledge and advising the federal government. Functioning in accordance with general policies determined by the Academy, the Council has become the principal operating agency of both the National Academy of Sciences and the National Academy of Engineering in providing services to the government, the public, and the scientific and engineering communities. The Council is administered jointly by both Academies and the Institute of Medicine. Dr. Ralph J. Cicerone and Dr. Charles M. Vest are chair and vice chair, respectively, of the National Research Council.

The **Transportation Research Board** is one of six major divisions of the National Research Council. The mission of the Transportation Research Board is to provide leadership in transportation innovation and progress through research and information exchange, conducted within a setting that is objective, interdisciplinary, and multimodal. The Board's varied activities annually engage about 7,000 engineers, scientists, and other transportation researchers and practitioners from the public and private sectors and academia, all of whom contribute their expertise in the public interest. The program is supported by state transportation departments, federal agencies including the component administrations of the U.S. Department of Transportation, and other organizations and individuals interested in the development of transportation. **www.TRB.org**

www.national-academies.org

COOPERATIVE RESEARCH PROGRAMS

CRP STAFF FOR ACRP REPORT 63

Christopher W. Jenks, *Director, Cooperative Research Programs*
Crawford F. Jencks, *Deputy Director, Cooperative Research Programs*
Lawrence D. Goldstein, *Senior Program Officer*
Eileen P. Delaney, *Director of Publications*

ACRP PROJECT 02-03A PANEL
Field of Environment

Renee L. Dowlin, *Portland (OR) International Airport* (Chair)
Robert A. Arnott, *Strategic Environmental Analysis, LLC, Greenwood Village, CO*
Steven L. Baughcum, *Boeing Commercial Airplanes, Seattle, WA*
Willard J. Dodds, *GE Aviation, McMinnville, OR*
Brenda L. Enos, *Massachusetts Port Authority, East Boston, MA*
Robert P. Howard, *Arnold Air Force Base, TN*
Eileen A. Murphy, *Rutgers, The State University of NJ*
Robert P. Newman, *EA Engineering, Science, and Technology, Sparks, MD*
Saadat Syed, *Pratt & Whitney, East Hartford, CT*
Darcy C.Z. Zarubiak, *Leigh Fisher, Dallas, TX*
Mohan Gupta, *FAA Liaison*
Nancy N. Young, *Airlines for America (A4A) Liaison*
Christine Gerencher, *TRB Liaison*

AUTHOR ACKNOWLEDGMENTS

John Kinsey, United States Environmental Protection Agency.
Art Kaucher, John Dayton, Tammy Kenney, Doug Rings, Phil Bursczak, and Elaine Karnes, Southwest Airlines.
Roger Petersen and Harold Roehrich, United Air Lines Engineering Operations Center.
Matthew Marich, Ray Hoffelt, and Aaron Frame, Chicago Department of Aviation.
Albert Presto and Allen Robinson, Carnegie Mellon University.
David Lewis, Connecticut College.
Matthew DeWitt, University of Dayton Research Institute.
Elena de la Rosa Blanca and Jim Hileman, Massachusetts Institute of Technology.
Prem Lobo, Stephen Achterberg, and Phillip Whitefield, Missouri University of Science and Technology.
Robert Howard, Arnold Engineering Development Center.
Williard Dodds and Russel Arey, GE Aviation.
Steven Baughcum and Douglas Dubois, The Boeing Company.
Luke Ziemba, NASA Langley.
Zhenhong Yu, Michael Timko, Jay Peck, and Chuck Kolb, Aerodyne Research, Inc.

FOREWORD

By Lawrence D. Goldstein
Staff Officer
Transportation Research Board

ACRP Report 63 presents the output of a comprehensive emissions test program designed to measure gaseous Hazardous Air Pollutants (HAPs) from in-production jet engines operating at a range of idle settings and ambient temperatures. The measurement program addressed two primary concerns: total hydrocarbons and speciated hydrocarbons, including HAPs, within the exhaust plume in reasonable proximity of the engine nozzle to capture emissions prior to condensation of volatile gasses; and emissions at a downstream location where the plume has cooled to near-ambient temperatures. The measurement program used commercial aircraft equipped with General Electric CFM56 wing-mounted engines, conducted during three separate campaigns at three different airports to evaluate the effects of change in environmental conditions as well as varying idle speeds. Although the data is attributed to and is defined by this particular engine, additional complementary data has been used to develop an estimation tool using measured data trends as a function of ambient temperature and fuel delivery rates.

Interest in this research emerged as the result of a recognized need, expressed by government agency and community groups, for more definitive information about emissions from aircraft and other airport-related sources. An important component of airport-related emissions, addressed by the National Environmental Policy Act (NEPA) and state-level environmental programs, is Hazardous Air Pollutants (HAPs). Unlike criteria air pollutants (particle pollution, ground-level ozone, carbon monoxide, sulfur oxides, nitrogen oxides, and lead), information on the emission, transformation, and transport of aviation-related HAPs has historically been limited. With a limited understanding of aviation HAP emissions, airport operators have neither been able to develop accurate inventories nor provide effective guidance to state and local constituencies. This research was envisioned as one of a series of studies undertaken or to be undertaken to address the broader question of measuring emissions from aircraft and other equipment operating at airports.

The specific need for this research was originally identified in an earlier ACRP study published in 2008. This earlier study identified gaps in then-current research on airport-related HAP emissions and recommended additional research to help understand potential impacts and how to measure them. That study, published as *ACRP Report 7: Aircraft and Airport-Related Hazardous Air Pollutants: Research Needs and Analysis,* concluded that an important source of airport-related HAP compounds at most commercial airports is idling jet engines and that understanding the scale and character of this emission source was, therefore, a high priority to the airport community. *ACRP Report 7* recommended a targeted research effort to document the contribution of idling jet engines to HAP emissions, which resulted in this report.

The results of this research can be used to improve the assessment of HAP emissions at airports based on specific operating parameters and changes in ambient conditions, recognizing that the engine emission data presented is limited to one class of engines. Despite that limitation, the analysis demonstrates that emissions vary as a function of ambient temperatures and idle speeds, and that these variations are significant and measurable. In the future, additional engine emissions performance testing to encompass different engine types would further improve air quality emissions assessment capability. The data provided in this study can still be used to improve emissions estimates that would otherwise not reflect changes linked to variation in ambient temperature and engine thrust characteristics experienced during passenger loading and unloading, and taxiing. In addition, the study outcome can motivate better data usage and suggest improved operations that would actually reduce emissions based on actual performance.

The research described in this report involved extensive interaction among technical experts in engine operations and engine emissions performance as well as experienced airport operators. The results contribute to the important objective of understanding and, eventually, managing airport-related emissions as a function of changes in capacity and service demand.

CONTENTS

SUMMARY

Measurement of Gaseous HAP Emissions from Idling Aircraft as a Function of Engine and Ambient Conditions

This project characterized the dependence of gaseous hazardous air pollutants (HAP) and other partially combusted fuel emissions from aircraft on ambient and near-idle engine conditions, including temperature and engine thrust setting. The measurement work focused on characterization of on-wing CFM56 engines installed on commercial aircraft and operated according to airline practice. This project also developed a simple empirical framework (based on measurement data collected on variants of the CFM56 engine) that can be used in emissions scenario analysis.

Three measurement campaigns were conducted at Chicago Midway Regional Airport (MDW), Chicago O'Hare International Airport (ORD), and Dallas Love Airport (DAL) in 2009 and 2010. Measurement tests focused on the CFM56-7B24 and -3B1 engine types. A single V2527 engine and a PW4090 engine were also characterized. The temperatures during these tests ranged from −8°C to 25°C (18°F to 77°F).

Engine conditions examined ranged from the minimum fuel flow rates used at airports (ground idle with zero bleed air demand) to the International Civil Aviation Organization (ICAO) certification thrust setting for taxi/idle (7% of maximum rated thrust). Exhaust from the measured aircraft engines was collected using state-of-the-art probe/sampling schemes and analyzed using instrumentation housed in a mobile laboratory. Speciated measurements of HAP compounds such as formaldehyde, benzene, and 1,3-butadiene were measured using high-time-response, research grade instrumentation.

The main HAP emissions from aircraft engines are volatile organic compounds (VOCs), with the important HAPs being formaldehyde, benzene, and acetaldehyde. Both the fuel-based emission indices (grams of benzene per kilogram of fuel combusted) and emission rates (grams of benzene per second) of VOCs increase with decreases in ambient temperature and fuel flow rate. A major accomplishment of this project's research is the formulation of a simple model (currently only applicable to selected variants of the CFM56 engine type) that outputs the *relative* change in VOC emission index compared with ICAO's reference temperature condition (15°C).

Findings

The findings of this project are summarized as follows:

1. Temperature dependence: VOC emission indices are approximately twice as high under cold conditions (−8°C to 0°C) as they are at 15°C for the CFM56-7B24.

2. Fuel flow rate dependence: For the engine states that are likely to be most representative of the operational aircraft taxiway engine state, the VOC emission indices for the CFM56-7B24 are approximately 40% greater than the ICAO certification engine state (7% thrust).
3. VOC speciation: The composition profile of the exhaust is constant. The ratios of individual VOCs (e.g., formaldehyde to 1,3-butadiene) remain constant over all thrust settings and temperatures encountered. The first two findings are thus expected to be applicable to all VOCs measured, with the exception that there is a dependence of benzene emissions on fuel aromatic content.

Implications for Airport Operators

The data collected and analyzed in this project can be used by airport operators to improve the accuracy of taxiway emissions for selected aircraft engine types. Inventory assessment, whether performed for regulatory needs or not, can help prioritize sources that may require mitigation. Organic gas emissions can influence air quality by direct toxicological influence (HAP compounds specifically) by accelerating the production of ozone (a criteria pollutant) and by contributing to secondary organic aerosol (with its visibility and potential health consequences).

This work has characterized the dependence of VOC engine emissions on ambient temperature under taxiway and terminal area operational engine states. These results can also be used to inform decisions on minimizing HAP emissions. The simple model developed in this work can be used to quantify the emissions benefits from proposed changes in airport operations. The results from this project can be used to relate the inventory of HAP emissions from aircraft engines during routine airport operation to emissions mitigation strategies such as single-engine taxiing or temporary engine shutdown practice during taxi delays.

SECTION I

Introduction

This document describes the results and findings of Airport Cooperative Research Program (ACRP) Project 02-03a, which characterized the emissions of gaseous hazardous air pollutants (HAPs) from idling aircraft engines during three measurement campaigns. The document begins with a discussion of the motivation for this project, and a summary of the test plan and approach is presented in Section II. Section III examines the effect of fuel flow on emissions. A method for scaling emission indices to reference values is described in order to enable data comparison of different engine technologies and different volatile organic compounds (VOCs). The relationship between emissions and ambient temperature is discussed in Section IV.

Data from this project, as well as from other complementary projects, have been used to develop a model for emission estimates when the engine is operating at near-idle power. The variability observed in the on-wing characterization of multiple engines will be discussed in the context of overall measurement uncertainty. Section V discusses a straightforward estimation tool that is based on the analysis of measured data trends. The estimation tool has direct applicability for quantifying emission levels in scenario evaluations and airport inventory modeling. The temperature and fuel flow corrections described here have been applied to a series of digital flight data records collected from in-use operations. Additional findings that occurred beyond the initial project statement are also summarized.

Section VI includes a discussion of the apparent engine warm-up effect, the near-idle hydrocarbon emission profile, and the effect of fuel properties on emissions. Section VII provides a discussion of the relevance of the project findings to airport practice.

Appendix A describes the results of the testing conducted for this project. The test matrix and test procedures developed specifically for the question of addressing near-idle emissions for on-wing engine testing are described in Appendix B. The methods employed for sampling specific VOCs without reactive or absorptive losses in the sampling probe are described in Appendix C. The data collected at the airport fence line (a mix of aircraft emissions and terminal area emissions) and its potential implications are described in Appendix D. The analytical methods used to characterize the engine exhaust and quality assurance procedures are collected in Appendix E.

The aircraft exhaust matrix potentially consists of thousands of specific molecules containing carbon, hydrogen, oxygen, nitrogen, and sulfur. Sets and subsets of these emitted compounds are denoted by various terms. A variety of terms have been used to describe the species of interest in this document, including volatile organic compounds, hydrocarbons, unburned hydrocarbons, and partially burned hydrocarbons.

Every attempt has been made in this document to keep the language concise and accurate. An important observation drawn from this work and previous measurements is that trends with near-idle engine state and ambient temperature in one volatile organic compound also apply to the compounds in the other classifications.

- A hazardous air pollutant (HAP) is defined by the U.S. Environmental Protection Agency (EPA) as a compound that causes or may cause cancer or other serious health effects. EPA lists 187 compounds as HAPs, 15 of which have been identified in aircraft exhaust.
- A hydrocarbon (HC) is a chemical compound that contains only carbon and hydrogen.
- An unburned hydrocarbon (UHC) refers to the total gas phase organic carbon content in the exhaust as measured by a flame ionization detector. This is the measurement reported by ICAO.
- A volatile organic compound (VOC) is defined by EPA as an organic compound that participates in atmospheric photochemical reactions. Originally, a VOC was defined based only on volatility, but the current definition makes the term inaccurate for describing the collection of gas phase organic compounds present in aircraft exhaust. Because the term

is, however, so prevalent in aircraft emissions literature, we continue to employ it in this document.

I.1 Aircraft Engine Emissions at Airports

Government agencies and community groups frequently ask airport operators to provide information that enables an assessment of the health impacts of toxic emissions from aircraft and other airport-related sources. Two important categories of pollutants, as classified by the Clean Air Act, are criteria pollutants (comprising particulate matter, ground-level ozone, carbon monoxide, sulfur dioxide, nitrogen dioxide, and lead) and HAPs (e.g., benzene and formaldehyde). Information on the emission, transformation, and transport of aviation-related HAPs and their health impacts is rudimentary. Without a better understanding of aviation HAP emissions, airport operators cannot develop accurate emission inventories or adequately respond to the queries from state and local constituencies.

The ACRP 02-03 study was undertaken in 2007 to examine and identify gaps in research on airport-related HAP emissions and to recommend and prioritize additional research to help understand potential impacts of those emissions. The study findings were published in *ACRP Report 7: Aircraft and Airport-Related Hazardous Air Pollutants: Research Needs and Analysis,* which concluded that idling jet engines are a key source of airport-related HAPs at most commercial airports (Wood et al. 2008). Understanding the scale and character of this emission source is a high priority for the airport community. The report recommended a targeted research effort to document the contribution of idling jet engines to HAP emissions. This report describes the resulting research project and the development of a model to estimate emissions from engines operating at near-idle engine states.

Testing from earlier measurement campaigns conducted as part of the Aircraft Particle Emissions Experiment (APEX) in 2004 and 2005 (Herndon et al. 2009, Knighton et al. 2007, Timko et al. 2010, Wey et al. 2006, Yelvington et al. 2007) confirmed that emissions of VOCs from modern jet engines, many of which are classified as HAPs, are relatively small at medium and high power settings, but higher at low power settings (engine idle) (Spicer et al. 1994). Notwithstanding the contributions from the APEX measurements, knowledge of VOC emissions from aircraft at idle power settings was still limited. VOC emissions vary as a function of engine state, environmental variables (especially ambient temperature), and engine type. To quantify airport HAP emissions in the context of an airport inventory, data are needed on HAP emission rates as a function of low power settings and ambient conditions.

This research project is aimed at arming airport operators with a simple methodology for improving estimates of HAP species in the airport operational context. The test program described here employs on-wing engine testing, pulling aircraft from active commercial service of cooperating airlines. The test matrix used in this project includes the engine state defined in the certification databank (ICAO 2006), but also includes engine states that reflect airport operational conditions developed with advice from airline propulsion engineers. The inclusion of different engines, each with a different maintenance history, implies that there may be variability in the results, particularly when probing an engine state far removed from the optimal combustor design. This project will attempt to "see through" whatever variability is present in the key data trends and develop a simple methodology that can be used to estimate HAP emissions at different ambient temperatures and in-use fuel flow rates at the airport.

Although every airport is unique and universal statements are not appropriate, several airport emission inventories report that the greatest source of HAP emissions is idling jet engines (Wood et al. 2008). At power (thrust) settings greater than idle, the combustion efficiency of modern jet engines is high, and emissions of carbon monoxide (CO) and VOCs, which are products of incomplete combustion, are thus small. Many of the VOCs are partially oxidized combustion hydrocarbons and are classified as HAPs (e.g., acetaldehyde). Aircraft engines operating at idle power settings are responsible for the majority of HAP emissions generated during landing/takeoff (LTO) cycles. This point can be illustrated by examining data from the emissions performance databank maintained by the International Civil Aviation Organization (ICAO). In Figure I-1, the emissions data (expressed as unburned hydrocarbon [UHC]) is depicted for an LTO cycle at an airport. The relationship between UHC and the gaseous HAP compounds has been established previously (Herndon et al. 2009) and will be expanded later.

In Figure I-1, the emission rate is estimated as a function of time during a hypothetical operation. The estimate depicted by the solid line is based on the tabulated emissions performance data for aircraft equipped with two CFM56-2B24 engines

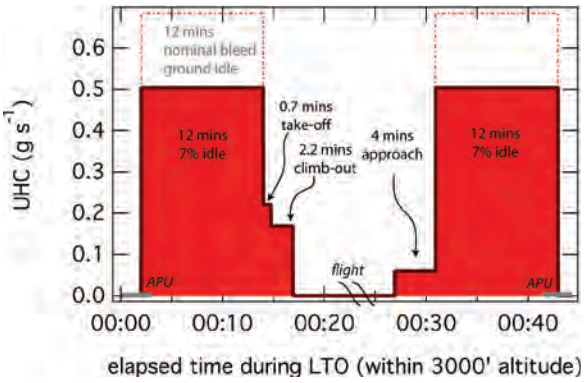

Figure I-1. UHC emissions during a landing/takeoff cycle.

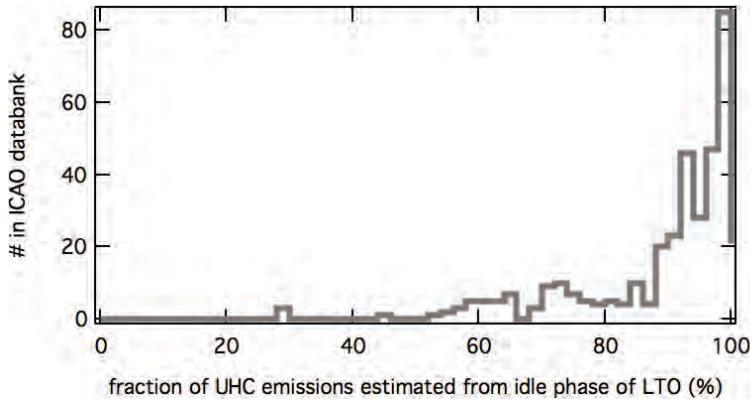

Figure I-2. Histogram of the emissions arising from the idle portion of the ICAO LTO for all engines.

operating at 15°C (59°F). The trace denoted by the dashed line is the estimate based on the emissions measurement observed in this work, assuming the entire idle phase is characterized by ground idle with a nominal bleed air demand (rather than the ICAO certification value of 7% thrust). For both cases the area under the particular mode is proportional to the total emissions. This figure demonstrates (for this engine) that the idle phase of airport activity in the standard LTO cycle is responsible for most of the hydrocarbon emissions from aircraft engines. The UHC emission rate for the auxiliary power unit (APU) has been taken from Table 6-1 of Wade (Wade 2002) and assumes a GTCP331-200 APU type. Other APU types that are typically installed on a narrow-body aircraft (Gerstle et al. 1999), such as that presumed by the CFM56-7B24 engine type in the example depicted in Figure I-1, have similar emission levels. The choice of time for APU use during the LTO is arbitrary and is included to provide a sense of how the APU emissions compare with those from the main engines.

UHC emissions arising from the idle phase in the example in Figure I-1 account for 94% of total UHC emissions (for the CFM56-7B22). This is fairly typical of the aircraft engines tabulated in the ICAO databank. Figure I-2 depicts a histogram of this calculation (fraction of total UHC emissions from the idle phase during a standard LTO cycle), which shows that the idle phase dominates total UHC emissions for the vast majority of engine types. This project has focused on characterizing selected HAPs, total UHC, and other specific VOCs emitted by aircraft engines during the idle phase.

I.2 Anatomy of the High-Bypass-Ratio Turbofan Engine

Modern commercial aircraft are powered by engines typically classified as high-bypass-ratio turbofan engines. The combustor uses a turbine-driven fan to draw air into the combustor, and the exhaust outflow goes through the core turbine. A hollow shaft connects the core turbine to the core compressor, and a second shaft passes through the core and is connected to the outer fan. This is the scheme for a two-spool engine. There are variants that use an additional stage of compression and are called three-spool engines. The reason these engines are generally referred to as high-bypass-ratio turbofans is that the majority of the air flow (and hence the thrust) does not go through the combustor region, but rather bypasses the engine core.

The generalized schematic depicted in Figure I-3 labels the major pieces of a turbofan engine, where pressure (P) and temperature (T) are noted with a number. For example, in this project, the effect of ambient temperature on the emissions of various HAP species would schematically manifest itself as a perturbation to T2, the temperature of the gas coming into the engine.

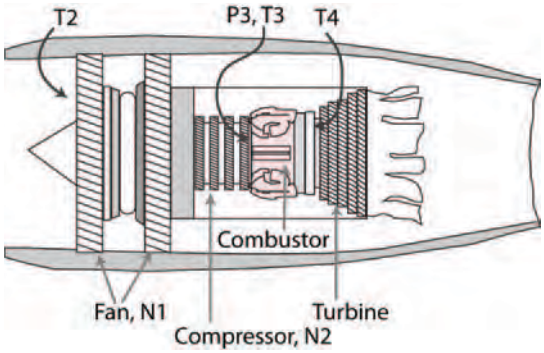

Figure I-3. Schematic of turbofan engine. The component pieces (labeled on the lower portion of the figure) of a turbofan engine are depicted with air flow proceeding from left to right. The station numbers T2, P3, T3, and T4 are taken from* Aircraft Engines and Gas Turbines *(Kerrebrock 1977) and are referred to in subsequent sections of this report.

I.3 Application of the Current Emission Model to Idle Phase Emissions

The Emissions and Dispersion Modeling System (EDMS) was developed by the Federal Aviation Administration (FAA) and the US Air Force to assess air quality impacts of proposed airport development projects (FAA 2006). It has become the preferred computer model for air quality analysis at airports (Anderson et al. 2007). The principal source of emissions data for the aircraft engines is the ICAO emission databank (ICAO 2006). The protocol for emissions performance testing for carbon monoxide, nitrogen oxides (NOx), and unburned hydrocarbons is described in *ICAO Annex 16* (ICAO 1993) and *SAE Aerospace Recommended Practice* (SAE 2006). The ICAO emissions databank tabulates exhaust emissions performance and other engine characteristics at four named conditions that are nominally indicative of operational states at the airport: takeoff, climb-out, approach, and idle. Each of the tabulated emissions values has either been measured at or scaled to the reference pressure (1 atm) and temperature (15°C).

To project the certification values to other temperatures and pressures, the EDMS uses the Boeing Fuel Flow Method 2 (BFFM2) (DuBois and Paynter 2006). The premier method for calculating the engine emissions uses established semi-empirical relationships between emissions and combustion pressure and temperature and is known as the P3T3 method. The P3T3 calculations (NEPAIR 2003, Sarli et al. 1975) are based on several parameters that are engine specific and not widely available or published. The BFFM2 approach is significantly more general and estimates emissions performance using only the engine databank values. The comparisons of NOx emissions predictions based on BFFM2 with those based on the P3T3 method are excellent for a wide variety of engines operating at different ambient temperatures, pressures (altitude), and relative humidity. The comparisons of CO and UHC emissions are reasonable, but there are discrepancies. It is particularly challenging for the BFFM2 to use the logarithmic extrapolation of the emissions data at 7% thrust and 30% thrust to project emissions at the lower thrust values typical of actual operational use (DuBois and Paynter 2006).

SECTION II

Project Plan and Approach

II.1 Project Stages and Tests

Figure II-1 depicts the four stages of this project. The first stage involved developing a test matrix suitable for probing near-idle engine states using in-service aircraft engines. The second and fourth stages were conducted at a cold weather airport in winter. For the third stage, the detailed probe work was conducted at a warm weather airport.

We quantified emissions from both staged aircraft and in-use aircraft. Staged aircraft tests involved running tests on an out-of-service aircraft under controlled conditions using a test matrix developed specifically for this project. Testing was conducted using one of four exhaust sampling methods (three based on a one-meter probe and one using the mobile laboratory as a mobile probe). A total of 12 aircraft were sampled with this approach at three airport campaigns: MDW 2009, DAL 2010, and MDW/ORD 2010. The analysis of these test results form the basis of the temperature dependence of the near-idle HAP/VOC emission indices.

In addition to the staged aircraft sampling, the emissions from in-use aircraft were also quantified. These tests were conducted in the provisional days at the end of each test, once the scheduled staged work was completed. To characterize the VOC emissions of in-use aircraft, exhaust plumes were continuously sampled and analyzed using high-time-response instrumentation downwind of an active taxiway. This approach measures diluted engine exhaust plumes formed under true operational conditions. Aircraft tail numbers were recorded and matched to time-coded video records to allow attribution of specific combustion plumes to the corresponding source engines. The in-use aircraft tests were conducted at various ambient temperatures and included a variety of aircraft engine types and taxiway operational throttle points. The analysis of the naturally diluted plume characterization produces a distribution of emission indices arising from aircraft operating with unknown fuel flow rates. To the extent that the precision in the trends observed in the staged aircraft testing is robust, the operational testing can yield information about the in-use engine state (Herndon et al. 2009). This type of data can also be used to investigate whether there are near-field atmospheric processes that could skew or undermine the effective use of an emissions inventory based exclusively on exhaust plane characterization.

II.2 Test Venues, Temperatures, and Engines

An overview of the test venues, ambient temperatures, and engines sampled is presented in Table II-1. In the MDW 2009 test, a subset of the complete instrument suite was deployed to characterize engine exhaust using a preliminary version of the test matrix that employed the mobile laboratory for sample acquisition.

In the DAL 2009 test, the same subset of analytical equipment was deployed, but the sampling probe developed by Robert Howard (Arnold Engineering Development Center) was coupled to the probe stand developed by Phil Whitefield (Missouri University of Science and Technology). At DAL 2009, various test protocols were used to compare and evaluate sampling methodologies using a probe and stand situated behind the aircraft engine. These included the use of a heated transfer line, immediate dilution at the probe tip, and dilution plus pressure drop. The same aircraft was also characterized on an abbreviated test matrix using the mobile lab sampling methodology used in the first test.

In the MDW 2010 test, a comprehensive set of instruments was used, including the instrumentation deployed by the Pacific Northwest National Laboratory's Environmental Molecular Sciences Laboratory. For the ORD 2010 test, the mobile laboratory sampling method was used for two different engine technologies (non-CFM56) that had not been previously studied.

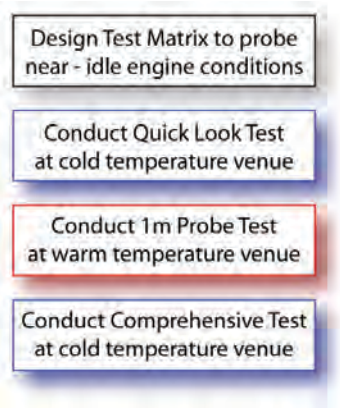

Figure II-1. Chronological depiction of the project stages.

Table II-1. Testing overview.

Test		Engine Types	Temperature
MDW 2009	Staged	CFM56-3B1 CFM56-7B24	-8°C to -4°C
	Airport Taxiway	Various	
DAL 2009	Staged	CFM56-7B24	23°C to 25°C
	Airport Runway	Various	
MDW 2010	Staged	CFM56-7B24	-6°C to -4°C
	Airport Taxiway	Various	
ORD 2010	Staged	V2527-A5 PW4090	-3°C to 2°C
	Airport Taxiway		

This project also seeks to construct an empirically based model that will estimate VOC emissions as a function of fuel flow and ambient temperature. The methodology this work adopts is to treat fuel flow and ambient temperature as parameters that influence the VOC emission index independently. Following the description and quantification of the near-idle fuel flow dependence, the data related to the ambient temperature dependence will be discussed.

SECTION III

Key Project Findings

Despite the complexities of the idle settings, an inverse relationship between emissions and fuel flow rate was observed.

Figure III-1 shows the fuel flow rate as a function of test point conditions during the MDW 2009 tests (with a CFM56-7 engine).

The operational categories in Figure III-1 are drawn from the nominal name given to each test point in the test matrix. The data points have been slightly offset horizontally within each category in order to better distinguish points that are very close in fuel flow rate.

In addition to fuel flow rate, two other engine characteristics—fraction of maximum rotational fan speed (N1) and exhaust gas temperature (EGT)—were varied as a consequence of the test point conditions. N1 is related to the rotational speed of the fan in the turbofan engine and is reported in units normalized by the maximum rotational speed for that engine and reported as a percentage. N1 = 25% defines the 7% idle condition for the CFM56 family of engines. Figure III-2 shows the relationship between N1 and fuel flow and the effect of test conditions on exhaust gas temperature.

At first glance the measurements suggest there are two disparate data groups that do not correlate well with fuel flow or EGT. Setting the data points with N1 greater than 23% aside, EGT generally increases with fuel flow (dark red at lowest fuel flow, orange and yellow at higher fuel flow). Because the engine bleed air demand is responsible for increasing fuel flow rate and there is no concomitant increase in the engine intake fan speed, relatively more combustion heat is available than at lower fuel flows, which increases the EGT. When the engine is set to produce a specified rotational speed (e.g., 25%), the outer fan speed ensures that the fuel-to-air ratio and the pressure in the combustor are scaled accordingly. The EGT is cooled with the increase in bypass air flow induced by N1.

This underscores the complex relationships in the near-idle on-wing regime between fuel flow, N1, and EGT. Similarly, the combustor pressure and fuel-to-air ratio do not vary linearly when bleed air demand is introduced. The overall carbon dioxide (CO_2) mixing ratio by volume at the engine exhaust plane is greater for the high bleed air demand condition than when N1 = 25%, which indicates a substantial shift in fuel-to-air ratio and thus combustion performance. The geometry of the turbomachinery is designed for maximum performance at continuous-cruise state, where the majority of fuel is consumed, and the use of variable bleed air during ground idle operation further exacerbates any combustion inefficiency.

The incorporation of variable bleed air demand into the test matrix employed in this study has required consideration of additional engine state parameters. The relationship that is depicted in Figure III-2 between fuel flow, N1, and EGT highlights the problem with assuming N1 (or thrust) varies linearly with fuel flow at idle. At this stage, we might be tempted to abandon this study in favor of more controlled combustion rig-based measurements. To do so, however, would fail to produce a meaningful capability to estimate HAP emissions for airport operations. As designed, this project was able to test 11 engines of the same model that were pulled from operational service. A mixture of newer and older engines was present in the test pool. We do not have detailed knowledge of each engine's clearances, tolerances, or overall efficiency. For some engines, documented maintenance histories were unavailable. The tally of potential system inefficiencies is further complicated by the fact that bleed air demand involved systems that are not part of the engine (e.g., cabin packs).

There were no a priori assumptions made as to which engine parameters would be needed for describing the emissions performance near idle. After examining the data tabulated in Appendix A and the detailed engine data recorded in the data recorder, fuel flow seems to best collapse the observed variability in emission indices for the speciated VOCs of interest. Several HAP compounds were quantified in this study and tended to exhibit highly correlated behavior, as will be shown later. Observed correlations among the measured

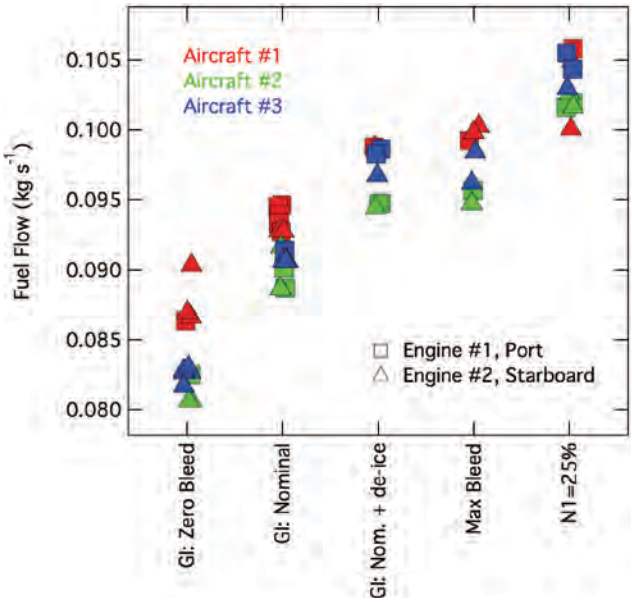

Figure III-1. Fuel flows resulting from the named engine condition in the near-idle test matrix (GI = ground idle). *These tests were conducted at ambient temperatures between 265K and 271K.*

emission indices for several VOC species are actually more precise than the capability to reproduce low-fuel-flow engine states. Although some important differences in the VOC profile have been uncovered in this study, the same trend will generally be present in other HAP species when data for a particular HAP or VOC are evaluated.

Figure III-3 presents all measured formaldehyde emission indices, from every test conducted when the ambient air was lower than 0°C in 2009 and 2010 at MDW, plotted versus fuel flow for 11 different CFM56-7B24 combustors. Of all parameters recorded in the digital flight data records, fuel flow best linearizes the trend in emission index. Similar patterns are observed in the other specific hydrocarbon measurements, including ethene, acetylene, and 1,3-butadiene.

III.1 Dependence of VOC on Fuel Flow Near Idle

The ICAO engine certification databank (ICAO 2006) defines the idle condition as 7% of rated thrust. An ICAO engine entry specifies the engine combustor and the thrust rating for each particular model certified for use on commercial aircraft. In some cases, the combustor technology is not drastically different for entries in the databank with different thrust ratings. Because the ICAO definition of idle is relative to maximum thrust, if the engines using the same combustor designs can be identified there may be preexisting data that can address the dependence of VOC emissions on fuel flow for near-idle operations (DuBois and Paynter 2006).

Examination of the tabulated total UHC emission indices should provide a qualitative guide for the UHC emissions-related performance to compare with the trend observed in Figure III-3.

Figure III-4 shows a selected portion of the ICAO emissions databank for total hydrocarbons. The blue data entries in the

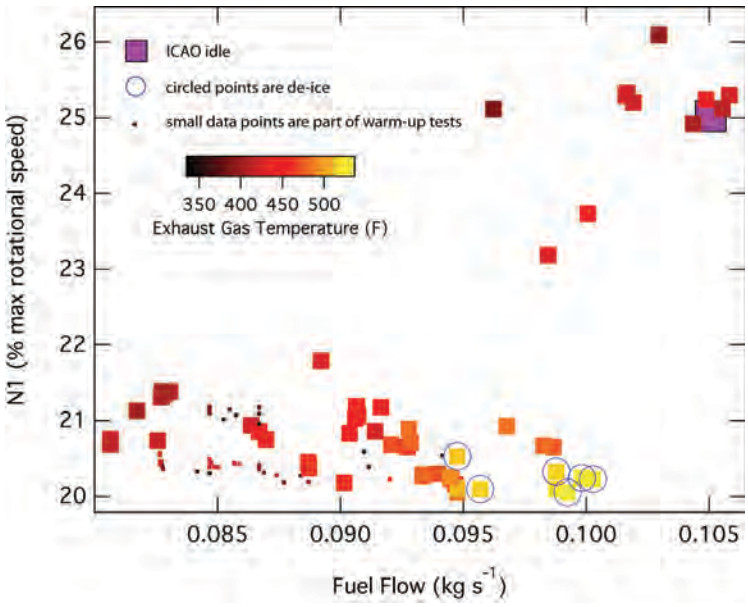

Figure III-2. N1 fan speed versus fuel flow rate. *The data points are colored by exhaust gas temperature. The small data points are the warm-up test points. The data circled in blue represent points where de-icing technologies were enabled.*

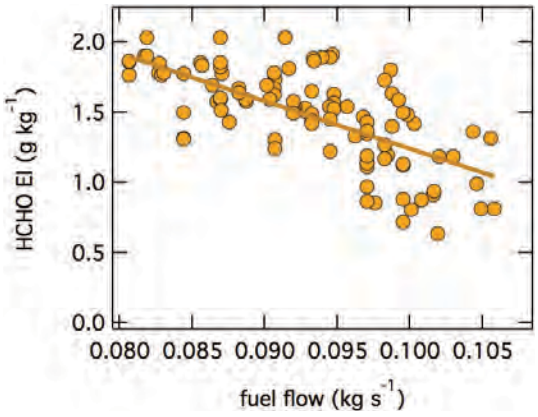

Figure III-3. Formaldehyde emission index versus fuel flow.

EI HC column are the UHC emission indices at idle thrust setting (7% thrust). The black entries labeled with black arrows are from combustors with similar characteristics. When the entry with the highest fuel flow/lowest emission index is used to normalize each entry, we can compare the relationship of the UHC emissions index with absolute fuel flow for the CFM56-7Bxx family of engines to the data collected in the tests conducted for this project.

Essentially, the exercise described in Figure III-4 uses the ICAO databank to form a generalized UHC dependence on fuel flow at near-idle condition. This procedure will be used to account for the engine-to-engine variability observed in absolute UHC emission indices for the on-wing engine tests in order to draw out whatever trend may exist in the UHC emission index with fuel flow. This procedure is also used to directly examine any systematic coupling between fuel flow and specific VOC emission indices.

The construct described in Figure III-4 is referred to in this document as the near-idle fuel flow dependence. Formally, the slope of this assumed line carries units of s kg^{-1}, and is the slope parameter in the following expression.

$$\frac{\mathrm{HC}(Fuel\ Flow)}{\mathrm{HC}(FF_{7\%})} = 1 + slope\left(\frac{s}{kg}\right)\left[Fuel\ Flow - FF_{7\%}\right]$$

In this case the fuel flow is the independent variable, and the result is effectively a multiplicative factor that can project the UHC emission index to fuel flows lower than the fuel flow at 7% thrust ($FF_{7\%}$) in the expression above.

III.2 Test Results for Engine SA012

The test results for the aircraft engine "SA012" in Appendix A are plotted in Figure III-5 using the normalization procedure described in Figure III-4.

UID No	Engine Identification	Eng Type	B/P Ratio	Press Ratio	Rated Output (kN)	EI HC Idle (g/kg)	Fuel Flow Idle (kg/s)
3CM029	CFM56-7B18	TF	5.5	21.59	86.74	3.50	0.097
3CM030	CFM56-7B20	TF	5.4	22.61	91.63	3.10	0.100
4CM039	CFM56-7B20/2	TF	5.4	22.77	91.63	8.11	0.102
3CM031	CFM56-7B22	TF	5.3	24.41	100.97	2.50	0.105
4CM040	CFM56-7B22/2	TF	5.3	24.61	100.97	7.26	0.105
3CM032	CFM56-7B24	TF	5.2	25.78	107.65	2.40	0.109
4CM041	CFM56-7B24/2	TF	5.2	25.95	107.65	6.55	0.109
3CM033	CFM56-7B26	TF	5.1	27.61	116.99	1.90	0.113
4CM042	CFM56-7B26/2	TF	5.1	27.80	116.99	5.88	0.113
3CM034	CFM56-7B27	TF	5.0	28.63	121.44	1.70	0.116
4CM043	CFM56-7B27/2	TF	5.0	28.84	121.44	5.56	0.115

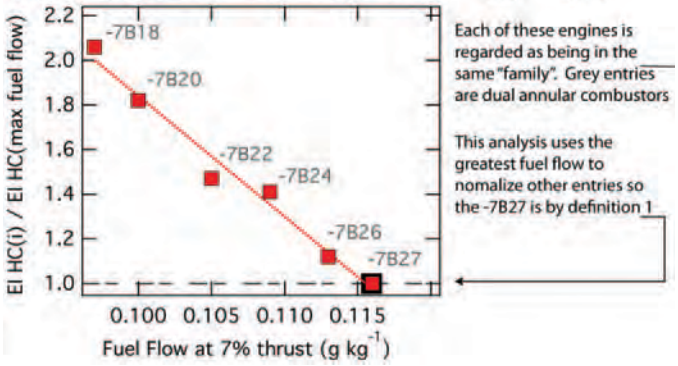

Figure III-4. ICAO emissions performance databank analysis. *The upper table shows selected columns and rows from the ICAO emissions performance databank. The inset graph depicts the results of an analysis scheme that addresses the relative UHC emission index increase caused by small changes in fuel flow for idling engine operation.*

The unnormalized data is depicted in Appendix A as Figure A01-E12b, and the three apparent ratios of the emission index (at a given fuel flow rate) relative to the measured emission index at the N1 = 25% fuel flow are tabulated in the legend. The uncertainties in the slopes are twice the standard error of the fitting procedure. This process can be extended to the entire dataset for all engines and all VOC species.

III.3 Ensemble Result for Fuel Flow Dependence

The entire dataset has been analyzed for each VOC following the procedure described in the preparation of Figures III-4 and III-5. The histogram of all these results has been plotted in Figure III-6. This result forms the basis of the fuel flow dependence that will be carried forward to a near-idle emissions index model described later. The goal of this project is to quantify HAP emissions from idling aircraft as a function of engine and ambient conditions. Despite the complexities of working with on-wing engines and the various bleed air operational states, the result depicted in Figure III-6 suggests an increase in the VOC emissions index with reduced fuel flow. The histogram for all the VOC project data fit to a

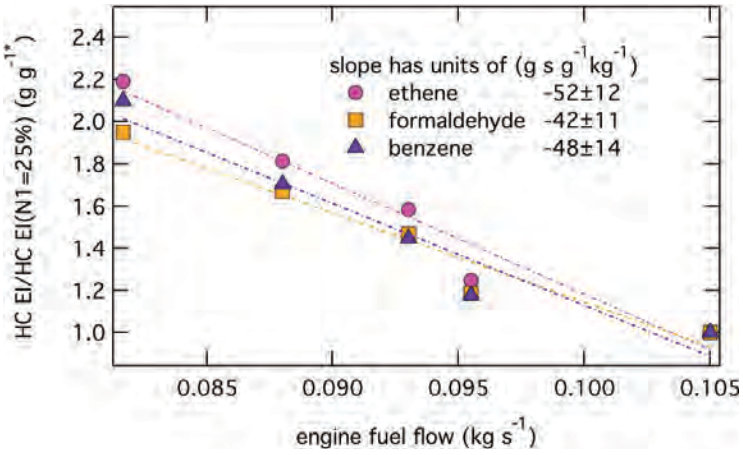

Figure III-5. Speciated VOC emissions data normalized to the N1 = 25% test result. *The data for this aircraft engine is SA012 and can be found in Appendix A. Ethene (circles), formaldehyde (squares), and benzene (triangles) have been plotted and fit as a function of fuel flow.*

Gaussian profile, depicted in Figure III-6 as the dashed-dot line, asserts a central value and Gaussian half width of −51±17 (s kg^{-1}), assuming the data are described by normal distribution. Whether this is a good assumption may not be known without measuring a much larger sample; however, it at least provides a metric for gauging the width of the distribution.

The two dominant VOC compounds by mass—ethene and formaldehyde—are characterized by average and standard deviation values of −60±16 and −49±10 (s kg^{-1}). The measured VOC/fuel flow dependence compares favorably with that determined for the UHC emission indices derived from the ICAO databank of −54±4 (s kg^{-1}) as depicted in Figure III-4. The width of this distribution will be revisited after a summary of the error analysis associated with the emission index measurements.

III.4 Systematic Error and Fuel Flow Dependence

The plume sampling methodology has a known bias of +2% (see Appendix A). Typically, the precision error in any single determination of an emissions index is much less than 5%

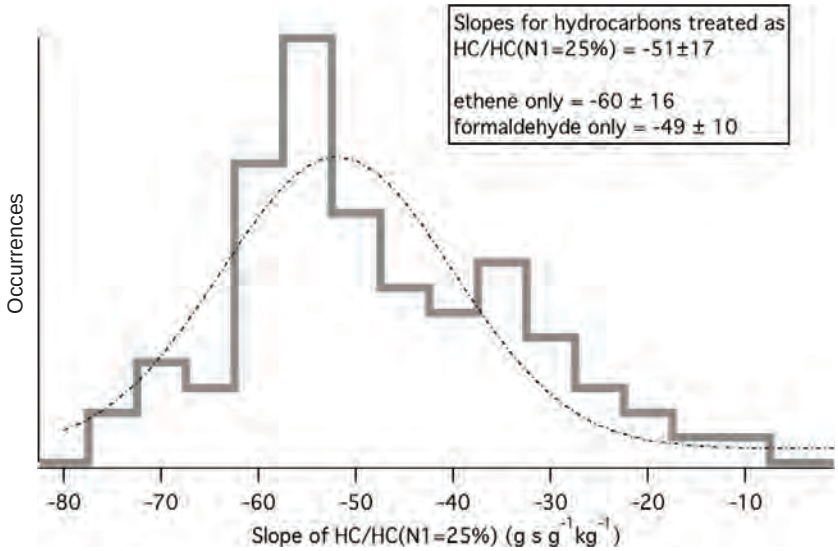

Figure III-6. Histogram of the measured dependence of VOC emission on fuel flow for all engines and speciated VOCs measured in the study. *The dashed-dot line is a Gaussian fit to the distribution.*

(see data tables, Appendix A). In this formalism, because ratios are used, the systematic error in the measurement of each specific hydrocarbon actually drops out. For example, if the proton transfer for reaction mass spectrometry (PTR-MS) measurement of styrene is systematically high by 25%, because the emission index is being divided by the emission index taken with the same test hour, the bias in this measurement will essentially cancel when the instrument is operating within its linear dynamic range.

Overall uncertainty estimates for the analytical instruments used in this study are discussed in Appendix E. An assessment of analytical instrument contribution to error, in the context of determining the near-idle fuel flow dependence of the emissions index, yields 5%. In this work, the emission index for CO_2 has been assumed to be a constant 3160 g kg^{-1}. This assumption is good to 3%. Furthermore, this work assumes that all fuel carbon is in the form of CO_2, which introduces a bias of up to 5%. Taken together, the combination of analytical instrument error and estimated analysis methodology uncertainty indicates an overall systematic uncertainty of 12%.

III.5 Fuel Flow Dependence and Variability

Based on the dominant VOCs as well as the ICAO UHC databank results, this study recommends a *near-idle* fuel flow dependence of −51 s kg^{-1} for the CFM56-7B engine variants. The overall uncertainty in this recommended central value of the near-idle fuel flow dependence parameter is ±23%. This has been estimated by combining the overall systematic uncertainty in the measurements of emission index with the average spread observed in the fuel flow dependence parameter for formaldehyde and ethene. The overall spread, however, of observed variability in this parameter when considering the entire distribution of VOCs measured in this study is large (see Figure III-6). The variability in the observations can be characterized by the 95% confidence limit. Twice the Gaussian half width of the distribution would imply a range of −86 to −18 s kg^{-1}. We attribute the width of this distribution to genuine engine-to-engine and intra-engine state variability.

A cursory examination of the test results in Appendix A reveals consistent patterns for all VOC and CO emission indices for a single test. This test pools the results from several engines, installed on different airframes, with operational parameters characterized by different on-board sensors, operating with different bleed air requirements, and with differing maintenance histories. This project assumes that each of these factors contributes to the observed width in the distribution of near-idle fuel flow dependences. The variability in these data should not be confused with error. In a model estimate of airport HAP emissions, the number of aircraft source engines will be much larger than the 11 studied here. If the influence of engine-to-engine variability effectively forms a normal distribution of idle fuel flow emissions dependence, then the uncertainty from this source of error in the tabulation of total airport emissions can be characterized by the uncertainties in the central value and the width of the emissions distribution. For these data, the uncertainty in the central value is much less than the width of the distribution.

SECTION IV

Relationship Between Emissions and Ambient Temperature

Previous studies have observed that ambient temperature has a profound effect on the emissions of CO and HC when the engine is operating at near-idle state (Lyon et al. 1979). They note that the change in emissions performance resulting from the influence of ambient pressure on the combustor intake pressure (P3 in Figure I-3) is not as significant as the effect of ambient temperature on the combustor inlet pressure (T3).

Gas turbine engines are optimized for operation at cruise power, so when they are operating at idle power, far from their optimal operation point, combustion efficiency can be non-ideal. Since the engine is operating at less than optimal efficiency, it is not surprising that it may be more sensitive to variations in ambient conditions. Physical conditions like temperature in the combustor strongly impact the combustion process. Figure IV-1 depicts the output of a simple GasTurb calculation to evaluate the potential magnitude that variations in ambient temperature (T2) can impact the temperature at the combustor exit (T4). This simple model should not be taken to be quantitatively accurate; however, it suggests the effect at low fuel flow, indicative of near-idle operation, has an effect on combustor temperature. The combustion temperature estimated using GasTurb (with combustor parameters for a CFM56-7B24 engine) results in a roughly linear relationship between T2 and T4 (see Figure I-3 for locations of the numbered temperature stages). Although the relationship between the ambient incoming air and the proxy combustion temperature is essentially linear in this simulation, the net efficiency of combustion falls dramatically at lower T2 values. Less efficient combustion produces higher emission levels of HAP compounds and other hydrocarbons.

IV.1 VOC Emissions and Ambient Temperature

The impact of ambient temperature on the combustion efficiency is illustrated using the measurements made for formaldehyde. The absolute formaldehyde emission index (expressed as grams of formaldehyde per kilogram of fuel) measured for each of the CFM56-7B24 engines tested during the testing phase of this project is depicted as a function of ambient temperature in Figure IV-2. The formaldehyde emission index measured at 7% thrust (N1 = 25%) and the ground idle (no bleed air demand) during the JETS/APEX2 test for the CFM56-7B24 engine have been included for comparison (OAK g.i. and OAK 7%). The two dashed lines added to Figure IV-2 suggest a simple linear temperature dependence for the two idle states: ground idle (brown) and the N1 = 25% definition of idle (yellow). The data plotted in Figure IV-2 includes all test points, and deliberate variations in fuel flow are responsible for what appears to be scatter in this depiction. Note that all of the cold weather (265K to 271K) data plotted in Figure IV-2 are also shown in Figure III-3 to vary systematically with fuel flow.

Prior to the testing undertaken by this project, the test points typically probed during on-wing emissions test projects were at ground idle (with no bleed air demand) and/or at the *ICAO* defined idle of N1 = 25% or 7% thrust. The previous section described the significant effect of the fuel flow rate on emissions when operating the on-wing engine below N1 = 25%. The data plotted in Figure IV-2 suggest that the magnitude of the influence of ambient temperature on the emission index is similar to the effect of engine operation at rotational speeds less than N1 = 25%.

IV.2 Emissions Index Temperature Dependence

The temperature dependence of the formaldehyde measurements is very similar to the dependence observed for ethene, propene, acetaldehyde, and other VOC species. Qualitatively, a similar temperature dependence was observed for the NASA DC-8 during APEX (2004). Because testing programs that use government-owned aircraft (such as APEX, JETS/APEX2,

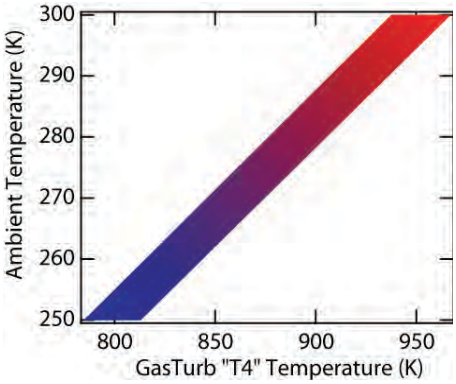

Figure IV-1. GasTurb simulation of combustor temperature for "idle" as a function of ambient temperature.

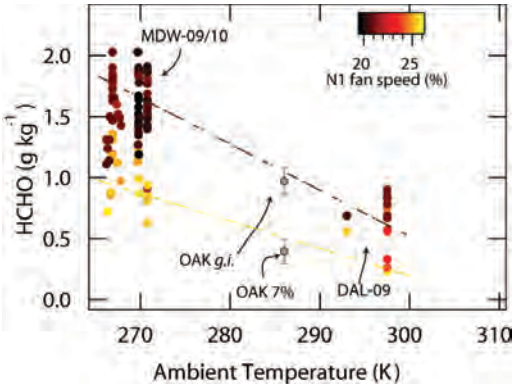

Figure IV-2. Formaldehyde emissions index versus ambient temperature for the CFM56-7Bxx family of engines. *The emission indices measured in this project are shaded by the N1 rotational fan speed to visually distinguish the N1 = 25% points (yellow) from the tests at ground idle with varying bleed air demand (darker reds). The gray data points from the JETS/APEX2 at OAK are included for comparison since the combustor type was the same as for the other data plotted here.*

APEX3, and the Alternative Aviation Fuel Experiment [AAFEX]) have access to an aircraft for long stretches of time, those tests have been able to probe a range of ambient temperatures. The limitation, however, is that they only test the ground idle and 7% idle conditions. In addition, the APEX and AAFEX testing on the NASA DC-8 do not have a measured record of the fuel flow that parallels the data collected by the digital flight data recorder (DFDR) during subsequent commercial aircraft tests.

To compare the temperature dependence from test results for different CFM56 combustor types, as well as to examine the temperature dependence using other available VOC measurements, a normalization scheme is adopted. The ICAO reference temperature is 288K (58.7°F). In the adopted normalization scheme the emission index is normalized by a measured or assumed emission index at 288K.

The normalized emission indices (at or near ground idle) for several measurement campaigns have been plotted as a function of ambient temperature in Figure IV-3. Overall,

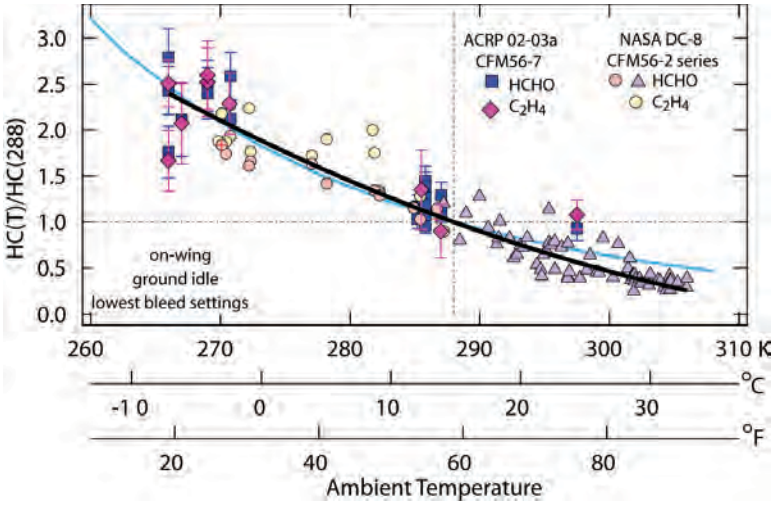

Figure IV-3. Normalized emission index versus ambient temperature. *The measured emission indices for formaldehyde and ethene have been normalized by the value at 288K for several datasets. The light blue line is a representation of the BFFM2, and the dark black line is a quadratic fit to the data.*

the emission indices of the VOCs are approximately twice as high between 0°C and −8°C as they are at 15°C.

In order to query the functional dependence of the temperature correction implicit in BFFM2 for *idle* data, the calculation was performed for temperatures ranging from 258K to 308K. The resulting emissions index data was divided by the result at 288K in order to extract the embedded temperature dependence (DuBois and Paynter 2006). The resulting curve is the light blue line in Figure IV-3 and agrees very well with the empirical results despite the potential misapplication of BFFM2 to fuel flow below the 7% reference fuel flow.

Figure IV-3 depicts the temperature dependence for the ground idle results only. When this analysis is performed on the ICAO 7% test data, the negative temperature dependence is still present, but not quite as steep. This result is not unanticipated because at the increased fuel flow rate the combustor temperature is increased and combustion efficiency increases.

SECTION V

Emissions Model Based on Near-Idle Fuel Flow and Ambient Temperature

The essential trend observed when an engine is operating at near-idle conditions is an increase in VOC emission indices with decreasing temperature. This negative temperature dependence was demonstrated for several VOCs. Scatter is present in the observations and the apparent engine-to-engine variability will be discussed later. An empirical model of the temperature dependence of near-idle emissions can be developed and locked to the ICAO emissions performance databank values. This empirical model can also account for the effect of ambient temperature and engine operation at rotation speeds less than the 7% thrust condition.

V.1 Proposed Empirical Model

In the empirical model proposed here, the effect of ambient temperature and sub-7% fuel flow are treated as independent factors that influence a base reference emission index defined at 288K and 7% thrust. This is how the ICAO databank idle reference conditions are incorporated into this model approach. Near-idle emissions scaling suggests that it is plausible to rely on the FAA and EPA's Speciate database (EPA 2008) VOC emissions profile to convert the tabulated UHC emission index to specific VOC (or specific HAP) species emission indices for a reference emission index.

The datasets and the measurement conditions they span are used to develop the empirical emissions index model shown in Figure V-1. The APEX1 datasets, which first showed a strong dependence of emissions on ambient temperature at the ground idle engine condition, were conducted at temperatures at or greater than the ICAO reference temperature (288K). The two idle conditions defined in that test matrix were ground idle (with no bleed air demand) and idle defined by N1 = 25%. Similarly, the AAFEX tests were conducted at the same engine conditions; however, the ambient temperatures encountered during that testing were essentially at or lower than the ICAO reference temperatures. Note that while the study goals of AAFEX were to study alternative fuel emissions, only the Jet A (proxy fuel for JP-8) data have been considered here. The JETS/APEX2 testing, also conducted at zero bleed air demand and N1 = 25% fuel flows, was performed on the CFM56-7B combustor, but only modest ambient temperature variations were encountered during the test. The testing protocol included tests at the ground idle (zero bleed) and N1 = 25% fuel flow points, but also probed intermediate fuel flows. These latter tests were conducted at both cold weather (MDW 2009/2010) and warm weather (DAL 2009) venues.

Figure V-1 indicates that, to the extent that the normalization of datasets can allow comparisons between different CFM56 combustors, empirical data from all quadrants of the fuel flow and ambient temperature space are available. The essential functional forms are a linear representation of the dependence of the emission index on fuel flow and a semilinear (weakly quadratic) dependence of the emission index on ambient temperature. A smooth interpolation has been applied between the temperature dependence observed for the ground idle fuel flow data and the N1 = 25% data.

An abbreviated encapsulation of the model developed for CFM56-7B22 engines is tabulated in Table V-1. At the reference fuel flow rate of 0.105 kg s^{-1} (7% thrust fuel flow) and temperature (288K) the emission index is by definition 1. If an application of this model were directed to estimate the effect of ambient temperature and non-7% fuel flow on an emission rate, the emission index could be multiplied by the factor in Table V-1. For example, the model predicts that emission rate for any VOC or HAP compound at 278 K and a fuel flow of 0.095 kg s^{-1} would be estimated by the following equation:

$$\text{Emission Rate}\left(\text{g s}^{-1}\right) = 2.1 \times 0.095\left(\text{kg s}^{-1}\right) \times \text{Reference Emission Index}\left(\text{g kg}^{-1}\right)$$

The data tabulated in Table V-1 are graphically depicted in Figure V-2.

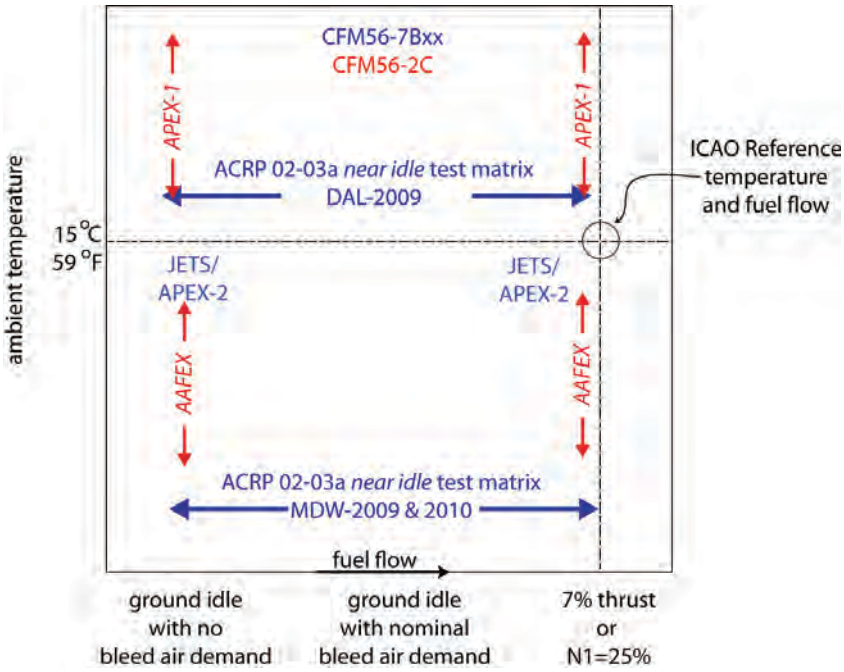

Figure V-1. Datasets available to develop fuel flow/ambient temperature model for predicting near-idle emissions. *The red datasets were collected for the CFM56-2C combustor on the NASA DC-8. The blue datasets for the CFM56-7B24 combustors were collected as part of this project.*

The emission index (grams of HAP per kilogram of fuel) multiplicative factor for the CFM56-7B22 depicted in Figure V-2 and tabulated in Table V-1 should not be interpreted as a direct multiplicative factor on the total emission rate (grams of HAP per second) when a fuel flow rate besides the reference fuel flow rate is considered.

The multiplicative factor is applied to the emissions index, with the total emission rate as the product of EI and fuel flow rate. Thus, at lower fuel flow rates, the emission rate is linearly reduced with the reduced fuel burn. This effect is accounted for in Figure V-3, which depicts the direct factor for the temperature dependent emission rate that accounts for

Table V-1. Emissions index correction factor for near-idle CFM56-7B22 operation.

	Ambient Temperature					
	273K	278K	283K	288K	293K	298K
	32°F	41°F	50°F	59°F	68°F	77°F
Fuel Flow						
(kg s^{-1})						
0.090	3.1	2.6	2.2	1.8	1.3	0.9
0.095	2.5	2.1	1.8	1.5	1.1	0.8
0.100	1.9	1.7	1.5	1.2	0.9	0.6
0.105	1.5	1.3	1.2	**=1.0**	0.7	0.5
0.110	1.1	1.0	0.9	0.7	0.6	0.4
0.115	0.7	0.6	0.6	0.5	0.4	0.2

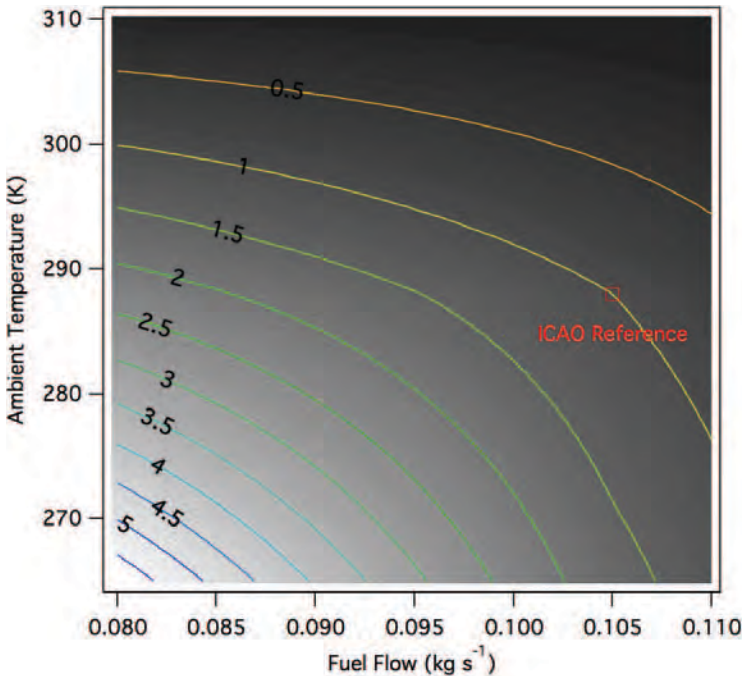

Figure V-2. Relative emission index as a function of ambient temperature and fuel flow. *The gray-scale shading and labeled contours are the multiplicative factor for the reference emission index.*

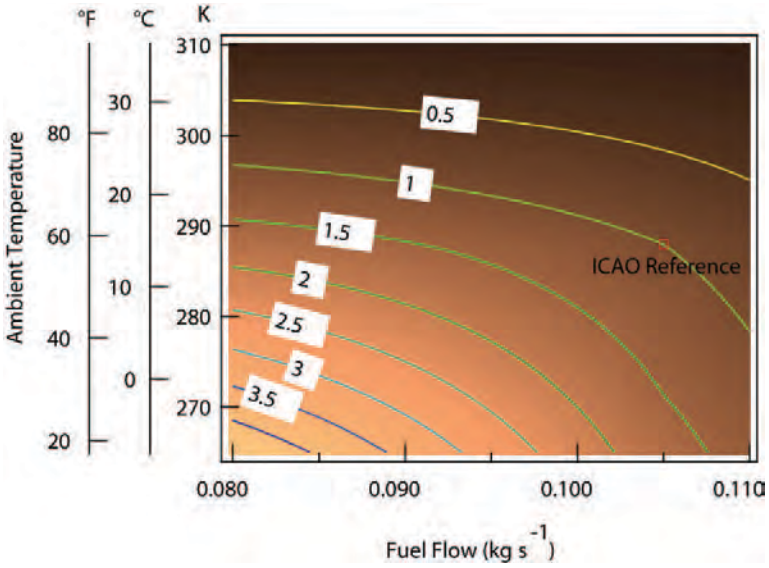

Figure V-3. Near-idle emission* rates *(not emission index) as a function of ambient temperature and fuel flow. *The contours and shading in the figure are derived from the data in Figure V-2. The effect of reduced fuel flow rate has been applied.*

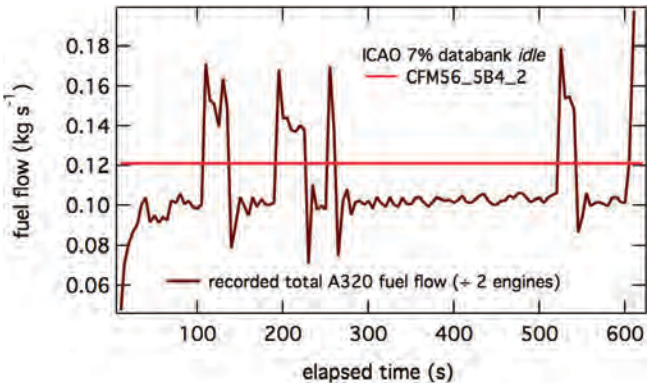

Figure V-4. Recorded fuel flow from an A320's taxiway phase is shown as a function of time since engine start. *The reference ICAO 7% thrust fuel flow is depicted in the horizontal line, and the trace is derived from the digital flight data record. The actual reported fuel flow has been divided by two since the original data source represents the sum from two engines.*

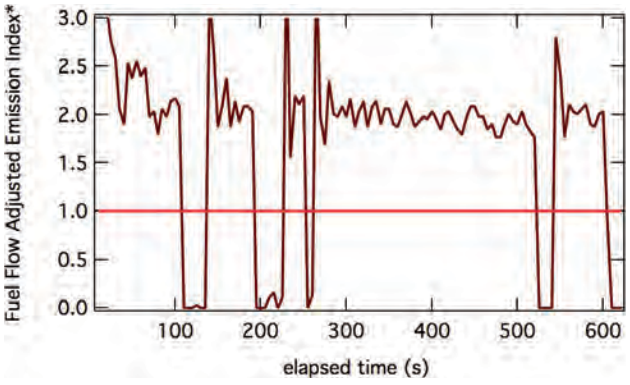

Figure V-5. Relative emission index adjusted for fuel flow rate for the example calculation described in the text.

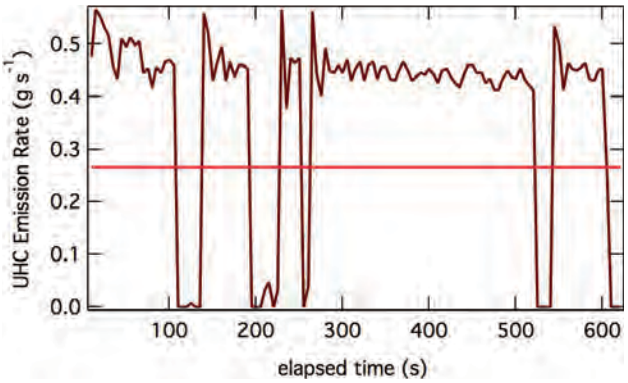

Figure V-6. Fuel dependent adjusted emission rate is depicted for two cases. *The brown trace is the example taxiway operation, and the light red trace is the ICAO emission rate for idle phase.*

the effects of both ambient temperature and fuel flow rate. The contours reflect that some of the dependence on fuel flow has been softened, relative to the dependence in Figure V-2.

V.2 Example Application of the Model

The overall approach adopted here is to convert the recorded fuel flow rates to instantaneous emission rates using both the temperature and fuel flow dependent emission index. The steps associated with the fuel flow conversion *only* are outlined here for a single operation for an A320 aircraft being operated at Zurich Airport. The ambient temperature during the operation was within 2°C of the reference temperature (15°C) and thus the temperature correction is very small.

In Figure V-4, shortly after engine start a sub-7% fuel flow is established. Periodically, the fuel flow actually increased above the 7% thrust, presumably to achieve "breakaway" thrust—the point where the aircraft begins to move.

The units of the emissions index correction factor are grams UHC/grams UHC$^{7\%}$ kg fuel$^{7\%}$/kg fuel. This is a multiplicative factor to the 7% thrust emission index; however, the potential difference in fuel flow needs to be treated explicitly.

Figure V-5 depicts the estimated adjusted emission index factor for the example fuel flow time series depicted in Figure V-1. In this example, the extrapolation is assumed to be linear above the 7% thrust value.

$$\frac{\mathrm{HC}(Fuel\ Flow)}{\mathrm{HC}(FF_{7\%})} = 1 + -52\left(\frac{s}{kg}\right)\left[Fuel\ Flow - FF_{7\%}\right]$$

In Figure V-6 the UHC emission rate is calculated for the time-dependent fuel flow rate from the example operation. As noted earlier, the fuel flow dependent model is probably not very accurate for the breakaway accelerations, but this example at least estimates this portion of the fuel flow only dependence. The ratio of the integrated emission for the example operation to the ICAO 7% emission of equivalent duration is 1.34 for this portion of the LTO.

SECTION VI

Additional Findings

VI.1 Engine Warm-Up Emissions

During engine ground start there are three basic temporal regimes to consider: pre-ignition, post-ignition/pre-idle acceleration, and post-ignition at ground idle. The pre-ignition VOC emissions will simply be the result of evaporated fuel. Around the moment of ignition there will be a mixture of fuel-like hydrocarbons and partially burned hydrocarbons. The post-ignition period will be characterized by increasing combustion efficiency, and VOC emissions will be accompanied by concomitant CO_2 emissions.

In the winter MDW 2009 test, an effort was made to characterize the post-ignition emissions to address the question of "warm-up." Whenever possible, the mobile laboratory was positioned about 40 m downwind of the engine during engine start. This was only done when the engines were known not to have been operated for at least two hours prior to the start. The order of the test matrix initially precluded measurement of the engine starts for engines one and two. We found we had sufficient flexibility with the sampling scheme, however, to attempt two additional near-start observations.

In Figure VI-1, a subset of the warm-up data offers insight into the time required to establish an equilibrium exhaust gas temperature. This result suggests that the exhaust gas temperature parameter requires three minutes to reach 90% of its steady-state value.

The formaldehyde emission index as a function of time following ignition is depicted in Figure VI-2. The time offset has been computed from the flight data recorder information and the time-coded notes taken in the mobile laboratory. The chemical information in the emissions profile at other engine-state changes has been used to refine the estimate of the time offset between the flight data recorder and mobile laboratory time. Conservatively, the absolute time since engine start is accurate within five seconds.

Figure VI-2 suggests that the CFM56-7B24 engines at the temperatures of this test (–7°C, –2°C) have two characteristic times. The first, initial rapid emissions change takes place within 20 to 60 seconds, where the emission index shows a rapid decay. The second change in emission index is longer and is characterized by a time constant of approximately two to three minutes.

The data suggest that following cold start, the VOC emission index is approximately doubled compared with that for warm operation for less than a minute. A simplistic approach to gauge the effect this has on inventory modeling of a 13-minute idle time (engine-on; taxi-out) is to add approximately one minute worth of additional emissions due to post-ignition warm-up.

The argument's weaknesses are that no study has systematically looked at the reproducibility of this observation or the time needed to return to cold start conditions. Furthermore, the initial ten seconds following ignition are not well represented in this dataset. The warm-up aspect of the study was secondary to the overall test goals, but these results could be used to further refine assessments of warm-up emissions, as well as to design better tests for future work.

VI.2 Near-Idle VOC Scaling

The relationships among exhaust concentrations of numerous VOCs (e.g., formaldehyde, benzene, acetaldehyde, ethene) have been discussed in several archival publications (Herndon et al. 2008, Herndon et al. 2009, Knighton et al. 2007, Yelvington et al. 2007). Briefly, it has been observed that VOC emissions all scale together (i.e., when the formaldehyde emission index doubles because of a decrease in temperature and/or fuel flow rate, so does the ethene emission index). These data and the initial detailed profile of Spicer and coworkers (Spicer et al. 1994, Spicer et al. 1992) have been used recently to refine the Speciate database (EPA 2008) VOC profile for commercial aircraft emissions (FAA Office of Environment and Energy and EPA Office of Transportation and Air Quality 2009). While this near-idle VOC scaling observation has proven

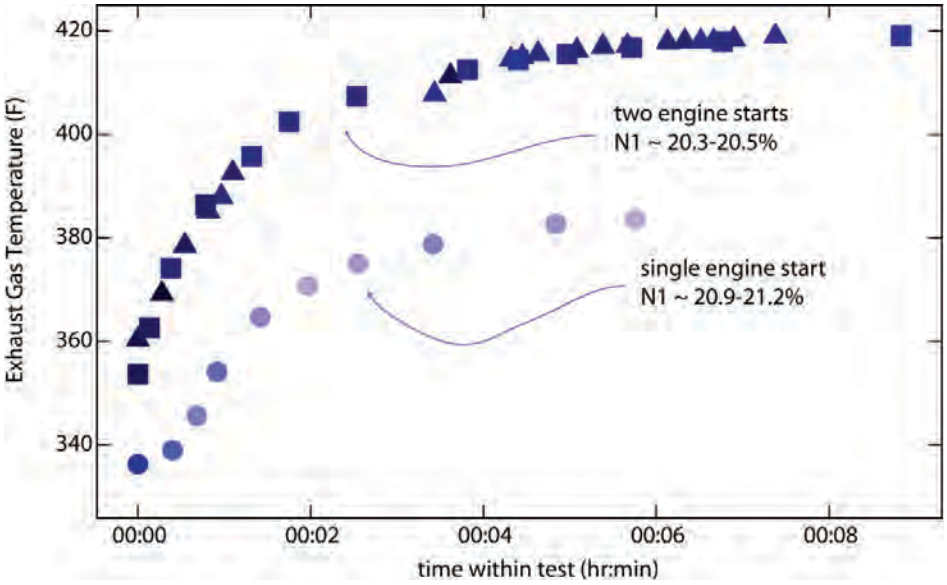

Figure VI-1. Measured exhaust gas temperature as a function of the approximate elapsed time since engine start. *Triangles, squares, and circles denote different aircraft tests. Dark blue points reflect lower N1 rotational speeds than the lighter blue points for two of the starts.*

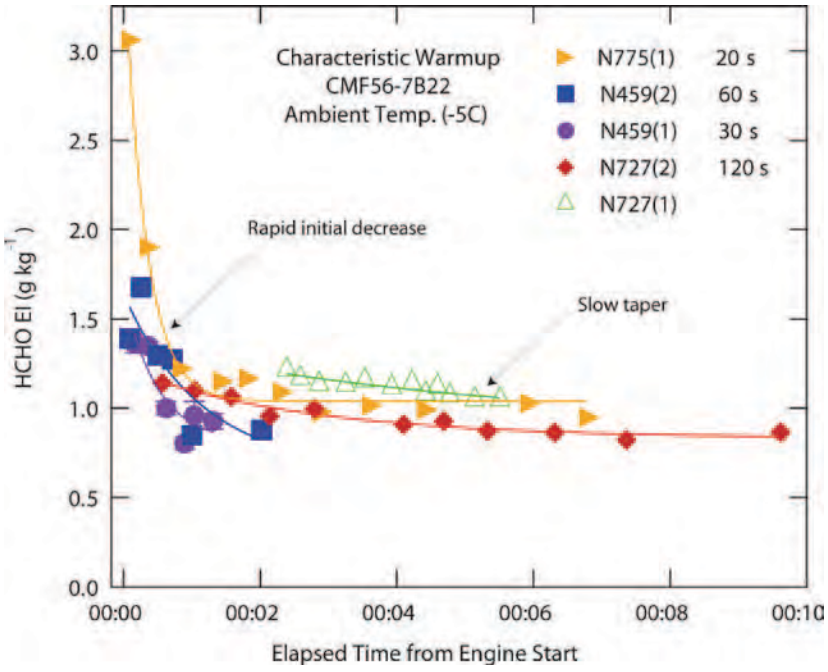

Figure VI-2. Formaldehyde emission indices are plotted as a function of the post-ignition warm-up time. *Although the relative times are precise, the absolute time following ignition for any of these curves is uncertain by five seconds. The solid lines represent fits of the data to an exponential decay. The approximate time constant associated with each curve is noted in the legend.*

to be a valuable guide, it is not universal. The tests undertaken by this project have, in conjunction with observations from other aircraft emission studies, revealed some subtle but important deviations of the near-idle VOC proportional scaling behavior. Two important observations derived from these tests are discussed below.

The emission of benzene in aircraft exhaust arises from several sources: unburned benzene in the fuel, dealkylation of higher molecular weight aromatics present in the fuel, and formation through radical-radical recombination reactions occurring within the combustor. The near-idle scaling observation permits these fuel effects to be extracted because it focuses on changes in the exhaust composition. Deducing compositional information from individual emission indices requires that one correct for the dominating influences of engine power and ambient temperature from the measurements. The scaling process naturally accomplishes this because the temperature and fuel flow corrections are applied equally to both compounds. The results presented in Sections III and IV demonstrated that different compounds were equally affected by fuel flow and ambient temperature.

The relationship of benzene and formaldehyde is investigated in Figure VI-3. The slopes of these plots provide information regarding the influence of fuel structure. While the variability in the plots appears to be scatter, a more complete analysis of all of the existing data reveals that the benzene emissions are in fact nonlinearly related to the aromatic fuel content. This result is discussed further in the fuel effects section.

A second example that demonstrates a deviation from the near-idle VOC scaling behavior is the emission of 1,3-butadiene, an important HAP. The development of the NO^+ reagent ion mode for the PTR-MS has permitted the first real-time measurement of 1,3-butadiene (Knighton et al. 2009). This technique was employed during this project.

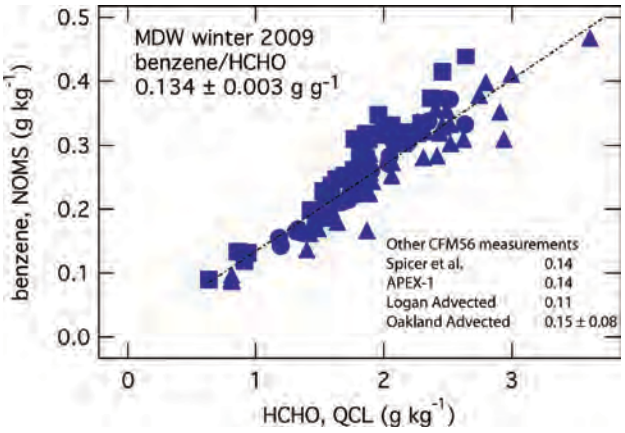

Figure VI-3. Correlation between emission indices of benzene and formaldehyde.

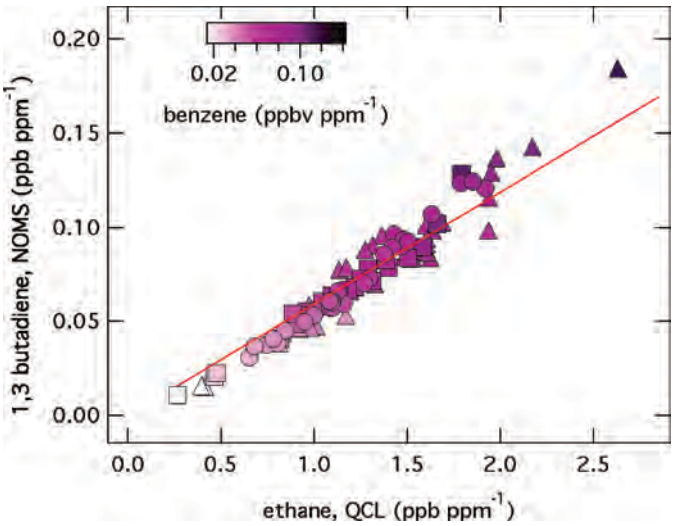

Figure VI-4. Correlation of 1,3-butadiene and ethane emissions.

A plot of the 1,3-butadiene emission index versus ethene emission index is shown in Figure VI-4. While the data are highly correlated, linear fits always suggest a negative intercept. Note that plots versus formaldehyde show similar results. This observation results from the fact that the emission of 1,3-butadiene has a stronger dependence on engine power than do other VOCs, producing a violation of the near-idle VOC proportional scaling rule. The emission of 1,3-butadiene scales more rapidly with changes in engine power, which demonstrates that errors (either positive or negative) can be made by applying a single-scaling variable drawn from EPA's Speciate database (EPA 2008).

VI.3 Effect of Fuel Composition on Emissions

Aromatic fuel content influences benzene emissions. The lower panel of Figure VI-5 depicts the scaled benzene emission index (normalized by the formaldehyde emission index) plotted versus the fuel aromatics content. In the upper panel, the shaded gray distribution of fuel aromatics was computed from the US military fuel stocks for 2007. Although the fuel stock used in commercial aviation is different from the military sources, it is likely that commercial aviation fuel typically contains 15%–22% aromatics. The larger blue points were collected at the MDW 2009 test and represent some of the most precise measurements of benzene performed to date. Additional data from other testing campaigns have been included for comparison purposes. The alternative fuels exhaust measurements in orange circles and red diamonds show that benzene emissions flatten out (i.e., do not decrease to zero for 0% aromatic content). It is plausible that at the

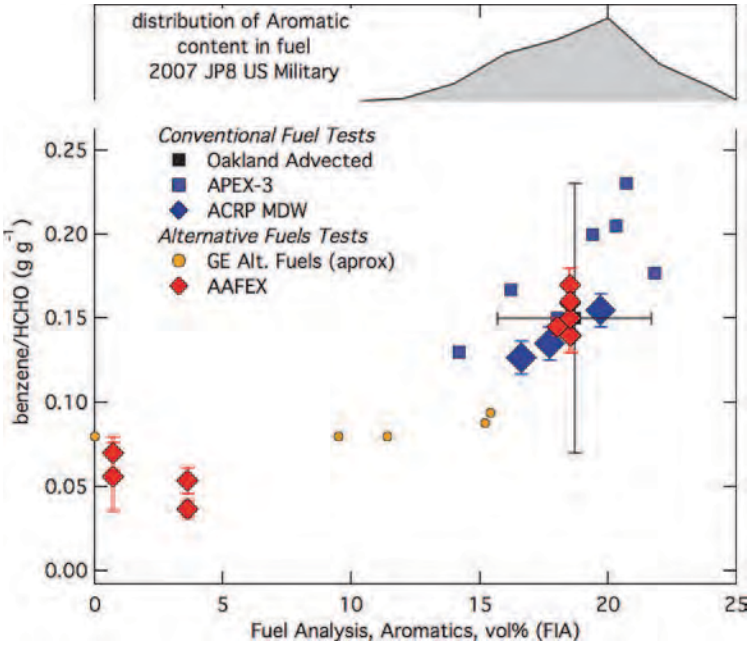

Figure VI-5. Benzene emission index and the aromatics fuel content. *The upper panel shows the distribution of aromatics in the fuel analysis for JP8 (assumed to be a good proxy for JetA). The lower panel contains the benzene/formaldehyde emission fraction.*

modest combustion temperatures at near-idle, there are two general pathways for the formation of benzene: one from assembly of small radical precursors and a second from the pyrolysis of larger aromatic compounds. The second pathway would have a dependence on the content of larger aromatic precursors, while the first would be less dependent on fuel aromatic content. These data imply that if benzene emissions are targeted for regulation, the fuel aromatic content could be reduced to cut benzene emissions. The data also suggest that there is a point of diminishing value from reducing fuel aromatics, with little benzene reduction below 12% aromatic content.

SECTION VII

Applicability to Airport Practice

This project has assessed the temperature dependence of idling aircraft engine emissions for selected variants of the CFM56 engine type. The project has characterized engine emissions of on-wing commercial aircraft (equipped with CFM56-7B24 engines) and explored the impact of fuel flows below the ICAO reference fuel flow rate for idle. The test matrix development process incorporated airline guidance on which fuel flow rates would be representative of actual idle phase during routine operation.

The project's results, together with data from other sources, have been assimilated into an empirical model that strives to describe the temperature and fuel flow dependence for near-idle VOC emissions. The model described in this work is only appropriately applied to idling aircraft engines and ambient temperatures between 260K and 310K (8°F to 98°F). It is currently based on the observations of the CFM56 engine. The project has proposed a framework for data assimilation that can tie future observations to ICAO certification data.

The approach described in this study can be used to estimate emissions during airport operations in the context of scenario analysis. The simple model described in this work can be used to help quantify the emissions benefit from proposed improvements to terminal area and taxiway operational protocols. Based on the observed temperature dependence, it is clear that practices that limit the amount of excess time spent at idle during the winter months will significantly limit the HAP emissions burden.

This project has completed the following for the CFM56-7B24 engine:

- Developed empirical corrections for fuel flow and temperature;
- Demonstrated applicability of the corrections to both individual VOC species and UHC;
- Corroborated the near-idle VOC scaling effect (described in Section VI.2);
- Demonstrated that emissions of HAP species can be estimated using the EPA Speciate profile with the ICAO databank UHC emissions performance value; and
- Provided a tool for airport operators to compute near-idle HAP and VOC emissions as a function of ambient temperature and airport operational conditions.

The results from this study can be applied in detailed analysis to study the HAP/VOC emissions trade-offs for a variety of scenarios, such as the following:

- Optimizing the takeoff queue length during operational pushes,
- Quantifying the benefit of switching to APU during cold weather ground stop, and
- Assessing HAP and VOC benefits from single engine taxiing.

SECTION VIII

References

Anderson, C., S. Augustine, D. Embt, T. Thrasher, and J. Plante. 2007. *Emissions and Dispersion Modeling System (EDMS) User's Manual,* AAE-07-01, Revision 3. Washington, DC: Federal Aviation Administration, Office of Environment and Energy.

DuBois, D., and G. C. Paynter. 2006. *"Fuel Flow Method2" for Estimating Aircraft Emissions.* SAE Technical Paper 2006-01-1987.

Federal Aviation Administration (FAA) Office of Environment and Energy and US Environmental Protection Agency (USEPA) Office of Transportation and Air Quality. 2009. *Recommended Best Practice for Quantifying Speciated Organic Gas Emissions from Aircraft Equipped with Turbofan, Turbojet, and Turboprop Engines.* Washington, DC: Federal Aviation Administration and US Environmental Protection Agency.

Federal Aviation Administration (FAA). 2006. *Emissions Dispersion Modeling System (EDMS).* www.faa.gov/about/office_org/headquarters_offices/aep/models/edms_model/.

Gerstle, T., P. Virag, and M. Wade. 1999. *Aircraft Engine and Auxiliary Power Unit Emission Testing: Vol. 1.* United States Air Force: IERA, RS-BR-TR-1999-0006.

Herndon, S. C., J. T. Jayne, P. Lobo, T. Onasch, G. Fleming, D. E. Hagen, P. D. Whitefield, and R. C. Miake-Lye. 2008. Commercial Aircraft Engine Emissions Characterization of In-Use Aircraft at Hartsfield-Jackson Atlanta International Airport. *Environmental Science & Technology* 42: 1877–1883.

Herndon, S. C., E. C. Wood, M. J. Northway, R. C. Miake-Lye, L. Thornhill, A. Beyersdorf, B. E. Anderson, R. Dowlin, W. Dodds, and W. B. Knighton. 2009. Aircraft Hydrocarbon Emissions at Oakland International Airport. *Environmental Science & Technology* 43: 1730–1736.

International Civil Aviation Organization (ICAO). 1993. International Standards and Recommended Practices, Environmental Protection. *ICAO Annex 16,* edited.

International Civil Aviation Organization (ICAO). 2006. *ICAO Aircraft Engine Emissions Databank.* www.caa.co.uk/docs/702/070716%20Introduction.pdf.

Kerrebrock, J. L. 1977. *Aircraft Engines and Gas Turbines.* Cambridge, Massachusetts and London, England: The MIT Press.

Knighton, W. B., E. C. Fortner, S. C. Herndon, E. C. Wood, and R. C. Miake-Lye. 2009. Adaptation of a Proton Transfer Reaction Mass Spectrometer Instrument to Employ NO+ as Reagent Ion for the Detection of 1,3-butadiene in the Ambient Atmosphere. *Rapid Communications in Mass Spectrometry* 23 (20): 3301–3308.

Knighton, W. B., T. Rogers, C. C. Wey, B. E. Anderson, S. C. Herndon, P. E. Yelvington, and R. C. Miake-Lye. 2007. Quantification of Aircraft Engine Hydrocarbon Emissions Using Proton Transfer Reaction Mass Spectrometry. *Journal of Propulsion and Power* 23 (5): 949–958.

Lyon, T. F., W. J. Dodds, and D. W. Bahr. 1979. *Determination of the Effects of Ambient Conditions on CFM56 Aircraft Engine Emissions.* US Environmental Protection Agency. nepis.epa.gov/Exe/ZyPURL.cgi?Dockey=9100XT8Y.txt.

NEPAIR. 2003. *Development of the technical basis for a New Emission Parameter covering the whole AIRcraft operation.* NEPAIR Final Technical Report, WP4/WPR/01(G4RD-CT-2000-00182).

SAE. 2006. *Procedure for the Continuous Sampling and Measurement of Gaseous Emissions from Aircraft Turbine Engines.* SAE Aerospace Recommended Practice: 1256C.

Sarli, V. J., D. C. Eiler, and R. L. Marshall. 1975. *Effects of operating variables on gaseous emissions.* Paper presented at the Air Pollution Control Association Specialty Conference on Air Pollution Measurement Accuracy as it Relates to Regulation Compliance, New Orleans.

Spicer, C. W., M. W. Holdren, R. M. Riggin, and T. F. Lyon. 1994. Chemical Composition and Photochemical Reactivity of Exhaust from Aircraft Turbine Engines. *Annales Geophysicae* 12: 944–955.

Spicer, C. W., M. W. Holdren, D. L. Smith, D. P. Hughes, and M. D. Smith. 1992. Chemical Composition of Exhaust from Aircraft Turbine Engines. *Journal of Engineering for Gas Turbines and Power* 114 (1): 111–117.

Timko, M. T., S. C. Herndon, E. C. Wood, T. B. Onasch, M. J. Northway, J. T. Jayne, M. Canagaratna, R. C. Miake-Lye, and W. B. Knighton. 2010. Gas Turbine Engine Emissions—Part 1: Volatile Organic Compounds and Nitrogen Oxides. *Journal of Engineering for Gas Turbines and Power* 132 (6): 061504.

US Environmental Protection Agency. 2008. Speciate. www.epa.gov/ttnchie1/software/speciate.

Wade, M. D. 2002. *Aircraft/Auxiliary Power Units/Aerospace Ground Support Equipment Emission Factors.* United States Air Force Institute of Environment, Safety and Occupational Health Risk Analysis, IERA-RS-BR-SR-2003-0002.

Wey, C. C., et al. 2006. *Aircraft Particle Emissions Experiment (APEX).* NASA/TM-2006-214382, ARL-TR-3903.

Wood, E., S. Herndon, R. C. Miake-Lye, D. D. Nelson Jr., and M. Seeley. 2008. *ACRP Report 7: Aircraft and Airport-Related Hazardous Air Pollutants: Research Needs and Analysis.* Washington, DC: Transportation Research Board.

Yelvington, P. E., S. C. Herndon, J. C. Wormhoudt, J. T. Jayne, R. C. Miake-Lye, W. B. Knighton, and C. C. Wey. 2007. Chemical Speciation of Hydrocarbon Emissions from a Commercial Aircraft Engine. *Journal of Propulsion and Power* 23: 912–918.

Acronyms and Abbreviations

AAFEX	Alternative Aviation Fuel Experiment
APEX	Aircraft Particle Emissions Experiment
APU	auxiliary power unit
BFFM2	Boeing Fuel Flow Method 2
CO	carbon monoxide
CO_2	carbon dioxide
DAL	Dallas Love Airport
DFDR	digital flight data recorder
EDMS	Emissions and Dispersion Modeling System
EGT	exhaust gas temperature
EI	emissions index
EPA	US Environmental Protection Agency
FAA	Federal Aviation Administration
GI	ground idle
HAP	hazardous air pollutant
HC	hydrocarbon
ICAO	International Civil Aviation Organization
LTO	landing/takeoff
MDW	Chicago Midway Airport
N1	rotational fan speed
NO_x	nitrogen oxides
ORD	Chicago O'Hare Airport
PTR-MS	proton transfer reaction mass spectrometry
UHC	unburned hydrocarbon
VOC	volatile organic compound

APPENDIX A

Project Results

Introduction

Staged tests were performed with both a stationary one-meter probe or by using the Aerodyne Mobile Laboratory as a mobile probe driving through the exhaust plume with a prevailing headwind. Staged tests performed at DAL 2009 and MDW 2010 provided an opportunity to test with a one-meter probe placed directly behind and engine operating at various ground idle conditions. Tests performed on the taxiways of all three airports visited under this project allowed measurements of exhaust plumes after natural dilution. In these latter measurements specific information on the engine operating conditions is not known, however this constitutes a dataset comprised of a multitude of different engines sampled while in-use. The testing from DAL 2009 can be compared to testing at MDW and ORD to get comparison of emissions at different ambient temperatures. DAL 2009 was conducted with warm ambient temperatures (24°C) while MDW and ORD tests were performed during the winter (–5°C). The dataset produced from this project is described in this appendix. The dataset is available as an excel format spreadsheet.

A01—Staged Aircraft Testing from the MDW 2009 Mission

The testing conducted during the MDW 2009 mission involved staging four Boeing 737 aircraft on two separate early mornings where the weather forecast called for cool precipitation free conditions. A single 737-300 and three 737-700 were tested. The 737-700 aircraft were equipped with a digital flight data record system that specified the engine state during the test. The 737-700 aircraft tested were equipped with CFM56-7B22 engines that had been upgraded via software to perform as a CFM56-7B24 engine type.

This section of the Appendix will briefly discuss the sampling and analysis method before discussing the results of the MDW 2009 measurement campaign.

Sampling and Analysis Methodology

Figure A01-1 depicts a schematic of the methodology used to sample engine emissions during the MDW 2009 quick look study. In this approach, the aircraft engine is not operated above N1 = 25% (CFM56-7B24), which ensures that the engine thrust does not damage the mobile laboratory in the thrust wake.

The air mass, sampled continuously, consists of a dynamic mixture of core-flow emissions mixed with an unknown and dynamically varying dilution fraction. The measurement as a function of time can be described by the following equation.

$$[X]_{measured} = f \times [X]_{post-combustion-core-emission} + (1-f) \times [X]_{ambient} \quad \text{(A-1)}$$

The method used to distinguish the core-flow plume constituents from the ambient is based on time series analysis (Herndon et al. 2004). The measurement at each of the continuous instruments will be a comprised of a mixture of core-flow combustion and ambient mixing ratios.

In expression (A-1), f represents the time dependent volume fraction of core flow that is being sampled. The quantity $f(t)$ is modulated by the engine by-pass flow turbulently mixing with the atmospheric shear field. Should $f(t)$ be zero for an entire sampling period, there will be no capacity to estimate $[X]_{post\text{-}combustion\text{-}core\text{-}emission}$ with the dataset.

To illustrate how (A-1) has been used to deduce $[X]_{post\text{-}combustion\text{-}core\text{-}emission}$ the time series for multiple measured quantities are used. The apparent baseline magnitudes for each of these species are equivalent to the ambient values measured when the mobile lab is outside of the engine flow (e.g., *upwind of the aircraft*) or when a crosswind component is pushing the engine core flow away from the sample location.

Using equation (A-1) for compounds such as those in Figure A01-2, it can be shown that for a time series containing time periods from non zero values of $f(t)$ the relationship

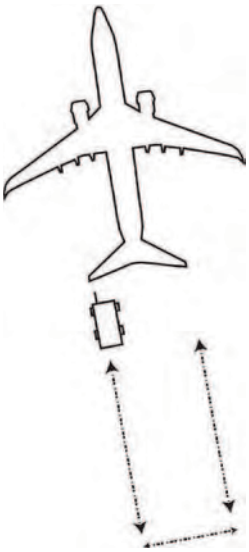

Figure A01-1. Sampling Scheme using the mobile laboratory inlet as the exhaust probe.

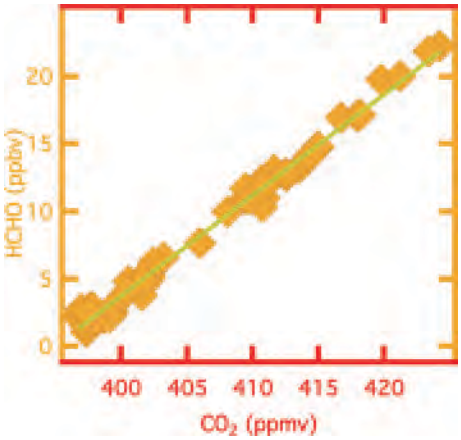

Figure A01-3. Correlation plot of HCHO and CO2 from MDW 2009 testing.

between two species, as X in (A-1) in the exhaust can be determined by,

$$\frac{[a]_{measured}-[a]_{ambient}}{[b]_{measured}-[b]_{ambient}}=\frac{-[a]_{ambient}}{[b]_{post-combustion-core-emission}-[b]_{ambient}}=m \qquad \text{(A-2)}$$

$$[a]_{post-combustion-core-emission}$$

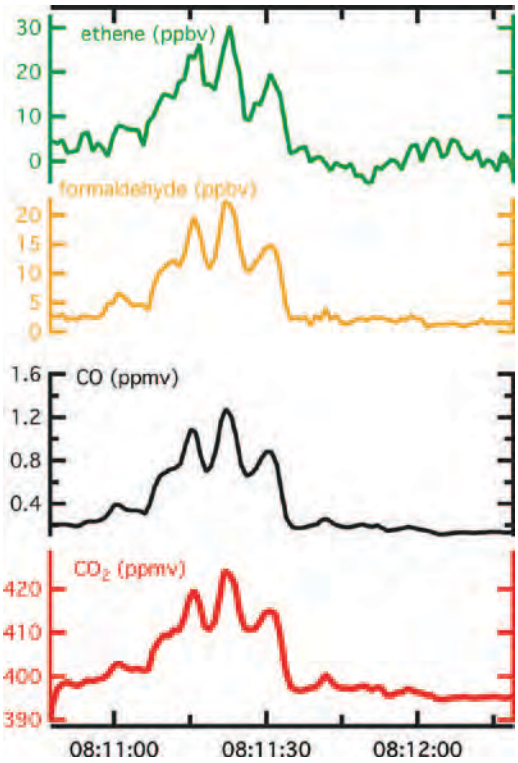

Figure A01-2. Example time series of CO2, CO, formaldehyde and ethene during a plume encounter at MDW (2009).

If the time response of both species a and b is matched in time and any potential lag between the two measurements accounted for, when the measurement of a is plotted against the measurement of b, for a time interval that contains non-zero $f(t)$ a linear fit of the correlation plot will yield a slope, m, in (A-2).

The slope of the fit of HCHO with respect to CO_2 (depicted in Figure A01-3) is 0.75±0.02 with units of ppbv $pppm^{-1}$ ($R^2 = 0.98$) where the error bar tabulated is twice the standard error of the slope parameter.

The slope is related to the desired quantity, the emission ratio of a (depicted in Figure A01-3 as HCHO) to CO_2 (labeled b in the formulas) in the post-combustion-exhaust by rearranging *without approximation* to yield equation (A-3).

$$\frac{[a]_{post-combustion-core-emission}}{[b]_{post-combustion-core-emission}}=m\left(1-\frac{[b]_{ambient}}{[b]_{post-combustion-core-emission}}\right)+\frac{[a]_{ambient}}{[b]_{post-combustion-core-emission}} \qquad \text{(A-3)}$$

In the case of using CO_2 to act as the dilution tracer the following limits can be used to estimate the systematic error inherent to this approach by making the reasonable assumption that the CO_2 in the core flow is 2% (or 20,000 ppmv) and CO_2 in the ambient is ~390 ppmv.

$$\frac{[a]_{post-combustion-core-emission}}{[b]_{post-combustion-core-emission}}=m\left(1-\frac{390\,ppmv}{20{,}000\,ppmv}\right)+\frac{[a]_{ambient}}{20{,}000\,ppmv} \qquad \text{(A-3a)}$$

The first term in this expression suggests that the error introduced by assuming that m is equivalent to the ratio of

the *a* to CO_2 in the core flow is less than 2%. The second term in this expression depends on the magnitude of $[a]_{ambient}$ which is compound specific, however it can be asserted that this error is much less than 0.01% for CO and the hydrocarbon compounds.

An uncorrected application of the methodology of compound slopes diluted to an unknown extent in the ambient, systematically biases calculated emission indices high by 1.7 to 2.1% for aircraft exhaust emissions when the CO_2 core flow is ~1.9 to 2.2% by volume and the species being studied is present in the ambient at less than 1 ppmv.

Results from CFM56-7B24 MDW 2009, DAL 2010 and MDW 2010 Testing

The results from the testing conducted where the digital flight data record is available are tabulated and depicted below. The table and figure numbers have been generated based on the engine test in question. The number following the letter E denotes which engine index is associated with the test result. At the request of the cooperating airline, the associated aircraft tail number and additional information is available by special request only and not part of the public release of this project.

Table A01-E1a. Selected test results for engine SA001 (MDW2009), aircraft test conducted from 3/3/09 04:00 to 3/3/09 05:00, ambient temperature 266.9±1K, relative humidity 71%.

Fuel Flow	2σ	N1	2σ	CO EI	S	FID EI	2σ
kg s^{-1}	kg s^{-1}	%	%	g kg^{-1}	g kg^{-1}	g kg^{-1}	g kg^{-1}
0.0910		20.900	0.000	78.340	0.800	8.170	0.410
0.0985	0.0007	20.650	0.071	73.955	0.616	8.275	0.502
0.1050	0.0014	25.000	0.141	56.055	0.895	6.030	0.439
Engine SA_001							
Fuel Flow	2σ	C_2H_4 EI	2σ	HCHO EI	2σ	Benzene EI	2σ
kg s^{-1}	kg s^{-1}	g kg^{-1}	g kg^{-1}	g kg^{-1}	g kg^{-1}	g kg^{-1}	g kg^{-1}
0.0910		2.990	0.010	2.480	0.050	0.270	0.007
0.0985	0.0007	2.450	0.098	2.155	0.055	0.215	0.006
0.1050	0.0014	1.785	0.063	1.630	0.028	0.160	0.006
Engine SA_001							
Fuel Flow	2σ	Toluene EI	2σ	C2-Benzene	2σ	Styrene	2σ
kg s-1	kg s-1	g kg-1	g kg-1	g kg-1	g kg-1	g kg-1	g kg-1
0.091		0.173	0.003	0.166	0.003	0.113	0.003
0.0985	0.0007	0.137	0.004	0.122	0.005	0.102	0.002
0.105	0.0014	0.111	0.002	0.112	0.004	0.087	0.004

Table Notes. The 2σ value is computed as twice the standard error of the fit emission ratio converted to emission index. When multiple data points have been averaged at the noted fuel flow rate, these errors have been added in quadrature.

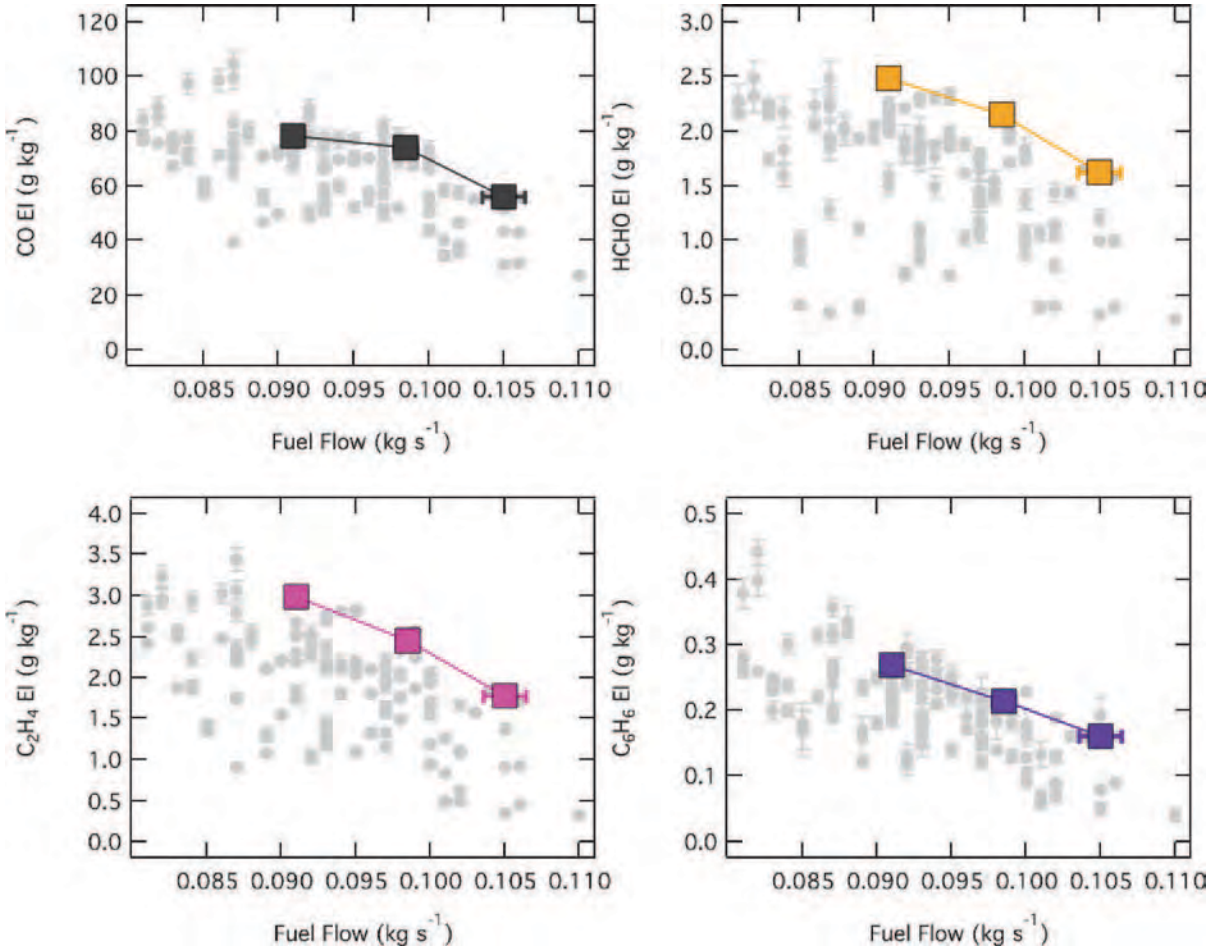

Figure A01-E1b. Emission Index for engine SA001 for CO, HCHO, C2H4, and C6H6. The four figures depict the emission indices in grey with the precision-based error bar from the entire CFM56-7B24 dataset. The colored data points are the emission index for the species in question averaged for the nominal engine state during the test of engine index SA-001. In many cases the precision based error bar for the emission index is smaller in magnitude than the size of the data point. See companion table for precision-based error bars. The absolute averaged emission indices for the fuel flow repeats during the test are depicted in the four panels; upper left CO in black; upper right HCHO in orange; lower left ethene (C2H4) in magenta; and lower right benzene (C6H6) in violet.

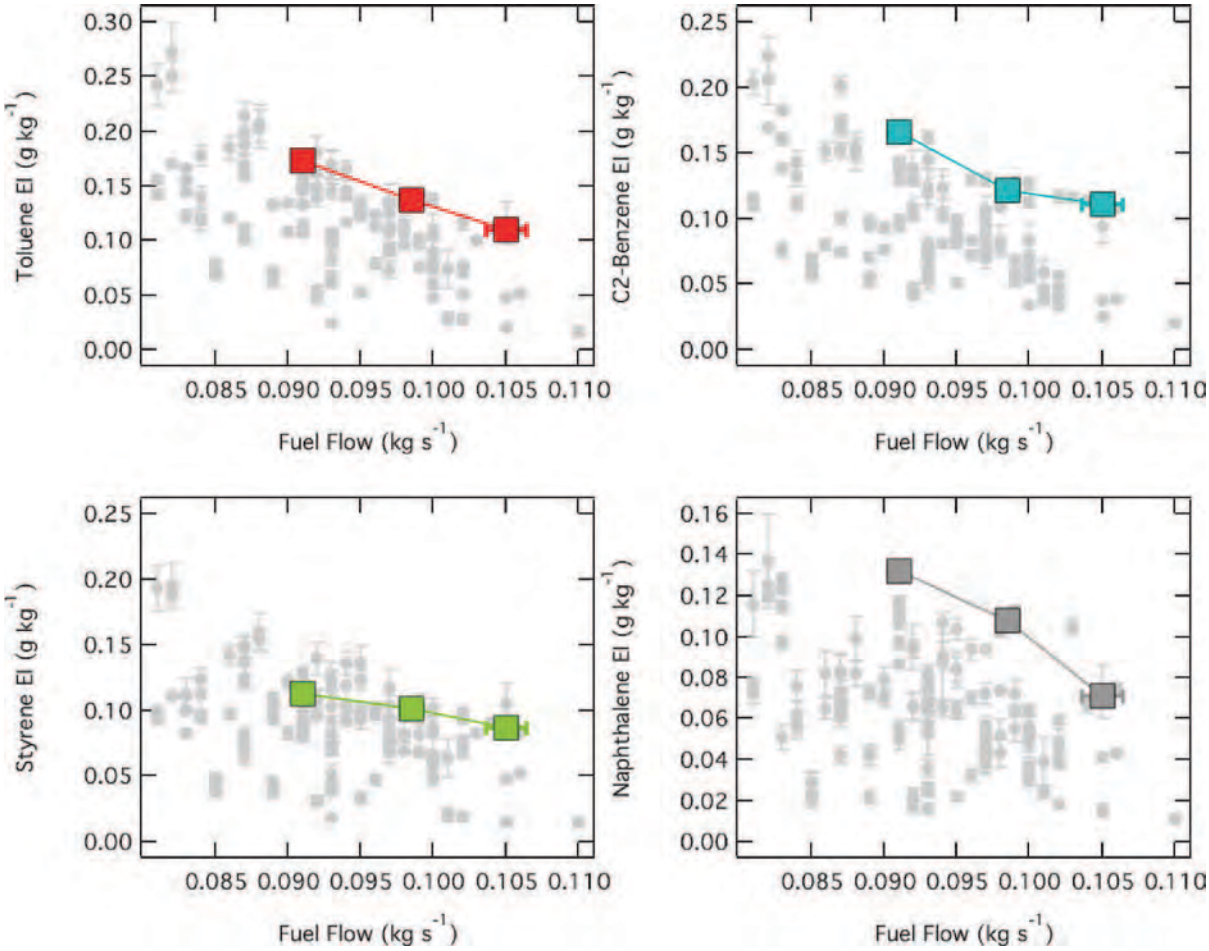

Figure A01-E1c. Emission Index for engine SA001 for Toluene, C2-Benzene, Styrene, and Naphthalene. C2-Benzene refers to the sum of the xylene isomers and ethyl-benzene. The four figures depict the emission indices in grey with the precision-based error bar from the entire CFM56-7B24 dataset. The colored data points are the emission index for the species in question averaged for the nominal engine state during the test of engine index SA-001. In many cases the precision based error bar for the emission index is smaller in magnitude than the size of the data point. See companion table for precision-based error bars. The absolute averaged emission indices for the fuel flow repeats during the test are depicted in the four panels; upper left Toluene in red; upper right C2-Benzene in light-blue; lower left Styrene in light green; and lower right naphthalene in the larger grey squares.

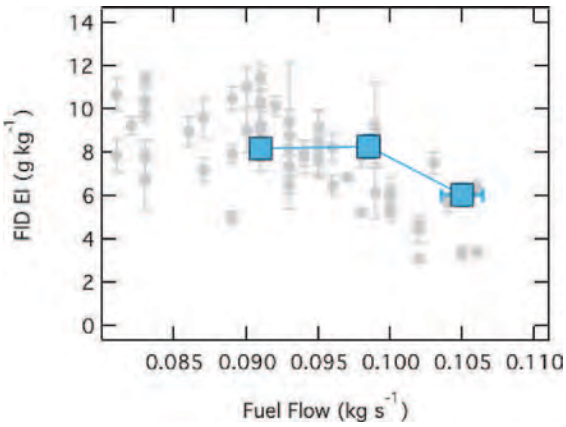

Figure A01-E1d. Emission Index for engine SA001 using the continuous FID instrument. The grey data points and error bars are the full FID EI dataset collected during the project, which only includes CFM56-7B24 data at MDW 2009. The larger points, in blue are the results for engine 1.

Table A01-E2a. Selected test results for engine SA002 (MDW 2009). Aircraft test conducted from 3/3/09 04:00 to 3/3/09 05:00, ambient temperature 266.9±1K, relative humidity 71%.

Fuel Flow	2σ	N1	2σ	CO EI	2σ	FID EI	2σ
kg s^{-1}	kg s^{-1}	%	%	g kg^{-1}	g kg^{-1}	g kg^{-1}	g kg^{-1}
0.0828	0.0004	21.320	0.130	76.0	1	9.7	0.75
0.0910		21.200	0.000	71.25	0.4	9.0	0.29
0.0965	0.0007	23.000	2.970	63.1	4	7.5	0.67
0.1030		26.100	0.000	55.3	1.1	7.5	0.50
Engine SA_001							
Fuel Flow	2σ	C_2H_4 EI	2σ	HCHO EI	2σ	Benzene EI	2σ
kg s^{-1}	kg s^{-1}	g kg^{-1}	g kg^{-1}	g kg^{-1}	g kg^{-1}	g kg^{-1}	g kg^{-1}
0.0828	0.0004	2.616	0.07	2.21	0.05	0.242	0.007
0.0910		2.190	0.01	1.99	0.03	0.210	0.006
0.0965	0.0007	1.875	0.06	1.70	0.07	0.175	0.006
0.1030		1.570	0.02	1.44	0.05	0.160	0.008
Engine SA_001							
Fuel Flow	2σ	Toluene EI	2σ	C2-Benzene	2σ	Styrene	2σ
kg s-1	kg s-1	g kg-1	g kg-1	g kg-1	g kg-1	g kg-1	g kg-1
0.0828	0.0004	0.158	0.005	0.163	0.007	0.101	0.005
0.0910		0.132	0.002	0.136	0.002	0.088	0.001
0.0965	0.0007	0.112	0.002	0.119	0.010	0.086	0.009
0.1030		0.100	0.003	0.116	0.003	0.083	0.003

Table Notes. The 2σ value is computed as twice the standard error of the fit emission ratio converted to emission index. When multiple data points have been averaged at the noted fuel flow rate, these errors have been added in quadrature.

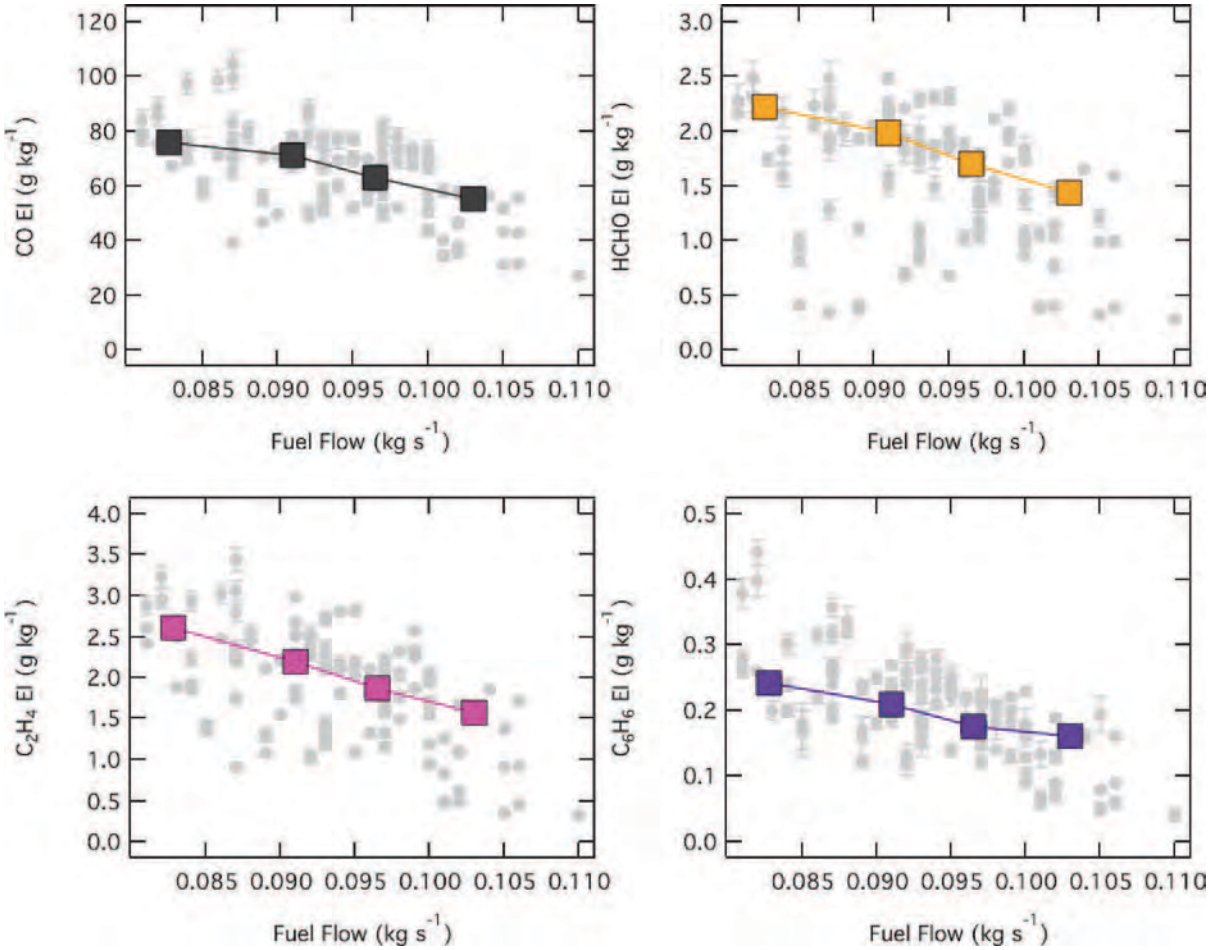

Figure A01-E2b. Emission Index for engine SA002 for CO, HCHO, C2H4, and C6H6. The four figures depict the emission indices in grey with the precision-based error bar from the entire CFM56-7B24 dataset. The colored data points are the emission index for the species in question averaged for the nominal engine state during the test of engine index SA-002. In many cases the precision based error bar for the emission index is smaller in magnitude than the size of the data point. See companion table for precision-based error bars. The absolute averaged emission indices for the fuel flow repeats during the test are depicted in the four panels; upper left CO in black; upper right HCHO in orange; lower left ethene (C2H4) in magenta; and lower right benzene (C6H6) in violet.

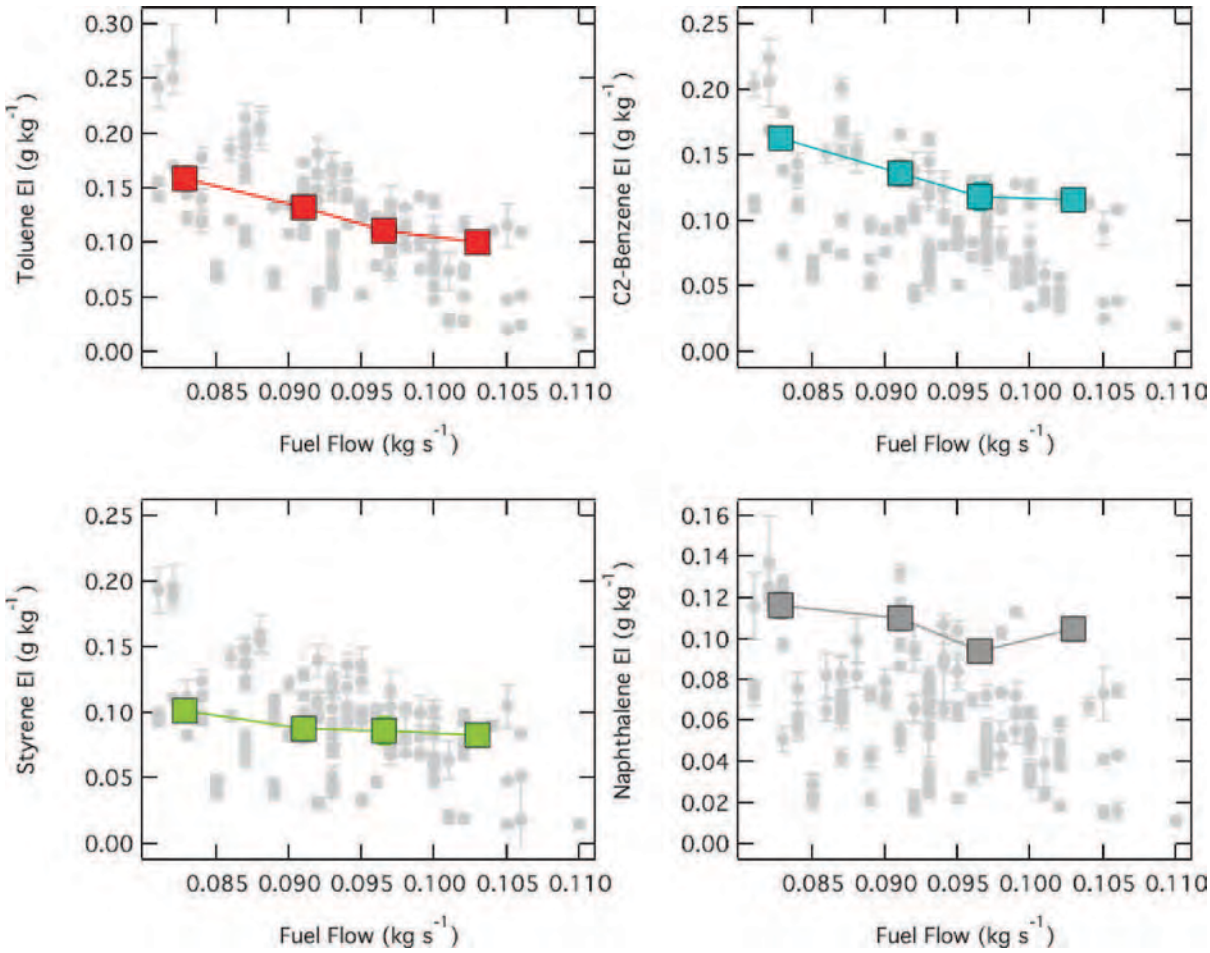

Figure A01-E2c. Emission Index for engine SA002 for Toluene, C2-Benzene, Styrene, and Naphthalene. C2-Benzene refers to the sum of the xylene isomers and ethyl-benzene. The four figures depict the emission indices in grey with the precision-based error bar from the entire CFM56-7B24 dataset. The colored data points are the emission index for the species in question averaged for the nominal engine state during the test of engine index SA002. In many cases the precision based error bar for the emission index is smaller in magnitude than the size of the data point. See companion table for precision-based error bars. The absolute averaged emission indices for the fuel flow repeats during the test are depicted in the four panels; upper left Toluene in red; upper right C2-Benzene in light-blue; lower left Styrene in light green; and lower right naphthalene in the larger grey squares.

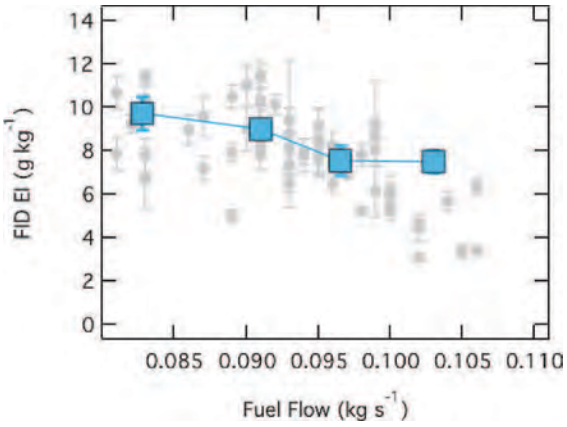

Figure A01-E2d. Emission Index for engine SA002 using the continuous FID instrument. The grey data points and error bars are the full FID EI dataset collected during the project, which only includes CFM56-7B24 data at MDW 2009. The larger points, in blue are the results for engine 2.

Table A01-E3a. Selected test results for engine SA003 (MDW 2009). Aircraft test conducted from 3/4/09 03:45 to 3/4/09 04:30, ambient temperature 270.8±1K, relative humidity 53%.

Fuel Flow	2σ	N1	2σ	CO EI	s	FID EI	2σ
kg s^{-1}	kg s^{-1}	%	%	g kg^{-1}	g kg^{-1}	g kg^{-1}	g kg^{-1}
0.0830		20.70		67.5	1.7	6.7	1.4
0.0895	0.0007	20.30	0.14	72.0	0.9	9.5	1.4
0.0953	0.0006	20.10		70.4	1.2	7.6	1.0
0.1020		25.20		38.2	0.4	3.2	0.2
Engine SA_001							
Fuel Flow	2σ	C_2H_4 EI	2σ	HCHO EI	2σ	Benzene EI	2σ
kg s^{-1}	kg s^{-1}	g kg^{-1}	g kg^{-1}	g kg^{-1}	g kg^{-1}	g kg^{-1}	g kg^{-1}
0.0830		1.880	0.020	1.74	0.06	0.200	0.014
0.0895	0.0007	2.155	0.046	1.99	0.06	0.240	0.011
0.0953	0.0006	2.147	0.031	1.93	0.05	0.230	0.015
0.1020		0.620	0.010	0.77	0.06	0.090	0.003
Engine SA_001							
Fuel Flow	2σ	Toluene EI	2σ	C2-Benzene	2σ	Styrene	2σ
kg s-1	kg s-1	g kg-1	g kg-1	g kg-1	g kg-1	g kg-1	g kg-1
0.0830		0.123	0.006	0.076	0.006	0.112	0.013
0.0895	0.0007	0.134	0.002	0.094	0.003	0.116	0.006
0.0953	0.0006	0.128	0.005	0.085	0.005	0.120	0.011
0.1020		0.051	0.001	0.039	0.001	0.093	0.003

Table Notes. The 2σ value is computed as twice the standard error of the fit emission ratio converted to emission index. When multiple data points have been averaged at the noted fuel flow rate, these errors have been added in quadrature.

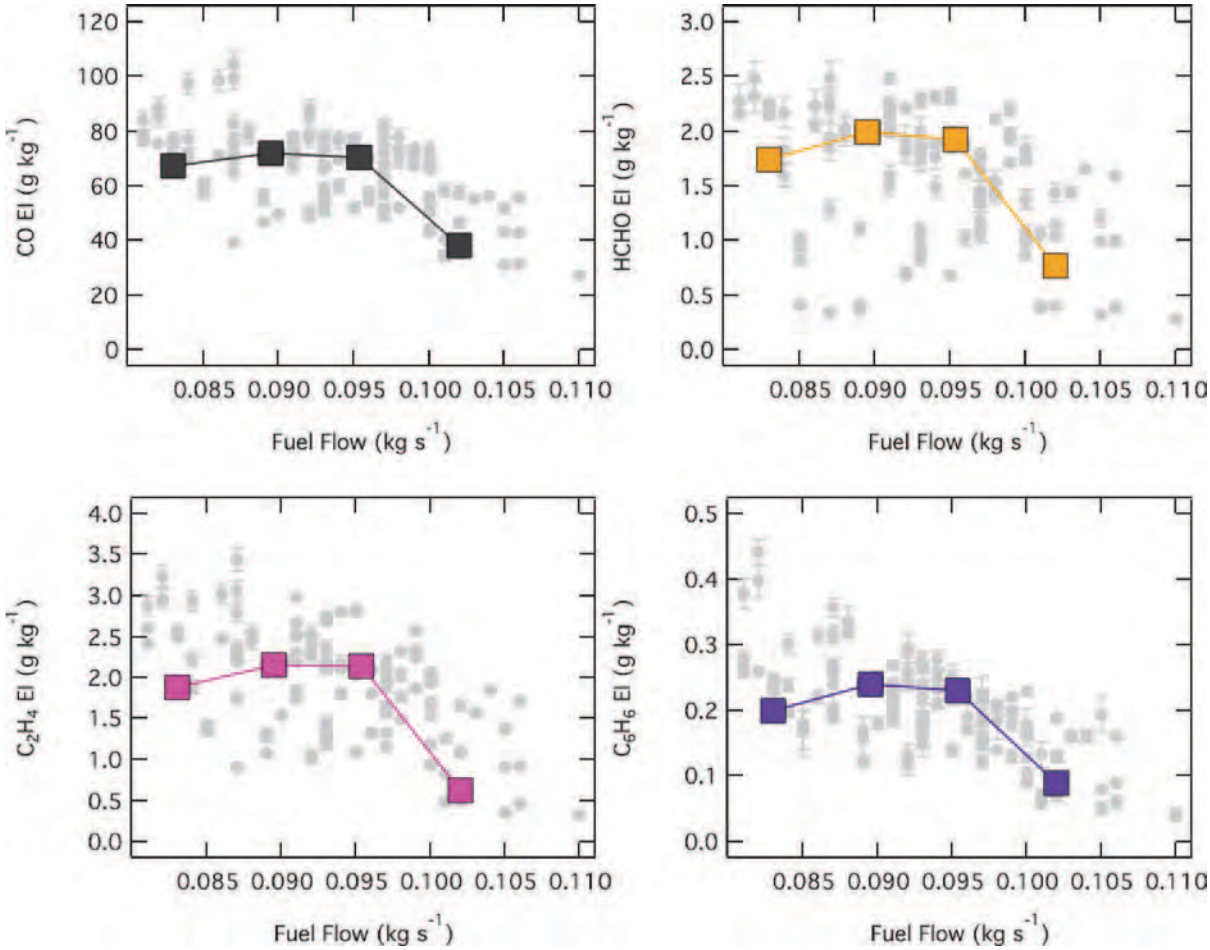

Figure A01-E3b. Emission Index for engine SA003 for CO, HCHO, C2H4, and C6H6. The four figures depict the emission indices in grey with the precision-based error bar from the entire CFM56-7B24 dataset. The colored data points are the emission index for the species in question averaged for the nominal engine state during the test of engine index SA003. In many cases the precision based error bar for the emission index is smaller in magnitude than the size of the data point. See companion table for precision-based error bars. The absolute averaged emission indices for the fuel flow repeats during the test are depicted in the four panels; upper left CO in black; upper right HCHO in orange; lower left ethene (C2H4) in magenta; and lower right benzene (C6H6) in violet.

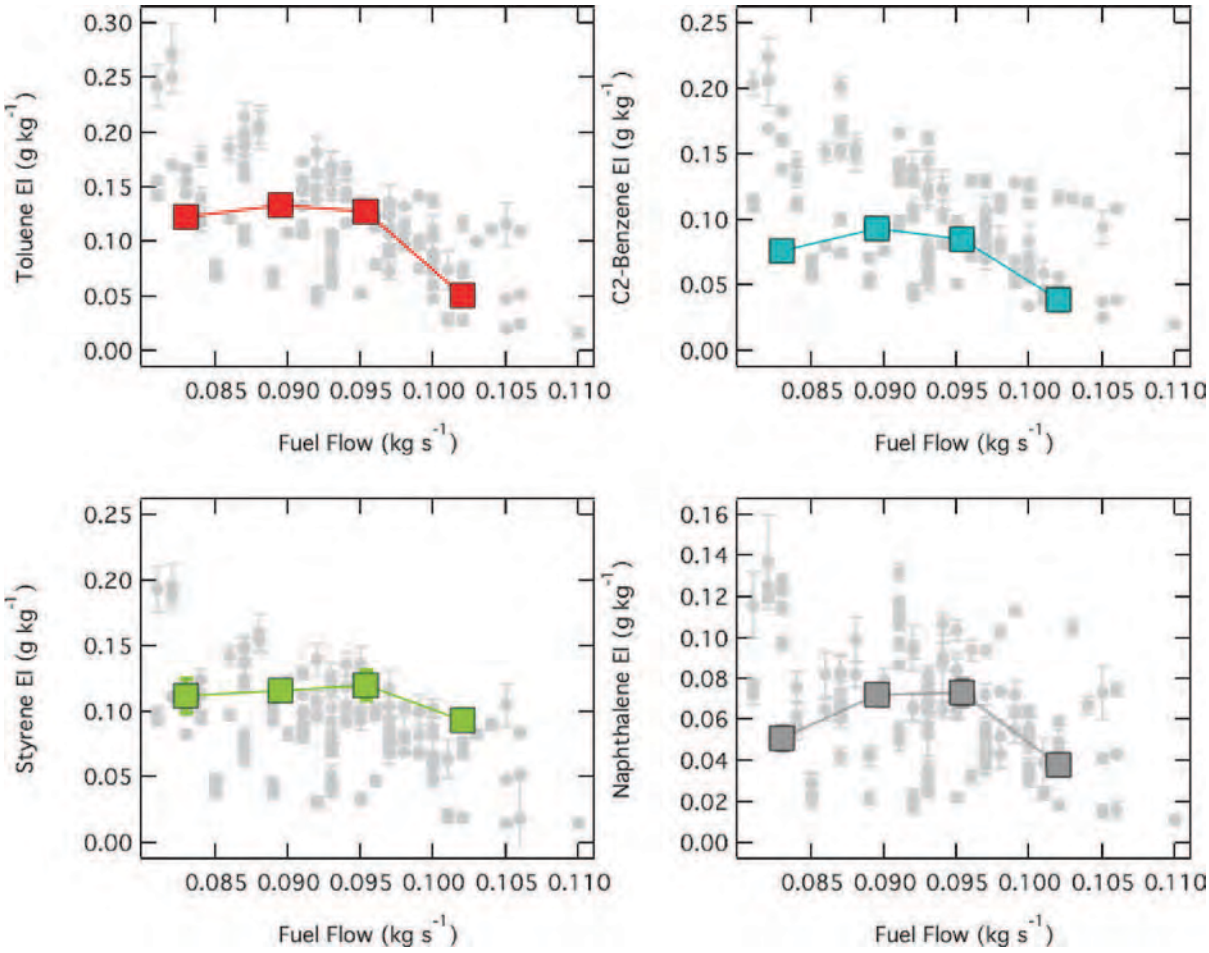

Figure A01-E3c. Emission Index for engine SA003 for Toluene, C2-Benzene, Styrene, and Naphthalene. C2-Benzene refers to the sum of the xylene isomers and ethyl-benzene. The four figures depict the emission indices in grey with the precision-based error bar from the entire CFM56-7B24 dataset. The colored data points are the emission index for the species in question averaged for the nominal engine state during the test of engine index SA003. In many cases the precision based error bar for the emission index is smaller in magnitude than the size of the data point. See companion table for precision-based error bars. The absolute averaged emission indices for the fuel flow repeats during the test are depicted in the four panels; upper left Toluene in red; upper right C2-Benzene in light-blue; lower left Styrene in light green; and lower right naphthalene in the larger grey squares.

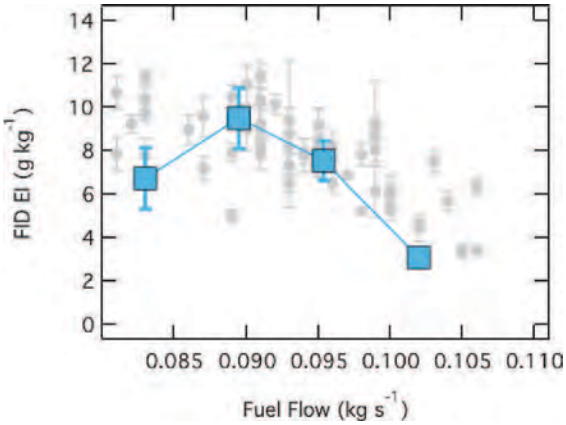

Figure A01-E3d. Emission Index for engine SA003 using the continuous FID instrument. The grey data points and error bars are the full FID EI dataset collected during the project, which only includes CFM56-7B24 data at MDW 2009. The larger points, in blue are the results for engine 3.

Table A01-E4a. Selected test results for engine SA004 (MDW 2009). Aircraft test conducted from 3/4/09 03:45 to 3/4/09 04:30, ambient temperature 270.8±1K, relative humidity 53%.

Fuel Flow	2σ	N1	2σ	CO EI	2σ	FID EI	2σ
kg s^{-1}	kg s^{-1}	%	%	g kg^{-1}	g kg^{-1}	g kg^{-1}	g kg^{-1}
0.0810	0.0000	20.75	0.07	77.625	1.277	9.260	1.314
0.0920	0.0000	21.20	0.00	78.260	1.070	10.150	0.450
0.0945	0.0007	20.40	0.14	69.400	0.677	7.765	0.713
0.1020	0.0000	25.30	0.00	46.710	0.760	4.470	0.620
Engine SA_001							
Fuel Flow	2σ	C_2H_4 EI	2σ	HCHO EI	2σ	Benzene EI	2σ
kg s^{-1}	kg s^{-1}	g kg^{-1}	g kg^{-1}	g kg^{-1}	g kg^{-1}	g kg^{-1}	g kg^{-1}
0.0810	0	2.510	0.083	2.215	0.049	0.270	0.012
0.0920	0	2.520	0.020	2.210	0.030	0.290	0.009
0.0945	0.0007	2.070	0.026	1.865	0.027	0.220	0.011
0.1020	0	1.100	0.010	1.150	0.010	0.130	0.009
Engine SA_001							
Fuel Flow	2σ	Toluene EI	2σ	C2-Benzene	2σ	Styrene	2σ
kg s-1	kg s-1	g kg-1	g kg-1	g kg-1	g kg-1	g kg-1	g kg-1
0.0810	0.0000	0.149	0.007	0.113	0.004	0.096	0.005
0.0920	0.0000	0.163	0.004	0.130	0.003	0.096	0.003
0.0945	0.0007	0.120	0.003	0.083	0.003	0.097	0.005
0.1020	0.0000	0.070	0.003	0.047	0.003	0.068	0.005

Table Notes. The 2σ value is computed as twice the standard error of the fit emission ratio converted to emission index. When multiple data points have been averaged at the noted fuel flow rate, these errors have been added in quadrature.

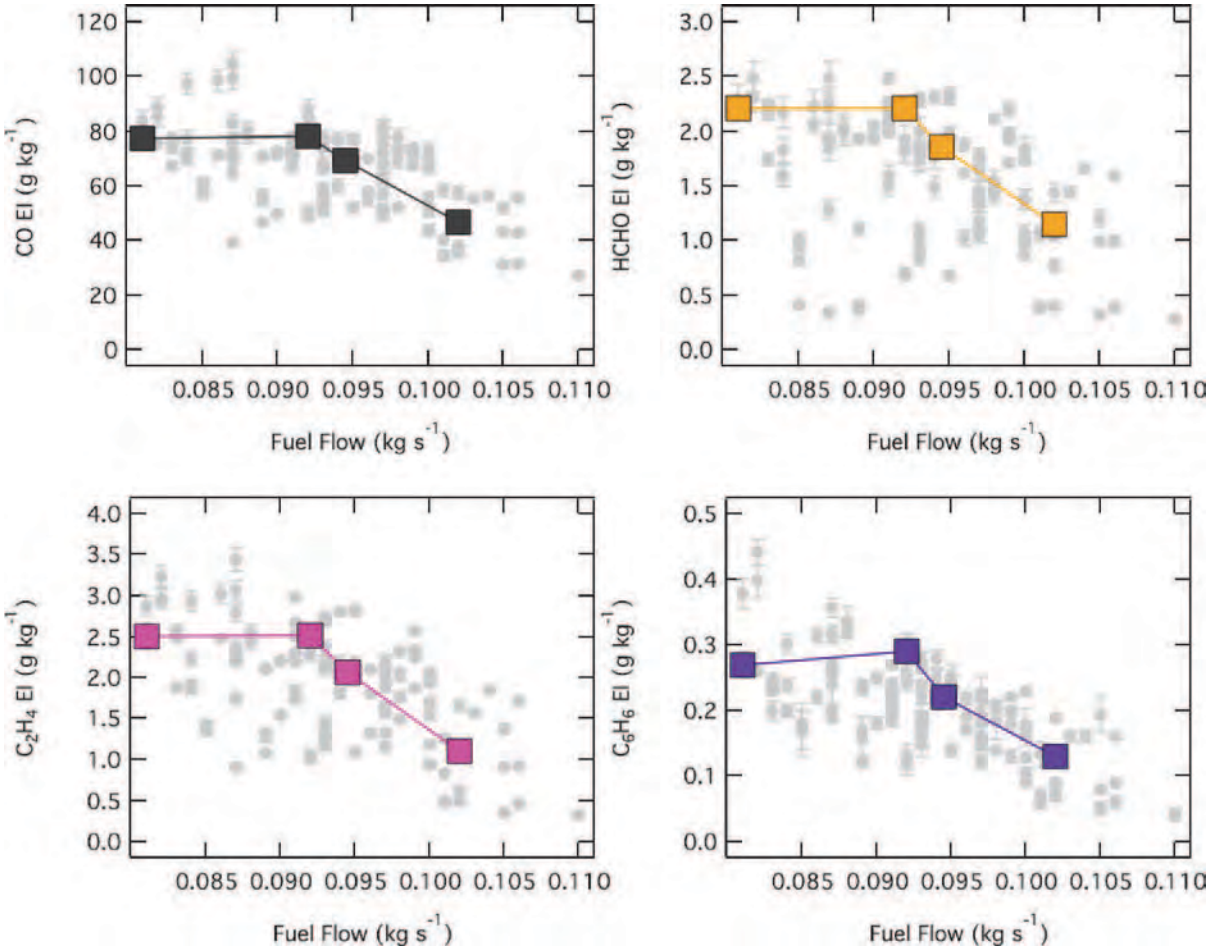

Figure A01-E4b. Emission Index for engine SA004 for CO, HCHO, C2H4, and C6H6. The four figures depict the emission indices in grey with the precision-based error bar from the entire CFM56-7B24 dataset. The colored data points are the emission index for the species in question averaged for the nominal engine state during the test of engine index SA004. In many cases the precision based error bar for the emission index is smaller in magnitude than the size of the data point. See companion table for precision-based error bars. The absolute averaged emission indices for the fuel flow repeats during the test are depicted in the four panels; upper left CO in black; upper right HCHO in orange; lower left ethene (C2H4) in magenta; and lower right benzene (C6H6) in violet.

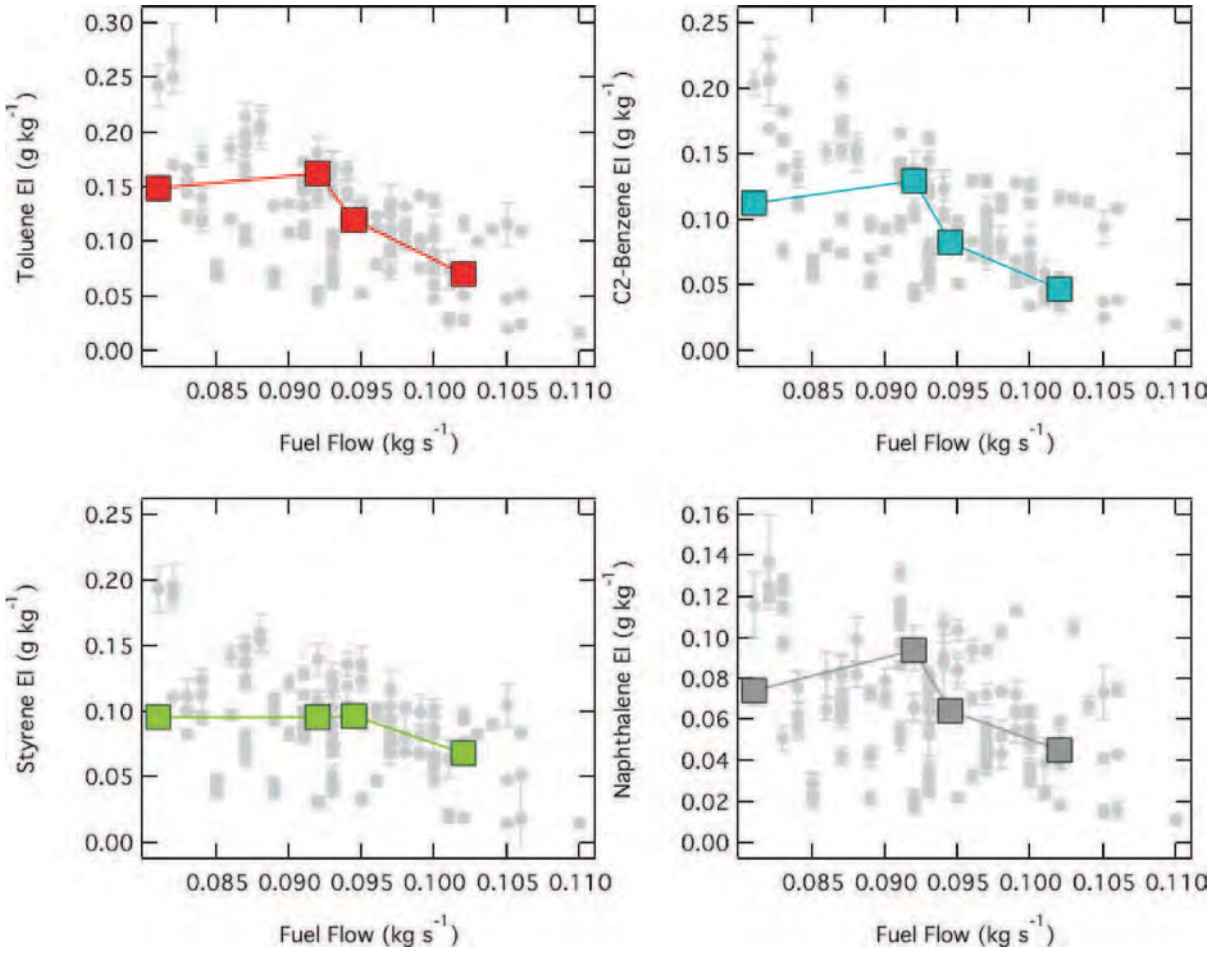

Figure A01-E4c. Emission Index for engine SA004 for Toluene, C2-Benzene, Styrene, and Naphthalene. C2-Benzene refers to the sum of the xylene isomers and ethyl-benzene. The four figures depict the emission indices in grey with the precision-based error bar from the entire CFM56-7B24 dataset. The colored data points are the emission index for the species in question averaged for the nominal engine state during the test of engine index SA004. In many cases the precision based error bar for the emission index is smaller in magnitude than the size of the data point. See companion table for precision-based error bars. The absolute averaged emission indices for the fuel flow repeats during the test are depicted in the four panels; upper left Toluene in red; upper right C2-Benzene in light-blue; lower left Styrene in light green; and lower right naphthalene in the larger grey squares.

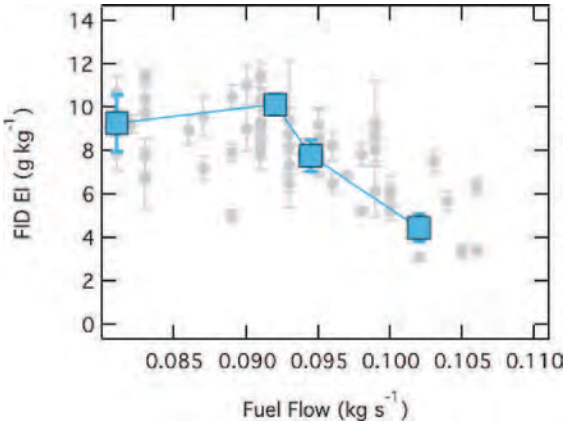

Figure A01-E4d. Emission Index for engine SA004 using the continuous FID instrument. The grey data points and error bars are the full FID EI dataset collected during the project, which only includes CFM56-7B24 data at MDW 2009. The larger points, in blue are the results for engine 4.

Table A01-E7a. Selected test results for engine SA007 (MDW 2009). Aircraft test conducted from 3/4/09 04:50 to 3/4/09 05:30, ambient temperature 270.8±1K, relative humidity 56%.

Fuel Flow	2σ	N1	2σ	CO EI	s	FID EI	2σ
kg s^{-1}	kg s^{-1}	%	%	g kg^{-1}	g kg^{-1}	g kg^{-1}	g kg^{-1}
0.0860		20.90	0.00	71.490	1.540	8.950	0.690
0.0938	0.001	20.32	0.15	75.320	2.087	8.283	1.397
0.0990		20.10	0.00	71.145	0.828	8.655	1.240
0.1060		25.30	0.00	42.860	0.690	3.410	0.090
Engine SA_001							
Fuel Flow	2σ	C_2H_4 EI	2σ	HCHO EI	2σ	Benzene EI	2σ
kg s^{-1}	kg s^{-1}	g kg^{-1}	g kg^{-1}	g kg^{-1}	g kg^{-1}	g kg^{-1}	g kg^{-1}
0.0860		2.480	0.010	2.060	0.060	0.220	0.009
0.0938	0.001	2.668	0.101	2.232	0.087	0.218	0.019
0.0990		2.295	0.039	1.970	0.049	0.190	0.011
0.1060		0.920	0.000	0.990	0.050	0.090	0.002
Engine SA_001							
Fuel Flow	2σ	Toluene EI	2σ	C2-Benzene	2σ	Styrene	2σ
kg s-1	kg s-1	g kg-1	g kg-1	g kg-1	g kg-1	g kg-1	g kg-1
0.0860		0.121	0.003	0.080	0.004	0.097	0.004
0.0938	0.001	0.120	0.008	0.082	0.009	0.090	0.009
0.0990		0.099	0.004	0.064	0.005	0.084	0.015
0.1060		0.052	0.001	0.039	0.001	0.052	0.001

Table Notes. The 2σ value is computed as twice the standard error of the fit emission ratio converted to emission index. When multiple data points have been averaged at the noted fuel flow rate, these errors have been added in quadrature.

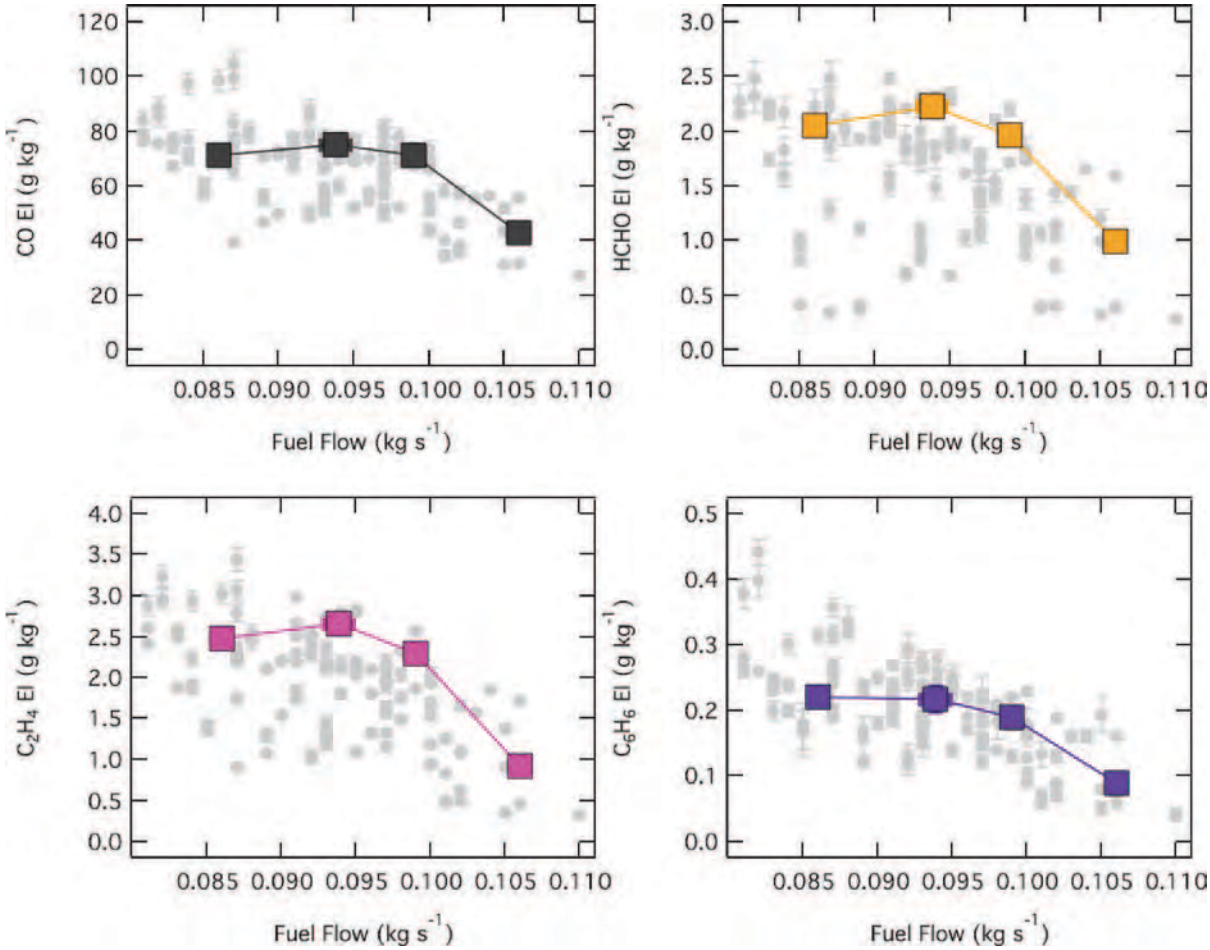

Figure A01-E7b. Emission Index for engine SA007 for CO, HCHO, C2H4, and C6H6. The four figures depict the emission indices in grey with the precision-based error bar from the entire CFM56-7B24 dataset. The colored data points are the emission index for the species in question averaged for the nominal engine state during the test of engine index SA007. In many cases the precision based error bar for the emission index is smaller in magnitude than the size of the data point. See companion table for precision-based error bars. The absolute averaged emission indices for the fuel flow repeats during the test are depicted in the four panels; upper left CO in black; upper right HCHO in orange; lower left ethene (C2H4) in magenta; and lower right benzene (C6H6) in violet.

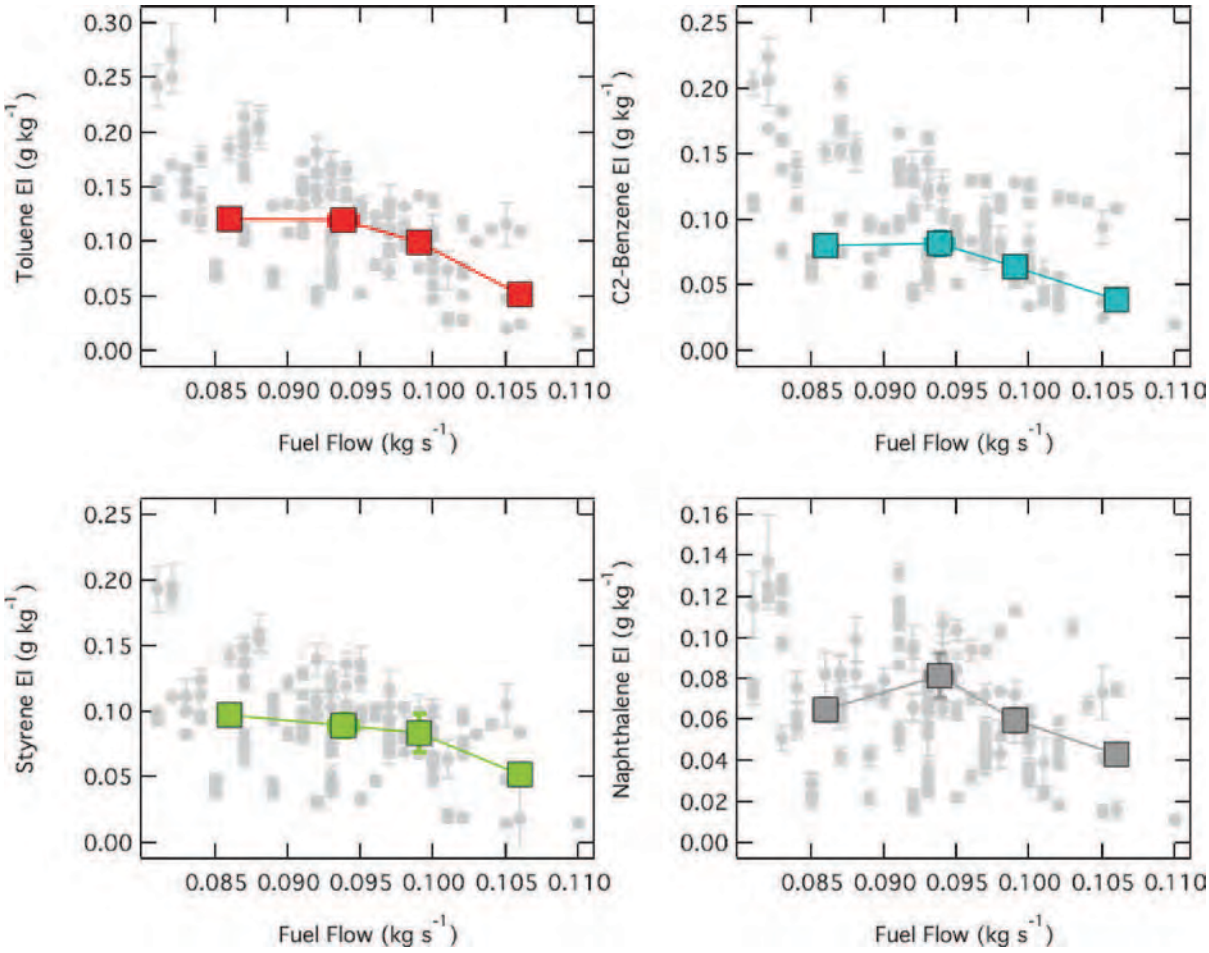

Figure A01-E7c. Emission Index for engine SA007 for Toluene, C2-Benzene, Styrene, and Naphthalene. C2-Benzene refers to the sum of the xylene isomers and ethyl-benzene. The four figures depict the emission indices in grey with the precision-based error bar from the entire CFM56-7B24 dataset. The colored data points are the emission index for the species in question averaged for the nominal engine state during the test of engine index SA007. In many cases the precision based error bar for the emission index is smaller in magnitude than the size of the data point. See companion table for precision-based error bars. The absolute averaged emission indices for the fuel flow repeats during the test are depicted in the four panels; upper left Toluene in red; upper right C2-Benzene in light-blue; lower left Styrene in light green; and lower right naphthalene in the larger grey squares.

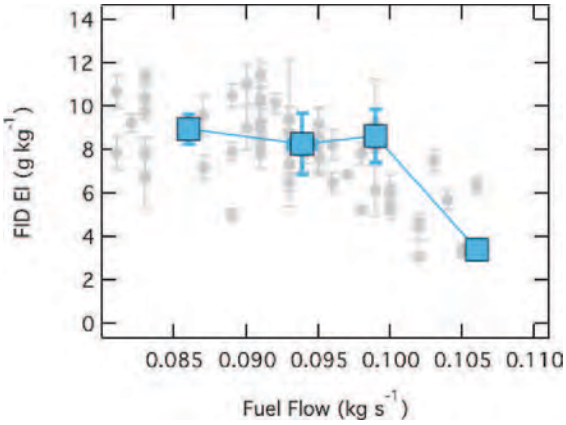

Figure A01-E7d. Emission Index for engine SA007 using the continuous FID instrument. The grey data points and error bars are the full FID EI dataset collected during the project, which only includes CFM56-7B24 data at MDW 2009. The larger points, in blue are the results for engine 7.

Table A01-E8a. Selected test results for engine SA008 (MDW 2009). Aircraft test conducted from 3/4/09 04:50 to 3/4/09 05:30, ambient temperature 270.8±1K, relative humidity 56%.

Fuel Flow	2σ	N1	2σ	CO EI	s	FID EI	2σ
kg s^{-1}	kg s^{-1}	%	%	g kg^{-1}	g kg^{-1}	g kg^{-1}	g kg^{-1}
0.0870		20.85	0.07	70.745	0.615	8.370	1.159
0.0900		20.80	0.00	71.310	0.490	8.990	1.000
0.0930		20.80	0.14	67.905	0.653	7.940	1.253
0.0997	0.0006	20.23	0.06	67.400	1.281	6.077	0.722
0.1050		25.20	0.00	43.340	0.580	3.360	0.310
Engine SA_001							
Fuel Flow	2σ	C_2H_4 EI	2σ	HCHO EI	2σ	Benzene EI	2σ
kg s^{-1}	kg s^{-1}	g kg^{-1}	g kg^{-1}	g kg^{-1}	g kg^{-1}	g kg^{-1}	g kg^{-1}
0.0870		2.230	0.028	1.935	0.025	0.195	0.008
0.0900		2.220	0.010	1.940	0.060	0.180	0.010
0.0930		2.140	0.026	1.850	0.033	0.185	0.007
0.0997	0.0006	1.947	0.045	1.750	0.050	0.153	0.014
0.1050		0.910	0.010	0.990	0.020	0.080	0.003
Engine SA_001							
Fuel Flow	2σ	Toluene EI	2σ	C2-Benzene	2σ	Styrene	2σ
kg s-1	kg s-1	g kg-1	g kg-1	g kg-1	g kg-1	g kg-1	g kg-1
0.0870		0.106	0.005	0.075	0.002	0.078	0.005
0.0900		0.108	0.004	0.076	0.003	0.083	0.005
0.0930		0.100	0.003	0.071	0.002	0.072	0.003
0.0997	0.0006	0.082	0.005	0.057	0.004	0.068	0.008
0.1050		0.048	0.001	0.037	0.001	0.048	0.002

Table Notes. The 2σ value is computed as twice the standard error of the fit emission ratio converted to emission index. When multiple data points have been averaged at the noted fuel flow rate, these errors have been added in quadrature.

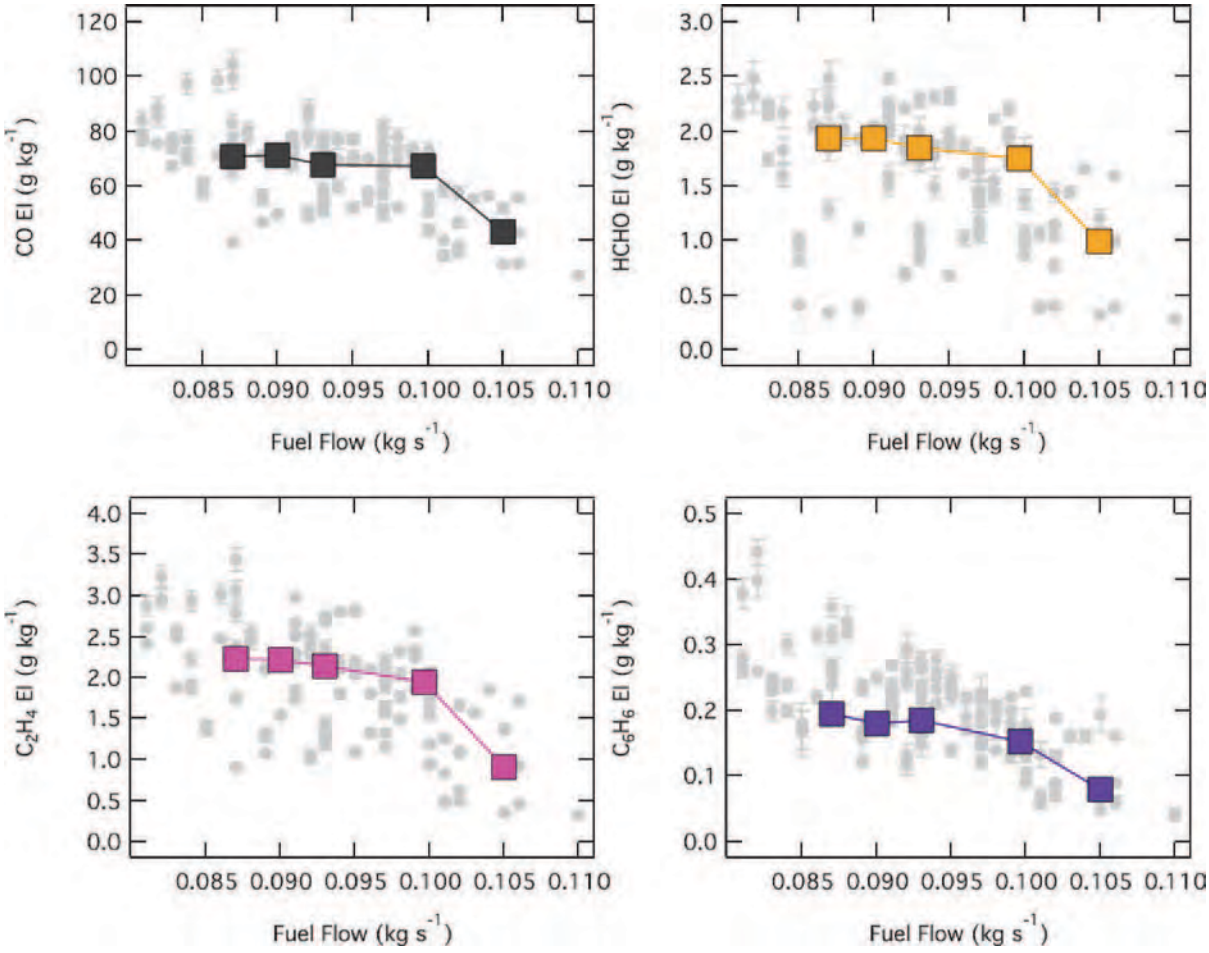

Figure A01-E8b. Emission Index for engine SA008 for CO, HCHO, C2H4, and C6H6. The four figures depict the emission indices in grey with the precision-based error bar from the entire CFM56-7B24 dataset. The colored data points are the emission index for the species in question averaged for the nominal engine state during the test of engine index SA008. In many cases the precision based error bar for the emission index is smaller in magnitude than the size of the data point. See companion table for precision-based error bars. The absolute averaged emission indices for the fuel flow repeats during the test are depicted in the four panels; upper left CO in black; upper right HCHO in orange; lower left ethene (C2H4) in magenta; and lower right benzene (C6H6) in violet.

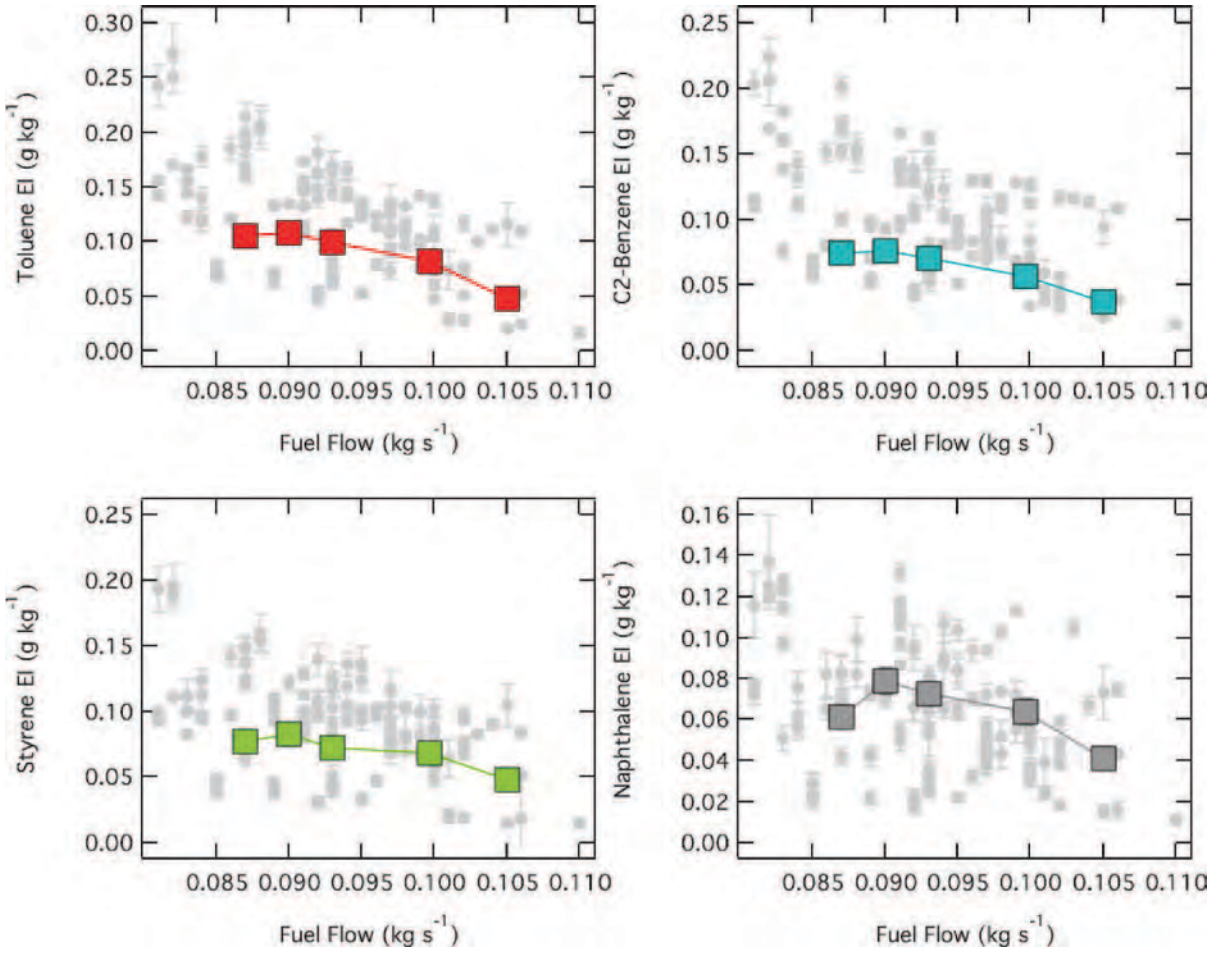

Figure A01-E8c. Emission Index for engine SA008 for Toluene, C2-Benzene, Styrene, and Naphthalene. C2-Benzene refers to the sum of the xylene isomers and ethyl-benzene. The four figures depict the emission indices in grey with the precision-based error bar from the entire CFM56-7B24 dataset. The colored data points are the emission index for the species in question averaged for the nominal engine state during the test of engine index SA008. In many cases the precision based error bar for the emission index is smaller in magnitude than the size of the data point. See companion table for precision-based error bars. The absolute averaged emission indices for the fuel flow repeats during the test are depicted in the four panels; upper left Toluene in red; upper right C2-Benzene in light-blue; lower left Styrene in light green; and lower right naphthalene in the larger grey squares.

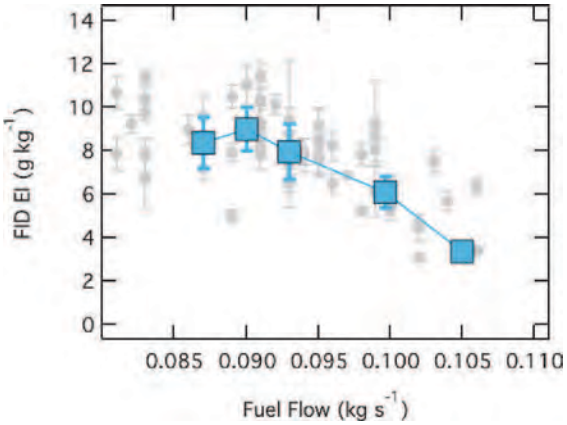

Figure A01-E8d. Emission Index for engine SA008 using the continuous FID instrument. The grey data points and error bars are the full FID EI dataset collected during the project, which only includes CFM56-7B24 data at MDW 2009. The larger points, in blue are the results for engine 8.

Table A01-E9a. Selected test results for engine SA009 (DAL 2009). Aircraft test conducted from 10/15/09 02:30 to 10/15/09 03:30, ambient temperature 297.5±1K, relative humidity 94%.

Fuel Flow	2σ	N1	2σ	CO EI	2σ		
kg s^{-1}	kg s^{-1}	%	%	g kg^{-1}	g kg^{-1}		
0.0854	0.0009	21.14	0.11	60.594	2.514		
0.0927	0.0005	22.07	1.50	53.100	2.397		
0.0955	0.0007	21.15	0.21	53.575	2.127		
0.1013	0.0006	22.20	0.95	34.903	1.240		
0.1050	0.0000	24.00	0.00	31.120	1.240		
0.1100	0.0000	25.60	0.00	27.430	1.100		
Engine SA_009							
Fuel Flow	2σ	C_2H_4 EI	2σ	HCHO EI	2σ	Benzene EI	2σ
kg s^{-1}	kg s^{-1}	g kg^{-1}	g kg^{-1}	g kg^{-1}	g kg^{-1}	g kg^{-1}	g kg^{-1}
0.0854	0.0009	1.456	0.087	0.896	0.142	0.186	0.032
0.0927	0.0005	1.212	0.077	0.880	0.085	0.155	0.022
0.0955	0.0007	1.210	0.105	0.850	0.146	0.165	0.024
0.1013	0.0006	0.490	0.018	0.393	0.024	0.067	0.009
0.1050	0	0.350	0.010	0.320	0.020	0.050	0.010
0.1100	0	0.320	0.010	0.280	0.020	0.040	0.010
Engine SA_009							
Fuel Flow	2σ	Toluene EI	2σ	C2- Benzene	2σ	Styrene	2σ
kg s-1	kg s-1	g kg-1	g kg-1	g kg-1	g kg-1	g kg-1	g kg-1
0.0854	0.0009	0.080	0.009	0.071	0.008	0.048	0.006
0.0927	0.0005	0.056	0.009	0.060	0.007	0.036	0.006
0.0955	0.0007	0.066	0.011	0.062	0.009	0.040	0.007
0.1013	0.0006	0.028	0.004	0.039	0.005	0.020	0.003
0.1050	0.0000	0.020	0.003	0.025	0.002	0.015	0.002
0.1100	0.0000	0.017	0.004	0.020	0.002	0.015	0.003

Table Notes. The 2σ value is computed as twice the standard error of the fit emission ratio converted to emission index. When multiple data points have been averaged at the noted fuel flow rate, these errors have been added in quadrature.

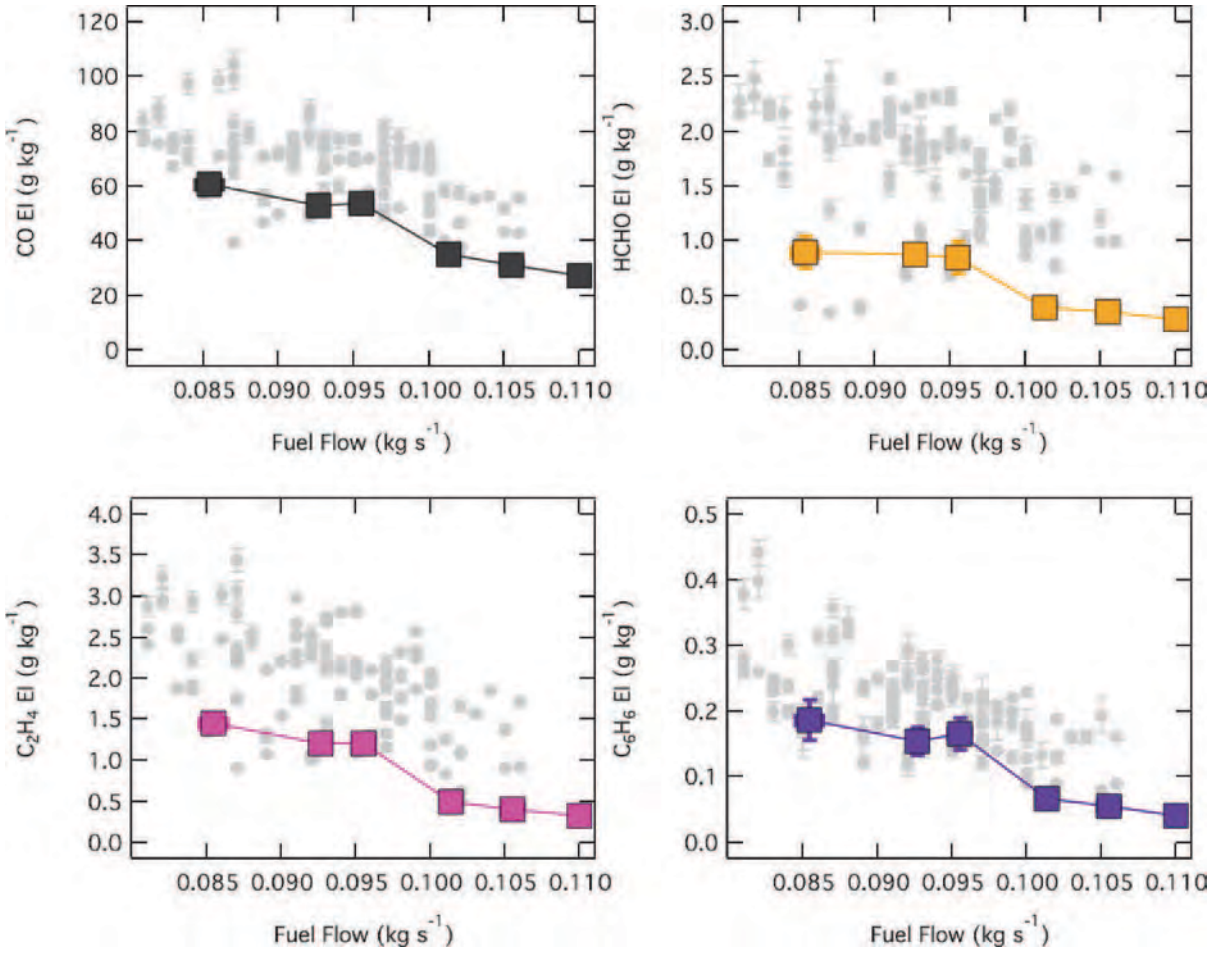

Figure A01-E9b. Emission Index for engine SA009 for CO, HCHO, C_2H_4, and C_6H_6. The four figures depict the emission indices in grey with the precision-based error bar from the entire CFM56-7B24 dataset. The colored data points are the emission index for the species in question averaged for the nominal engine state during the test of engine index SA009. In many cases the precision based error bar for the emission index is smaller in magnitude than the size of the data point. See companion table for precision-based error bars. The absolute averaged emission indices for the fuel flow repeats during the test are depicted in the four panels; upper left CO in black; upper right HCHO in orange; lower left ethene (C_2H_4) in magenta; and lower right benzene (C_6H_6) in violet.

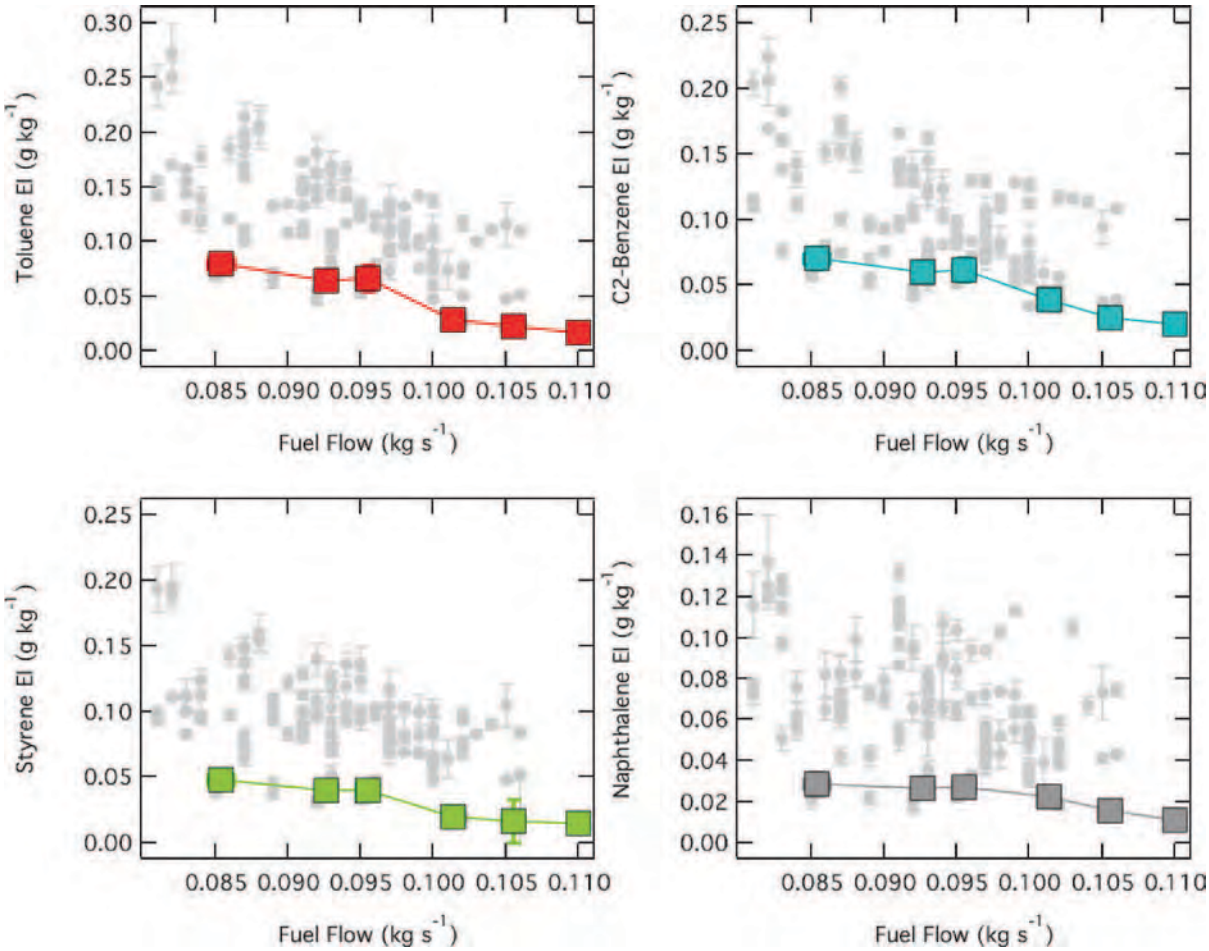

Figure A01-E9c. Emission Index for engine SA009 for Toluene, C2-Benzene, Styrene, and Naphthalene. C2-Benzene refers to the sum of the xylene isomers and ethyl-benzene. The four figures depict the emission indices in grey with the precision-based error bar from the entire CFM56-7B24 dataset. The colored data points are the emission index for the species in question averaged for the nominal engine state during the test of engine index SA009. In many cases the precision based error bar for the emission index is smaller in magnitude than the size of the data point. See companion table for precision-based error bars. The absolute averaged emission indices for the fuel flow repeats during the test are depicted in the four panels; upper left Toluene in red; upper right C2-Benzene in light-blue; lower left Styrene in light green; and lower right naphthalene in the larger grey squares.

Table A01-E10a. Selected test results for engine SA010 (MDW 2010). Aircraft test conducted from 2/15/10 04:50 to 2/15/10 05:30, ambient temperature 267.4±1K, relative humidity 78%.

Fuel Flow	2σ	N1	2σ	CO EI	2σ		
kg s^{-1}	kg s^{-1}	%	%	g kg^{-1}	g kg^{-1}		
0.0870	0.0000	21.37	0.40	78.183	3.468		
0.0930	0.0000	20.85	0.07	75.890	2.832		
0.0970	0.0000	22.95	2.62	61.680	8.640		
0.1007	0.0012	23.67	2.31	62.287	5.225		
Engine SA_001							
Fuel Flow	2σ	C_2H_4 EI	2σ	HCHO EI	2σ	Benzene EI	2σ
kg s^{-1}	kg s^{-1}	g kg^{-1}	g kg^{-1}	g kg^{-1}	g kg^{-1}	g kg^{-1}	g kg^{-1}
0.0870	0	2.487	0.157	2.007	0.150	0.280	0.018
0.0930	0	2.270	0.104	1.915	0.128	0.251	0.012
0.0970	0	1.690	0.299	1.460	0.242	0.184	0.032
0.1007	0.001154699	1.750	0.147	1.547	0.151	0.197	0.016
Engine SA_001							
Fuel Flow	2σ	Toluene EI	2σ	C2- Benzene	2σ	Styrene	2σ
kg s-1	kg s-1	g kg-1	g kg-1	g kg-1	g kg-1	g kg-1	g kg-1
0.0870	0.0000	0.175	0.012	0.182	0.010	0.132	0.010
0.0930	0.0000	0.155	0.010	0.154	0.009	0.113	0.010
0.0970	0.0000	0.113	0.018	0.114	0.014	0.088	0.014
0.1007	0.0012	0.121	0.010	0.119	0.005	0.096	0.007

Table Notes. The 2σ value is computed as twice the standard error of the fit emission ratio converted to emission index. When multiple data points have been averaged at the noted fuel flow rate, these errors have been added in quadrature.

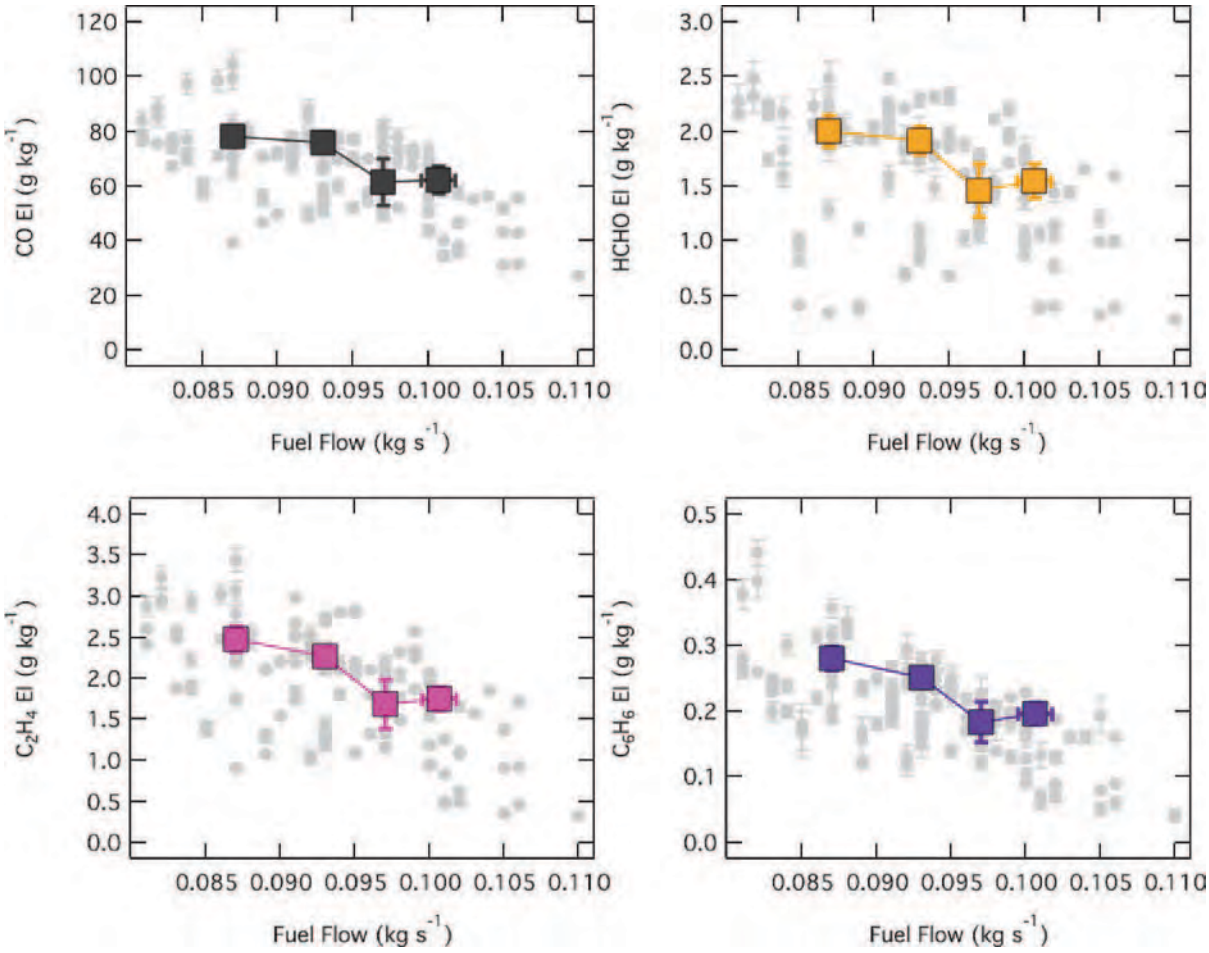

Figure A01-E10b. Emission Index for engine SA010 for CO, HCHO, C2H4, and C6H6. The four figures depict the emission indices in grey with the precision-based error bar from the entire CFM56-7B24 dataset. The colored data points are the emission index for the species in question averaged for the nominal engine state during the test of engine index SA010. In many cases the precision based error bar for the emission index is smaller in magnitude than the size of the data point. See companion table for precision-based error bars. The absolute averaged emission indices for the fuel flow repeats during the test are depicted in the four panels; upper left CO in black; upper right HCHO in orange; lower left ethene (C2H4) in magenta; and lower right benzene (C6H6) in violet.

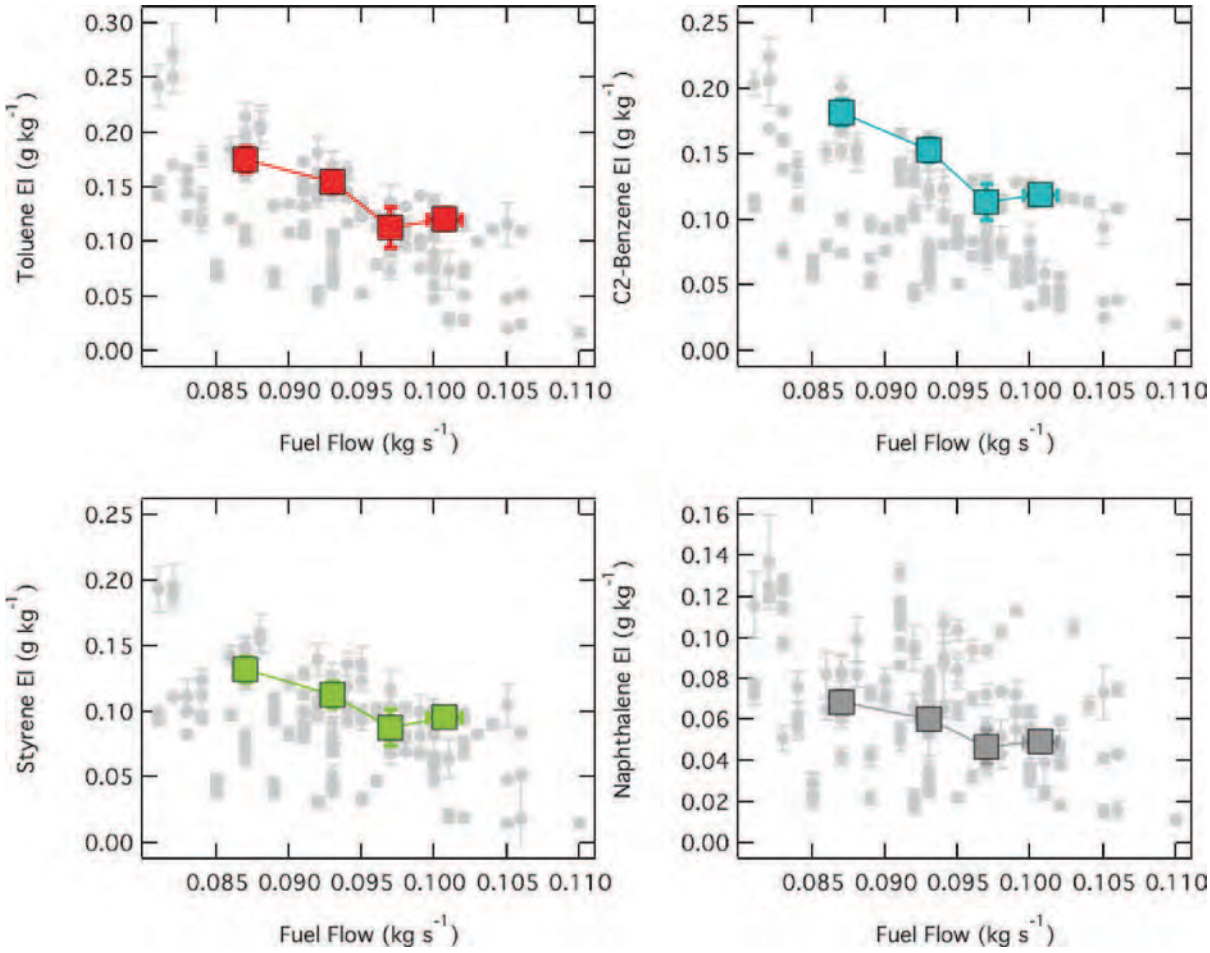

Figure A01-E10c. Emission Index for engine SA010 for Toluene, C2-Benzene, Styrene, and Naphthalene. C2-Benzene refers to the sum of the xylene isomers and ethyl-benzene. The four figures depict the emission indices in grey with the precision-based error bar from the entire CFM56-7B24 dataset. The colored data points are the emission index for the species in question averaged for the nominal engine state during the test of engine index SA010. In many cases the precision based error bar for the emission index is smaller in magnitude than the size of the data point. See companion table for precision-based error bars. The absolute averaged emission indices for the fuel flow repeats during the test are depicted in the four panels; upper left Toluene in red; upper right C2-Benzene in light-blue; lower left Styrene in light green; and lower right naphthalene in the larger grey squares.

Table A01-E11a. Selected test results for engine SA011 (MDW 2010). Aircraft test conducted from 2/15/10 07:00 to 2/15/10 07:40, ambient temperature 266.4±1K, relative humidity 77%.

Fuel Flow	2σ	N1	2σ	CO EI	2σ		
kg s^{-1}	kg s^{-1}	%	%	g kg^{-1}	g kg^{-1}		
0.0840	0.0000	21.10	0.26	72.837	3.116		
0.0910	0.0000	20.95	0.07	68.780	2.389		
0.0970	0.0000	20.70	0.00	63.460	2.102		
0.0990	0.0017	25.13	0.40	48.070	2.416		
Engine SA_001							
Fuel Flow	2σ	C_2H_4 EI	2σ	HCHO EI	2σ	Benzene EI	2σ
kg s^{-1}	kg s^{-1}	g kg^{-1}	g kg^{-1}	g kg^{-1}	g kg^{-1}	g kg^{-1}	g kg^{-1}
0.0840	0	2.000	0.123	1.677	0.116	0.212	0.013
0.0910	0	1.800	0.070	1.555	0.090	0.190	0.008
0.0970	0	1.595	0.053	1.370	0.075	0.159	0.005
0.0990	0.00173205	1.090	0.077	1.000	0.078	0.118	0.009
Engine SA_001							
Fuel Flow	2σ	Toluene EI	2σ	C2-Benzene	2σ	Styrene	2σ
kg s-1	kg s-1	g kg-1	g kg-1	g kg-1	g kg-1	g kg-1	g kg-1
0.0840	0.0000	0.126	0.009	0.119	0.007	0.101	0.008
0.0910	0.0000	0.111	0.005	0.097	0.004	0.087	0.006
0.0970	0.0000	0.092	0.004	0.074	0.003	0.074	0.005
0.0990	0.0017	0.069	0.007	0.065	0.007	0.060	0.007

Table Notes. The 2σ value is computed as twice the standard error of the fit emission ratio converted to emission index. When multiple data points have been averaged at the noted fuel flow rate, these errors have been added in quadrature.

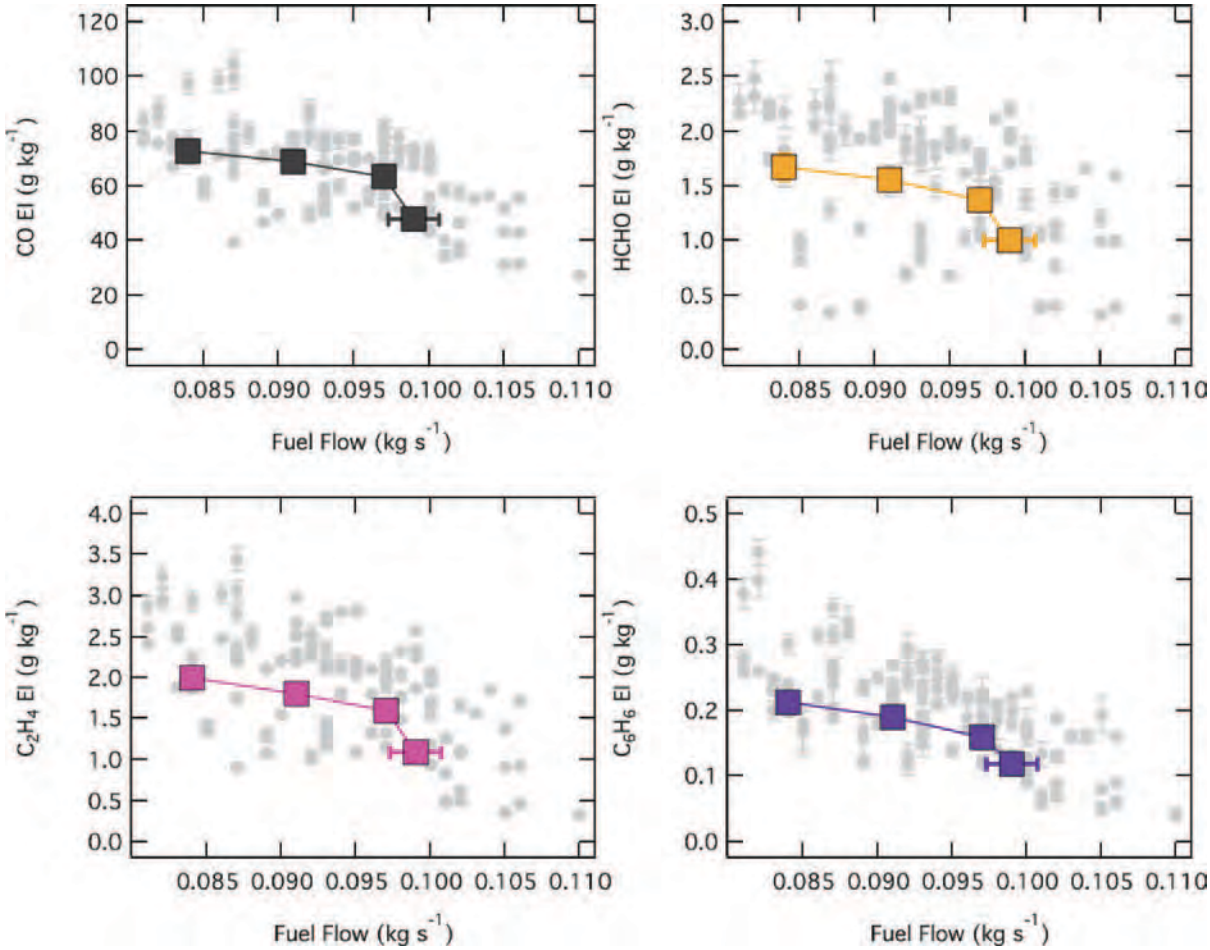

Figure A01-E11b. Emission Index for engine SA011 for CO, HCHO, C2H4, and C6H6. The four figures depict the emission indices in grey with the precision-based error bar from the entire CFM56-7B24 dataset. The colored data points are the emission index for the species in question averaged for the nominal engine state during the test of engine index SA011. In many cases the precision based error bar for the emission index is smaller in magnitude than the size of the data point. See companion table for precision-based error bars. The absolute averaged emission indices for the fuel flow repeats during the test are depicted in the four panels; upper left CO in black; upper right HCHO in orange; lower left ethene (C2H4) in magenta; and lower right benzene (C6H6) in violet.

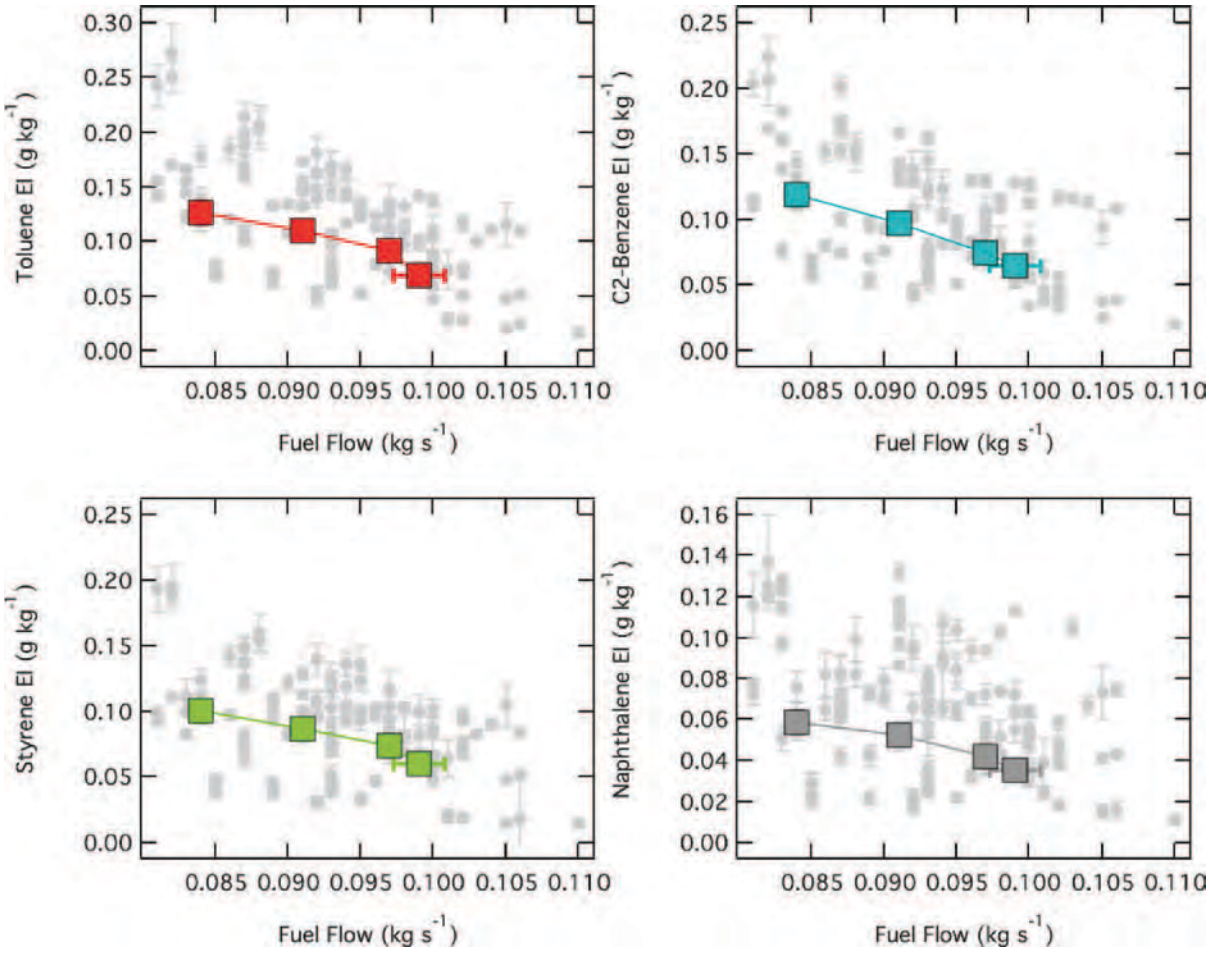

Figure A01-E11c. Emission Index for engine SA011 for Toluene, C2-Benzene, Styrene, and Naphthalene. C2-Benzene refers to the sum of the xylene isomers and ethyl-benzene. The four figures depict the emission indices in grey with the precision-based error bar from the entire CFM56-7B24 dataset. The colored data points are the emission index for the species in question averaged for the nominal engine state during the test of engine index SA011. In many cases the precision based error bar for the emission index is smaller in magnitude than the size of the data point. See companion table for precision-based error bars. The absolute averaged emission indices for the fuel flow repeats during the test are depicted in the four panels; upper left Toluene in red; upper right C2-Benzene in light-blue; lower left Styrene in light green; and lower right naphthalene in the larger grey squares.

Table A01-E12a. Selected test results for engine SA012 (MDW 2010). Aircraft test conducted from 2/16/10 02:30 to 2/16/10 03:10, ambient temperature 269.8±1K, relative humidity 80%.

Fuel Flow	2σ	N1	2σ	CO EI	2σ		
kg s^{-1}	kg s^{-1}	%	%	g kg^{-1}	g kg^{-1}		
0.0817	0.0006	20.17	0.23	86.163	3.228		
0.0880	0.0000	19.75	0.21	79.595	2.665		
0.0930	0.0008	19.80	0.34	76.555	2.761		
0.0955	0.0021	25.25	0.21	58.720	2.238		
Engine SA_001							
Fuel Flow	2σ	C_2H_4 EI	2σ	HCHO EI	2σ	Benzene EI	2σ
kg s^{-1}	kg s^{-1}	g kg^{-1}	g kg^{-1}	g kg^{-1}	g kg^{-1}	g kg^{-1}	g kg^{-1}
0.0817	0.0006	3.027	0.143	2.360	0.143	0.405	0.026
0.0880	0	2.505	0.090	2.020	0.107	0.329	0.016
0.0930	0.0008	2.185	0.085	1.778	0.108	0.279	0.018
0.0955	0.0021	1.725	0.084	1.440	0.088	0.228	0.024
Engine SA_001							
Fuel Flow	2σ	Toluene EI	2σ	C2-Benzene	2σ	Styrene	2σ
kg s-1	kg s-1	g kg-1	g kg-1	g kg-1	g kg-1	g kg-1	g kg-1
0.0817	0.0006	0.255	0.019	0.211	0.014	0.193	0.012
0.0880	0.0000	0.205	0.014	0.152	0.010	0.157	0.010
0.0930	0.0008	0.171	0.012	0.126	0.013	0.129	0.012
0.0955	0.0021	0.139	0.014	0.112	0.016	0.119	0.012

Table Notes. The 2σ value is computed as twice the standard error of the fit emission ratio converted to emission index. When multiple data points have been averaged at the noted fuel flow rate, these errors have been added in quadrature.

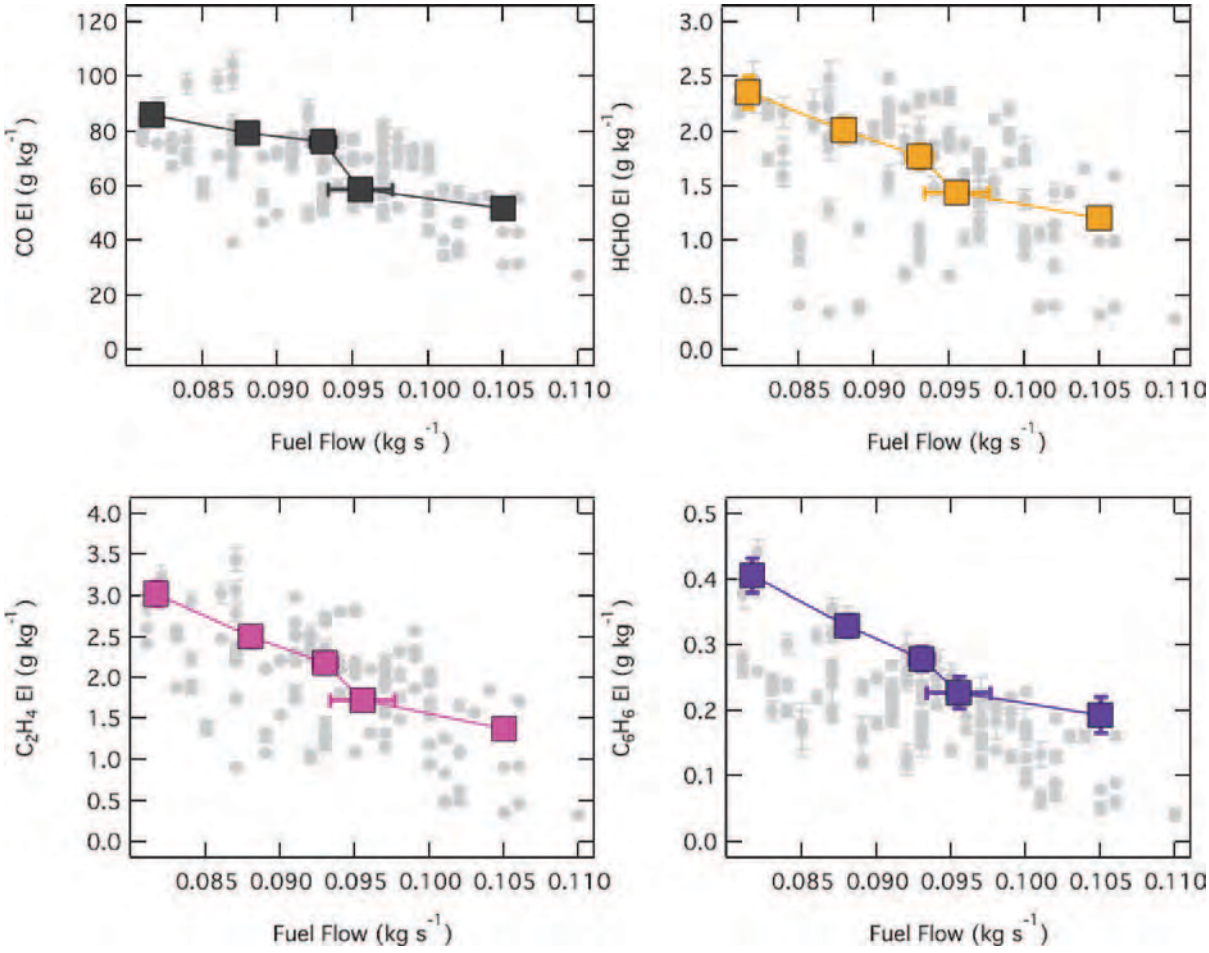

Figure A01-E12b. Emission Index for engine SA012 for CO, HCHO, C2H4, and C6H6. The four figures depict the emission indices in grey with the precision-based error bar from the entire CFM56-7B24 dataset. The colored data points are the emission index for the species in question averaged for the nominal engine state during the test of engine index SA012. In many cases the precision based error bar for the emission index is smaller in magnitude than the size of the data point. See companion table for precision-based error bars. The absolute averaged emission indices for the fuel flow repeats during the test are depicted in the four panels; upper left CO in black; upper right HCHO in orange; lower left ethene (C2H4) in magenta; and lower right benzene (C6H6) in violet.

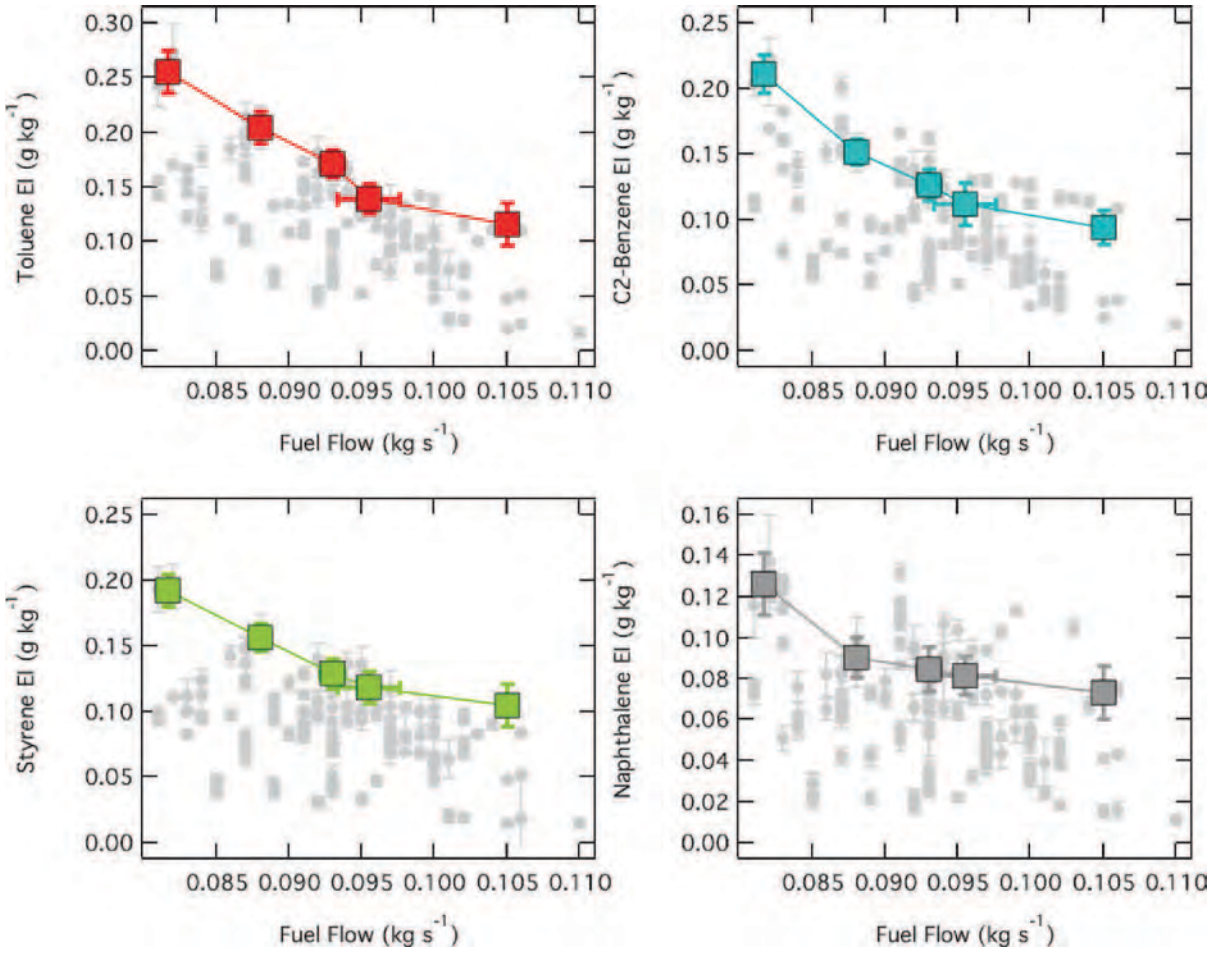

Figure A01-E12c. Emission Index for engine SA012 for Toluene, C2-Benzene, Styrene, and Naphthalene. C2-Benzene refers to the sum of the xylene isomers and ethyl-benzene. The four figures depict the emission indices in grey with the precision-based error bar from the entire CFM56-7B24 dataset. The colored data points are the emission index for the species in question averaged for the nominal engine state during the test of engine index SA012. In many cases the precision based error bar for the emission index is smaller in magnitude than the size of the data point. See companion table for precision-based error bars. The absolute averaged emission indices for the fuel flow repeats during the test are depicted in the four panels; upper left Toluene in red; upper right C2-Benzene in light-blue; lower left Styrene in light green; and lower right naphthalene in the larger grey squares.

Table A01-E13a. Selected test results for engine SA013 (MDW 2010). Aircraft test conducted from 2/16/10 04:30 to 2/16/10 05:15, ambient temperature 269.7±1K, relative humidity 80%.

Fuel Flow	2σ	N1	2σ	CO EI	2σ		
kg s^{-1}	kg s^{-1}	%	%	g kg^{-1}	g kg^{-1}		
0.0860	0.0014	20.55	0.42	100.033	3.885		
0.0920	0.0000	20.05	0.21	86.645	3.029		
0.0973	0.0005	20.20	0.45	78.808	3.093		
0.0997	0.0015	25.37	0.45	65.287	3.780		
Engine SA_001							
Fuel Flow	2σ	C_2H_4 EI	2σ	HCHO EI	2σ	Benzene EI	2σ
kg s^{-1}	kg s^{-1}	g kg^{-1}	g kg^{-1}	g kg^{-1}	g kg^{-1}	g kg^{-1}	g kg^{-1}
0.0860	0.0014	3.118	0.150	2.285	0.147	0.323	0.016
0.0920	0	2.450	0.101	1.875	0.111	0.251	0.013
0.0973	0.0005	2.070	0.098	1.580	0.104	0.209	0.012
0.0997	0.0015	1.577	0.149	1.290	0.124	0.165	0.025
Engine SA_001							
Fuel Flow	2σ	Toluene EI	2σ	C2-Benzene	2σ	Styrene	2σ
kg s-1	kg s-1	g kg-1	g kg-1	g kg-1	g kg-1	g kg-1	g kg-1
0.0860	0.0014	0.191	0.012	0.155	0.008	0.138	0.009
0.0920	0.0000	0.144	0.008	0.106	0.006	0.108	0.007
0.0973	0.0005	0.118	0.009	0.083	0.006	0.087	0.007
0.0997	0.0015	0.095	0.019	0.075	0.012	0.076	0.014

Table Notes. The 2σ value is computed as twice the standard error of the fit emission ratio converted to emission index. When multiple data points have been averaged at the noted fuel flow rate, these errors have been added in quadrature.

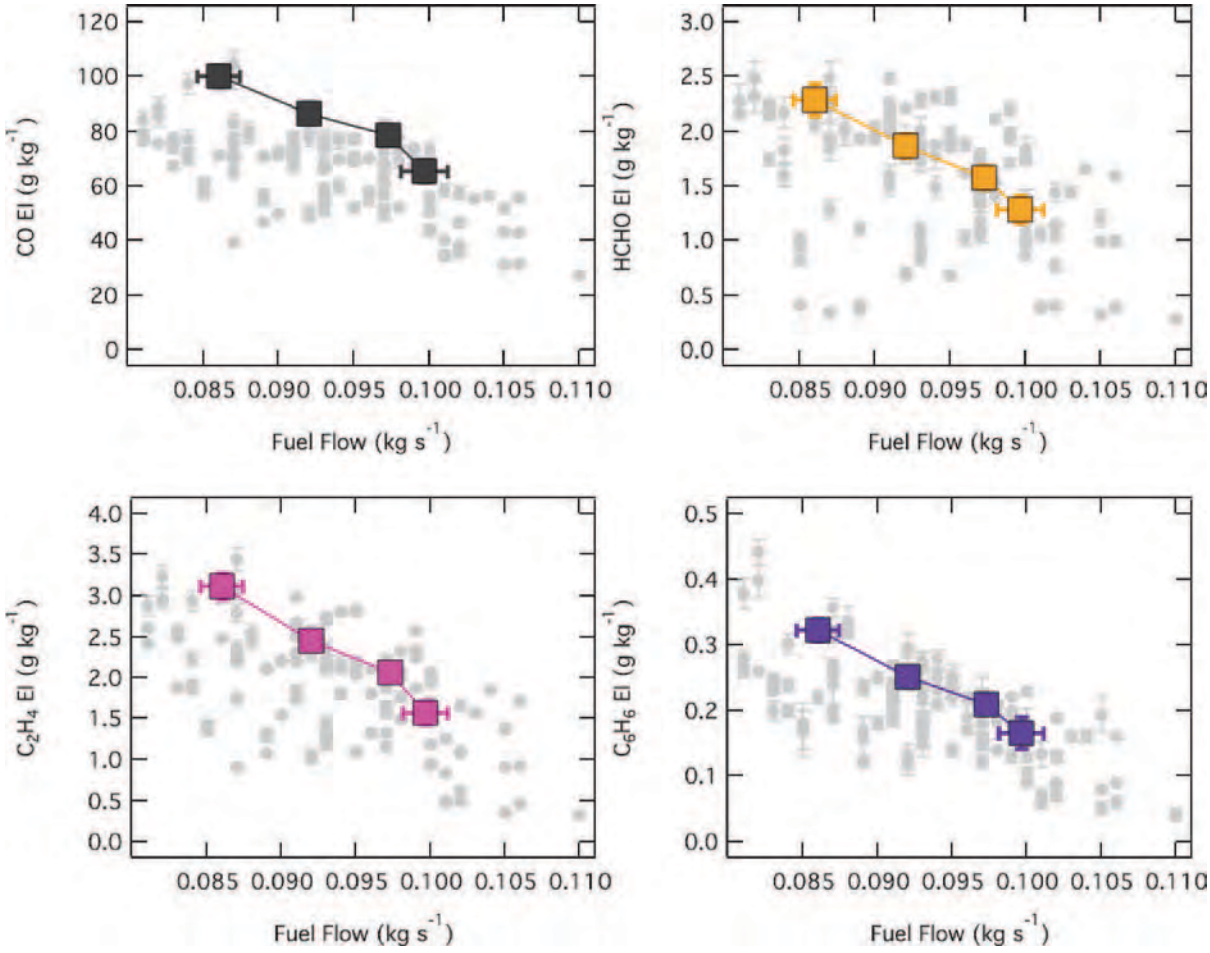

Figure A01-E13b. Emission Index for engine SA013 for CO, HCHO, C2H4, and C6H6. The four figures depict the emission indices in grey with the precision-based error bar from the entire CFM56-7B24 dataset. The colored data points are the emission index for the species in question averaged for the nominal engine state during the test of engine index SA013. In many cases the precision based error bar for the emission index is smaller in magnitude than the size of the data point. See companion table for precision-based error bars. The absolute averaged emission indices for the fuel flow repeats during the test are depicted in the four panels; upper left CO in black; upper right HCHO in orange; lower left ethene (C2H4) in magenta; and lower right benzene (C6H6) in violet.

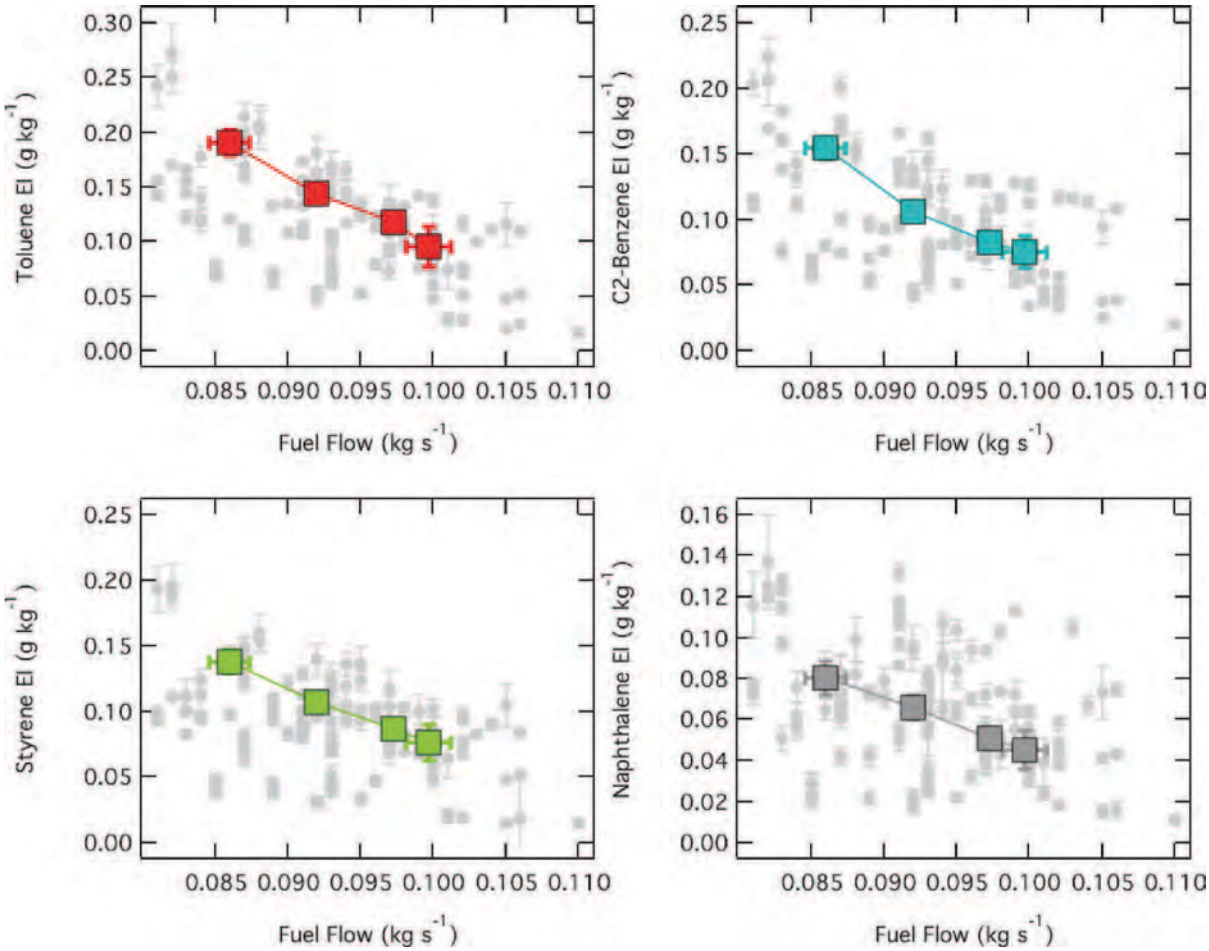

Figure A01-E13c. Emission Index for engine SA013 for Toluene, C2-Benzene, Styrene, and Naphthalene. C2-Benzene refers to the sum of the xylene isomers and ethyl-benzene. The four figures depict the emission indices in grey with the precision-based error bar from the entire CFM56-7B24 dataset. The colored data points are the emission index for the species in question averaged for the nominal engine state during the test of engine index SA013. In many cases the precision based error bar for the emission index is smaller in magnitude than the size of the data point. See companion table for precision-based error bars. The absolute averaged emission indices for the fuel flow repeats during the test are depicted in the four panels; upper left Toluene in red; upper right C2-Benzene in light-blue; lower left Styrene in light green; and lower right naphthalene in the larger grey squares.

Testing on the V2527-A5

At the conclusion of the MDW 2010 testing campaign, the mobile laboratory was driven to Chicago ORD airport in order to collect abbreviated test data on engine technologies in addition to the CFM56 type engine. One of the two aircraft tested in this phase of the project, provided by United Air Lines, was an A320-232 equipped with the V2527-A5 engine variant. The sampling style employed was identical to that used in the MDW 2009 phase, where the mobile laboratory was maneuvered behind the aircraft.

Figure A01-Va depicts the results of the determination of CO and HCHO emission indices as a function of fuel flow noted in the cockpit. All of the data collected in this test, {engine 1, engine 2 and at distances where the sample was a mixture of both engines} has been plotted together. Where the digital readout in the cockpit indicated a difference in fuel flow between the two engines and the sampling distance was such that we could not plausibly argue the sample was dominated by one engine or the other, the average has been used in the graphical representation.

The CO EI tabulated in the ICAO databank has been placed on the figure as a black diamond. The dashed line is approximately 37% greater than the ICAO databank value at a fuel flow rate of 0.128 kg/s. This qualitatively agrees with the trend observed in the CO EI temperature dependence in other work (AAFEX) as well as the temperature dependence derived for the near-idle hydrocarbon EI (see main project narrative). The simple two point temperature dependence derived from this single engine test indicates the engine is slightly less dependent on ambient temperature than the CFM56-7B24 and CFM56-2C1 engine tests. This engine type does warrant additional study in the future, but the single test described here should not be over-interpreted.

The ICAO databank HC EI for the V2527-A5 is 22 times lower than the HC emission index tabulated for the CFM56-7B24. As a result, the limits of detection in the analytical instrumentation preclude assigning any speciated VOC emissions for this engine type beyond formaldehyde. Using the tabulated emission index of 0.105 g HC per kg fuel, and the ratio of HCHO to HC measured in the MDW 2009 tests (0.2 g HCHO per "g" HC), it suggests the HCHO EI for this engine type at the 7% thrust fuel flow rate should be 21 mg HCHO per kg fuel. In the right hand panel of Figure A01-Va, this estimate is quite close to what is actually observed at the fuel flow rate of 0.128 kg s^{-1}. This would suggest that the dependence of HCHO EI on ambient temperature is weaker than that observed in the CFM56 engine testing.

Testing of the PW4090

Following the testing of the V2527-A5, the United Air Lines personnel suggested that a 777-222ER equipped with PW4090 be tested next. The data from this test are tabulated here, however it was unscheduled work and as a result the precise engine settings required to match the ICAO 7% engine condition were not known during the test. The PW4090 represents a much higher thrust engine class then either of the CFM56 or V2500 engine types and we had to trust the experience of the maintenance crew we were working with in order to keep a safe condition for the mobile laboratory maneuvering behind the idling engine.

Due to the spontaneous nature of the test, we did not attempt to operate the engines independently. The test matrix was

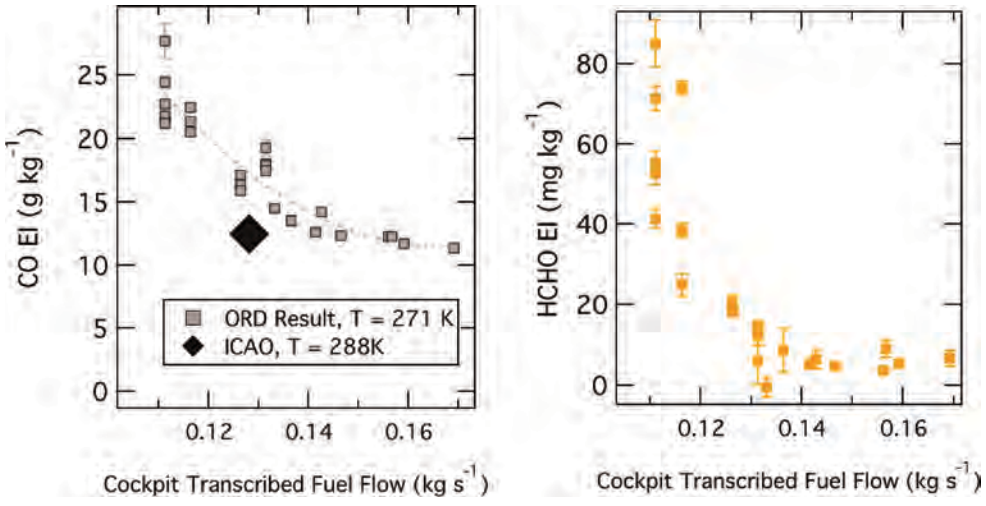

Figure A01-Va. Emission Indices for CO and HCHO for the V2527-A5 test. The left hand panel depicts the measured CO EI as a function of engine fuel flow rate. The right hand panel plots the measured HCHO EI (in mg kg^{-1}) as a function of fuel flow rate.

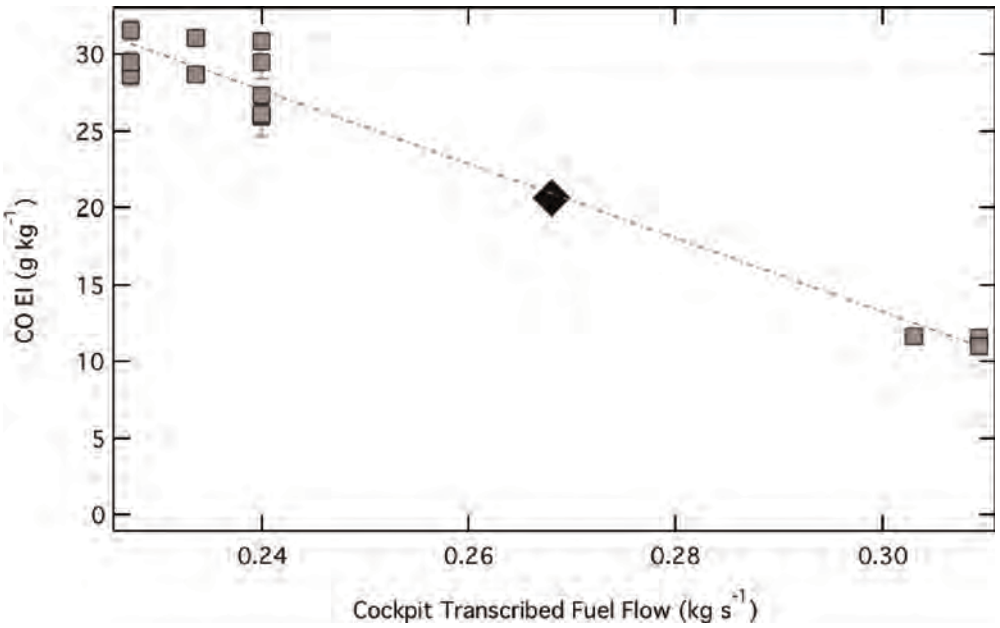

Figure A01-Pa. CO Emission Index vs Fuel Flow for PW4090. The Grey squares are the CO emission index plotted vs engine average fuel flow (see text for details). The black diamond is the ICAO reference CO EI at 7% fuel flow rate.

simplified to include the conditions described in Appendix B as ground-idle with zero bleed air demand, ground-idle with nominal bleed air demand and at N1 = 25%. This last test condition was a guess on what N1 setting would correspond to 7% thrust for this engine. The Figure A01-Pa depicts the CO emission index vs. the fuel flow rate for the test. Note that it is clear that the ICAO 7% fuel flow condition was not matched in this test. The range of noted N1 rotation speeds for the cluster of data measured below 0.24 kg s^{-1} were all in the range of 18.9 to 20.0%. The range of noted N1 rotation speeds for the three measurements above 0.3 kg s^{-1} were all 24.1 to 25.6%. In this engine test, the effect bleed air demand on fuel flow was considerably less than was observed in the CFM56 tests.

The comparison to the ICAO CO certification value is challenged because the fuel flow rate needed to match the 7% thrust condition was apparently not met. If the dashed line drawn between the cluster of CO points is taken to represent the CO emission index at intermediate fuel flows, then the comparison could be termed "favorable". The very puzzling aspect of this comparison, however is the apparent agreement. The ambient temperature was 270.3K (RH = 67%) for this test is sufficiently less than the ICAO reference temperature of 288K that the understanding of ambient temperature dependence developed in this study (based on the CFM56 tests) suggests the measured CO should have been greater. The qualitative observation of emission index trend with fuel flow is matched here though. The emission index for CO (and the hydrocarbons not depicted) is approximately double (N1 = 20% relative to N1 = 25%). Additional work will be needed to extract a quantitative comparison with ICAO for this engine test.

An additional evaluation can be performed that compares the hydrocarbon profile of this "large engine" to the more thoroughly tested CFM56 engines. The HC EI at 7% tabulated in ICAO is nearly identical for the PW4090 and the CFM56-7B24, indicating that unlike the comparison between the CFM56-7B24 and the V2527-A5, there should at least be hydrocarbons present of a similar magnitude to verify the hydrocarbon profile for the selected species measured at this test. Figure A01-Pb depicts the correlation of the emission indices of 1,3-butadiene and formaldehyde for the PW4090 test.

The grey dashed line in Figure A01-Pb is a linear least squares fit to the data forced through the origin which suggests the relationship between 1,3-butadiene and formaldehyde is 103±4 mg:g^{-1}. This compares favorably to the current value asserted in the SPECIATE profile (137 mg:g^{-1}).

Additional hydrocarbon ratios tabulated in Table A01-Pc suggest generally good agreement with the SPECIATE profile for this test (EPA 2008). While the compound ratios for the other VOCs, except for ethene, tend to be lower than that predicted by SPECIATE, such a good correlation might not have been expected given that SPECIATE is derived from CFM56 engine (EPA 2008). This singular comparison should not be over interpreted, but it does suggest that VOC emission profile is not highly dependent on combustor design.

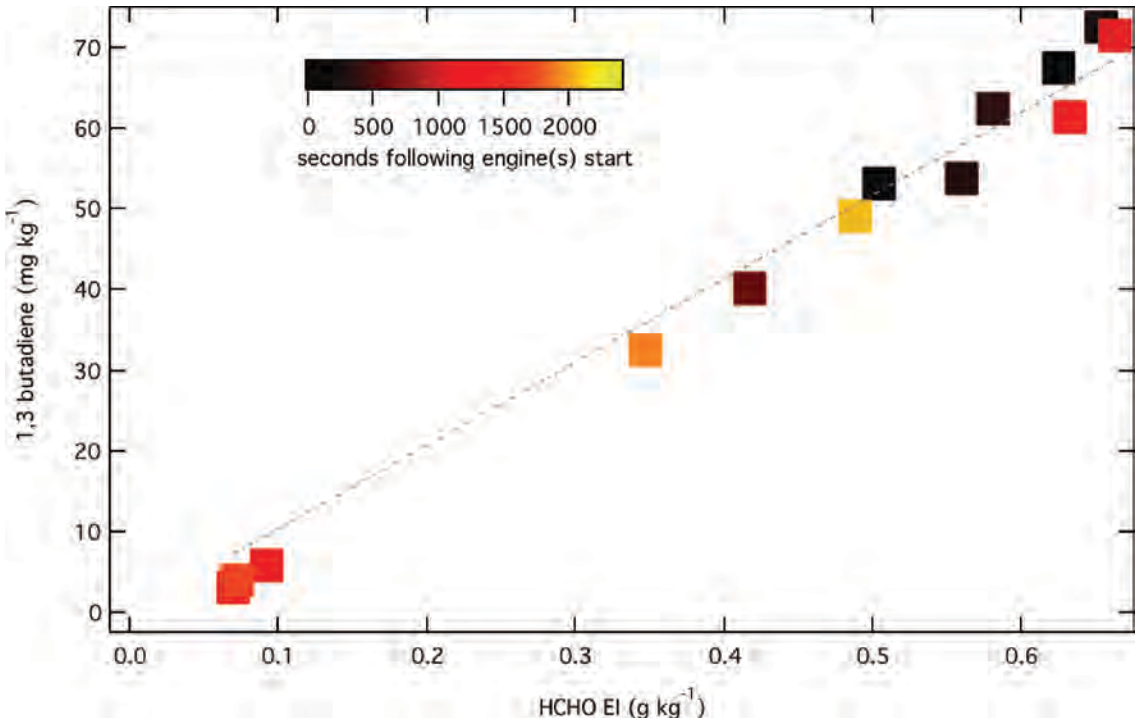

Figure A01-Pb. 1,3-butadiene EI vs. HCHO EI. The PW4090 test results for the NO-MS measurement of 1,3-butadiene are plotted against the QCL measurement of HCHO. The color scaling indicates the time since the engines were turned on. The ratio between these hydrocarbon species does not depend on the engine warm up.

Additional engines needed to be studied to further corroborate this finding.

A02—Additional Findings on the Near-Idle Hydrocarbon Emission Profile

Our characterization of VOC emissions from Jet aircraft engines has spanned a period of 8 years and 12 separate measurement opportunities (Herndon et al. 2006, Herndon et al. 2009, Knighton et al. 2007, Yelvington et al. 2007) (need to include AAFEX NASA reference). During these studies, we have observed a consistent and repeatable phenomenon, in which we find that nearly all of the VOC exhaust emissions components scale in a near-linear relationship with one another under low power conditions. We refer to this observation as near-idle emissions scaling. In this section, we first briefly review the instruments and sampling methods and then present results that illustrate the near-idle VOC emissions scaling phenomenon. This is followed by a discussion of how this relationship can be used to interrogate our analytical methodology, probe sampling effects, gaps in existing VOC speciation profile, and the validity of predicting VOC emissions that were not directly measured.

Table A01-Pc. PW4090 compound ratios.

	(g / g formaldehyde)	uncertainty	SPECIATE
Ethane	1.30	0.04	1.25
1,3 butadiene	0.103	0.004	0.137
Benzene	0.128	0.006	0.137
Toluene	0.036	0.006	0.052
C2-benzenes	0.046	0.008	0.050
Naphthalene	0.032	0.002	0.044

Before we present any data, it is important to review the analytical methods and sampling strategies employed. Sampling strategies differed in how the engine exhaust samples were delivered to the instruments. During MDW 2009, a down-wind plume intercept approach was used, which allowed the exhaust to cool and dilute naturally into ambient air. The concentration of the components within the exhaust plume dilutes continuously with down-wind distance and is modulated further by wind speed and direction. The plume intercept method requires that all of the instruments operate at 1 Hz. Extraction probes were used during DAL 2009 and MDW 2010 to transport the exhaust sample to the instruments. At DAL 2009, three different extraction probes were used and differed on how and where

Table A02-1. Instrumental methods used for the measurement of the selected VOCs.

Compound	MDW 2009	DAL 2009	MDW 2010
formaldehyde	QCL	QCL	QCL
ethene	QCL	QCL	QCL
acetaldehyde	PNL-H_3O^+	MSU-H_3O^+	PNL-H_3O^+
1,3-butadiene	MSU-NO^+	----	MSU-NO^+
benzene	MSU-NO^+	MSU-H_3O^+	MSU-NO^+
toluene	MSU-NO^+	MSU-H_3O^+	PNL-H_3O^+
styrene	MSU-NO^+	MSU-H_3O^+	PNL-H_3O^+
C2-benzenes	MSU-NO^+	MSU-H_3O^+	MSU-NO^+
naphthalene	MSU-NO^+	MSU-H_3O^+	PNL-H_3O^+

the exhaust was diluted. At MDW 2010 a single extraction probe was deployed.

VOC measurements were made using a total of four different instruments, one of which (MSU PTR-MS) was operated in two different chemical reagent ion modes. Formaldehyde and ethene were measured spectroscopically using QCL TILDAS instruments. The remaining VOCs were measured using a pair of chemical ionization mass spectrometers, except at DAL 2009 where only one instrument was deployed. Table A02-1 lists VOC species measured and identifies which instrument method was used. The compound list in Table A02-1 represents only those compounds that were measured during all of the deployments. The instruments are designated as follows: QCL represents the QCL TILDAS instruments. MSU H_3O^+ and MSU NO^+ refer to the MSU PTR-MS operated in standard proton transfer (H_3O^+) or alternative ion (NO^+) mode. The PNL PTR-MS was only operated in the standard H_3O^+ mode. In cases where the same species was measured by more than one instrument, only the "best" measurement is reported. At MDW 2010 the PNL PTR-MS measurements were chosen for styrene and naphthalene because of evidence that there were interferences to NO-MS measurements. For toluene, the calibration of the NO-MS is less robust and the PTR-MS measurement was considered as the best.

The near-idle VOC scaling phenomenon is illustrated in Figure A02-1, where we have taken the EI data for each of the VOC species and plotted it versus the corresponding ethene measurement. The plot colors identify the different measurements, MDW 2009 (red), DAL 2009 (green) and MDW 2010 (blue), while the different aircraft tested are identified by a different marker style. Overall, there is also a strong suggestion that all of the measurements are correlated in a near-linear fashion even though these profiles show varying degrees of scatter. Closer inspection reveals that the scatter in the plots, however, is not random. In most cases, the profiles exhibit a linear ray for each aircraft. It is from this behavior that the term near-idle VOC scaling concept arose. While it is not clear why near-idle VOC scaling should exist, it does collapse much of the variability observed in the absolute EI measurements. This is important, because it allows us to identify which measurements don't follow the trend and then interrogate those measurements more carefully.

We can now examine the profiles shown in Figure A02-1 more carefully with the goal of identifying the source or sources that lead to the observed variability. Formaldehyde and acetaldehyde both show similar behavior except for the five formaldehyde data points that lie below the rest of the data. These data were all measured using the gas probe during DAL 2009. This is not a sampling anomaly as the PTR-MS measurement of formaldehyde exhibited an identical result. It is not immediately obvious why formaldehyde should be lost or consumed within the gas probe, but it certainly casts some doubt about the use of this type of probe. In fact, it leads one to question if the reason why both formaldehyde and acetaldehyde measurements from MDW 2009 lie above those made using extractive probes isn't the result of a probe effect. We also note that there is some curvature in the formaldehyde and acetaldehyde plots at the highest emissions. This result seems to suggest that the fuel continues to decompose to ethene but that combustion begins to diminish under these conditions.

Inspection of the other profiles shows that there is inherently more variability in the hydrocarbon emissions, in part due to their lower concentrations (molar basis). It is logical to question whether this variability originates from the measurements or reflects differences in the engine exhaust emissions. In cases where the results show obvious differences between the test periods (i.e., 1,3-butadiene),

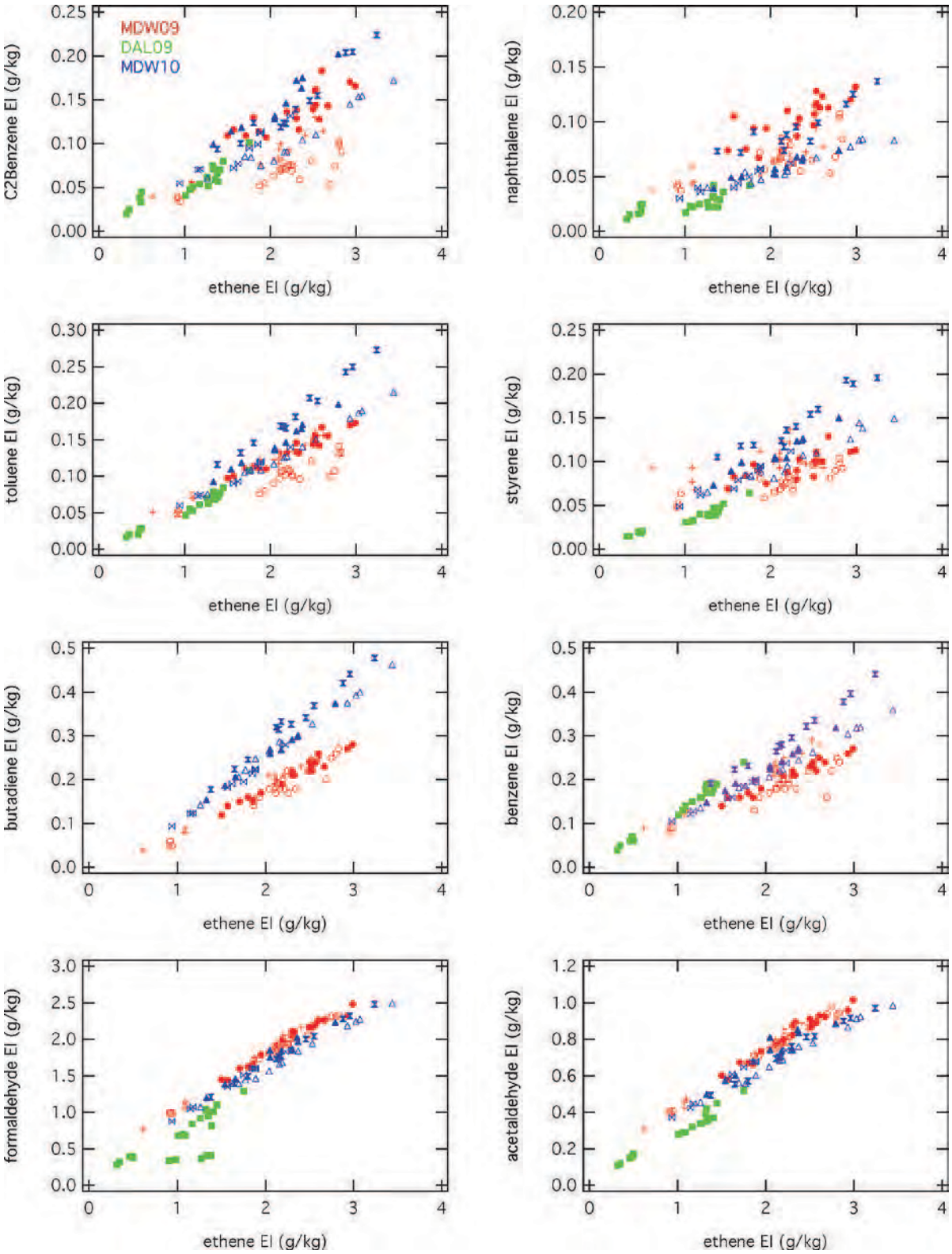

Figure A02-1. Near-idle VOC emissions scaling profiles. Marker color indicates the measurement date and location. Marker styles identify the different aircraft.

it seems logical to question if the variability isn't the result of the analytical measurement. An incorrect instrument calibration factor could lead to such a result, even though every effort was made to check the calibrations before, during and after the studies. When differences are observed within the aircraft studied at a given test, it would appear that the variability is related either to the fuel, the engine or some other unknown external influence.

We can now examine the results of this study to that reported elsewhere, such as SPECIATE or our previous AAFEX results (Anderson et al. 2010, EPA 2008). To make this comparison we have normalized our data to that of ethene and fit the frequency distribution to a Gaussian. The centroid of the Gaussian distribution is taken as the best value with the width representing the uncertainty. For 1,3-butadiene the average and standard deviation are reported, because the frequency distribution is bimodal. These results are summarized in Table A02-2 along with those reported in SPECIATE (EPA 2008) and from AAFEX for JP-8 (Anderson et al. 2010). The ACRP data agree within the uncertainty limits with the other measurements except for acetaldehyde, which is approximately 30% high.

Near-idle VOC emissions scaling allows us to decouple changes in the VOC composition of the exhaust from the variability in the absolute VOC EIs exerted by engine power and ambient temperature. The near-linear relationships observed in Figure A02-1 and the overall agreement between the ethene normalized EIs found here with that reported elsewhere, strongly suggests that the VOC composition is relatively insensitive to engine condition or fuel composition, at least over the limited range of engines studied and fuel compositions. The relative consistency of the VOC exhaust composition allows one to then project the emissions of chemical species not directly measured by scaling the emissions to that of ethene. The obvious question arises. Over what range of conditions can the near-idle VOC emission scaling be applied? To address this question we need to examine how our speciated VOC emissions vary with CO and UHC (unburned hydrocarbons).

Figures A02-2 and A02-3 examine the relationship between the emission of ethene with those of CO and UHC as measured with an FID. Two very different behaviors emerge. When the ethene EI is less than 2g/kg the ethene emissions appear to scale in a near-linear fashion with both CO and UHC. As the ethene EIs increase above 2g/kg nonlinearities appear. The CO emissions stop increasing at the same rate and the UHC emissions start increasing more rapidly with respect to ethene. This result suggests that the engine reaches a condition where it is no longer burning most of the fuel. If one views combustion as a simple two step process, where the fuel pyrolyzes decomposes into smaller molecules (ethene) followed by combustion (oxidation), then it follows that ethene production would continue longer than the combustion process. Likewise, the ethene production will diminish relative to the UHC at the point where unburned fuel actually escapes from the combustor. While this argument explains the relationship between ethene and UHC, why don't the VOCs in Table 2 (i.e., the aromatics) exhibit more non-linearity at the higher EIs?

Some of the species in Table A02-2 are only combustion products and are not present in the liquid fuel. Others, such as the aromatics, are both combustion products and components of the liquid fuel. It is beyond the scope of this report to do a detailed examination of how the VOC emissions vary with fuel composition, but the observation of the near-idle VOC emission scaling exhibited by the aromatics infers that, under the conditions studied, their presence in the exhaust is dominated by combustion and not the escape of unburned fuel into the exhaust. In contrast the FID is most sensitive to the presence of large hydrocarbons, such as the long chained alkanes that make

Table A02-2. Comparison of compound EIs normalized to ethene.

Species	Speciate EI_x/EI_{ethane}	AAFEX EI_x/EI_{ethene}	ACRP EI_x/EI_{ethene}
formaldehyde	0.80	0.75	0.79 (0.12)
acetaldehyde	0.28	0.27	0.35 (0.04)
1,3-butadiene	0.11	----	0.10 (0.03)
Benzene	0.11	0.12	0.10 (0.04)
Toluene	0.042	0.057	0.056 (0.007)
Styrene	0.020	0.026	0.043 (0.016)
C2-benzenes	0.040	(0.053)[a]	0.047 (0.026)
Naphthalene	0.035	0.028	0.028(0.015)

(a) The PTR-MS determination reports the sum of the C2-benzenes + benzaldehyde. The data entry here has been adjusted to correct for the benzaldehyde contribution assuming that 43% of the response is from benzaldehyde.

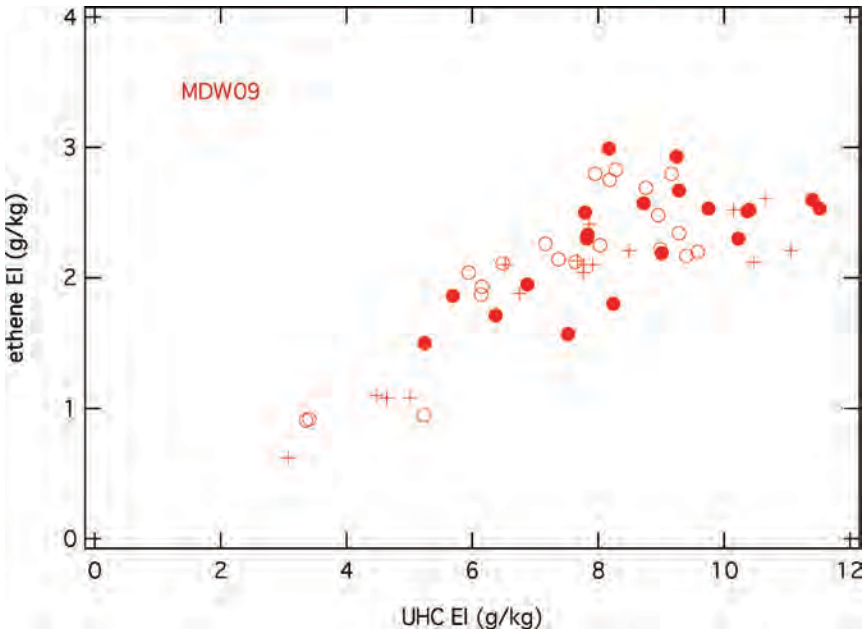

Figure A02-2. Correlation scatter plot of ethene EI versus unburned hydrocarbon UHC EI.

up a large fraction of the liquid fuel. The bias in the UHC towards the presence of unburned fuel is further exacerbated by the fact that FID detector response is diminished to carbons that are bonded to an oxygen. The FID is essentially blind to the presence of formaldehyde, which represents approximately 12% of the organic carbon in the exhaust.

Scaling emissions from either CO or UHC measurements using databases such as SPECIATE (EPA 2008) need to recognize the limits where these relationships become non-linear. Anecdotally, it appears that there is little error introduced under moderate to warm ambient temperatures. A linear scaling to CO or UHC is not appropriate at low ambient temperatures.

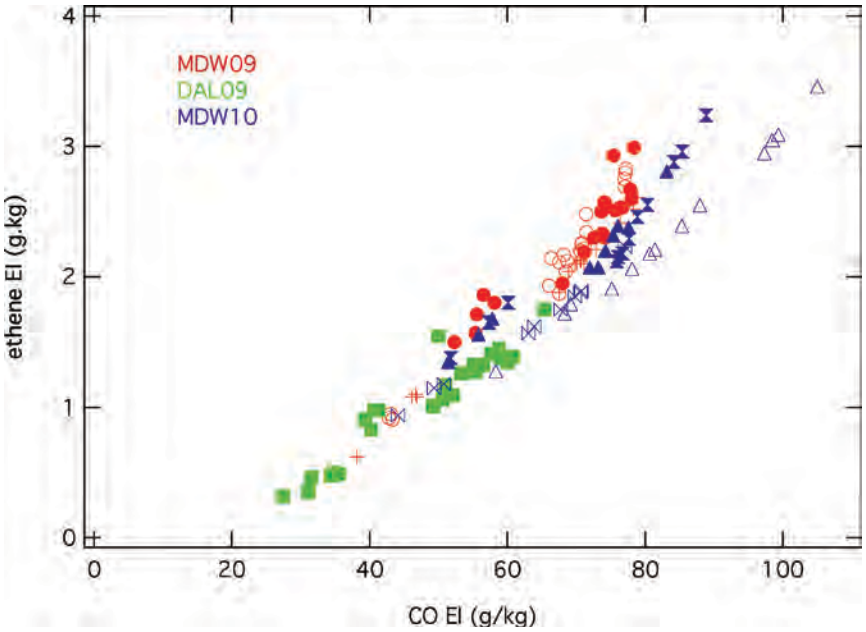

Figure A02-3. Correlation scatter plot of ethene EI versus CO EI.

Near-idle VOC emissions scaling can be a valuable tool for projecting jet engine exhaust emissions, providing it is properly applied. Its validity, however, is only as good as the knowledge of VOC speciation profile. Databases such as SPECIATE (EPA 2008) contain extensive listing, but are still not comprehensive and only identify 70% of the VOC mass emissions. The bulk of the missing mass is most likely in the higher molecular hydrocarbons, which are difficult to conclusively identify by GC/MS because of their similar mass spectral fragmentation patterns. There is also evidence from studies conducted elsewhere (Anderson et al. 2010, Timko et al. 2011) using a GC/PTR-MS that indicates the presence of unsaturated aldehydes, corresponding to C4H6O and C5H8O that are not included in SPECIATE (EPA 2008). These species are more likely to be on the HAPs list and thus represent species of concern.

References Cited in Appendix A

Anderson, B. E., et al. 2010. Alternative Aviation Fuel Experiment (AAFEX) *Rep.*

EPA. 2008. SPECIATE, edited. US EPA.

Herndon, S. C., T. Rogers, E. J. Dunlea, R. C. Miake-Lye, and B. Knighton. 2006. Hydrocarbon emissions from in-use commercial aircraft during airport operations. *Environmental Science and Technology.* 40 (14): 4406–4413.

Herndon, S. C., E. C. Wood, M. J. Northway, R. C. Miake-Lye, L. Thornhill, A. Beyersdorf, B. E. Anderson, R. Dowlin, W. Dodds, and W. B. Knighton. 2009. Aircraft Hydrocarbon Emissions at Oakland International Airport, *Environ Sci. Technol.* 43. 1730–1736.

Herndon, S. C., et al. 2004. NO and NO2 Emissions Ratios Measured from in use Commercial Aircraft during Taxi and Take-Off. *Environ. Sci. Technol.* 38: 6078–6084.

Knighton, W. B., T. Rogers, C. C. Wey, B. E. Anderson, S. C. Herndon, P. E. Yelvington, and R. C. Miake-Lye. 2007. Quantification of Aircraft engine Hydrocarbon Emissions Using Proton Transfer Reaction Mass Spectrometry. *Journal of Propulsion and Power* 23 (5): 949–958.

Timko, M. T., S. Herndon, E. de la Rosa Blanco, E. Wood, Z. Yu, R. C. Miake-Lye, W. B. Knighton, L. Shafer, M. DeWitt, and E. Corporan. 2011. Combustion Products of Petroleum Jet Fuel, a Fischer Tropsch Synthetic Fuel, and a Biomass Fatty Acid Methyl Ester Fuel for a Gas Turbine Engine. *Combust. Sci. Technol.* in press.

Yelvington, P. E., S. C. Herndon, J. C. Wormhoudt, J. T. Jayne, R. C. Miake-Lye, W. B. Knighton, and C. C. Wey. 2007. Chemical Speciation of Hydrocarbon Emissions from a Commercial Aircraft Engine. *Journal of Propulsion and Power.* 23: 912–918.

APPENDIX B

Development of the "Near-Idle" Test Matrix

Introduction

This section describes the development of the text matrix used to characterize the temperature dependence of HAP emissions from idling aircraft. It outlines background material and motivates the development of a *new* near-idle test matrix for use with on-wing aircraft engine testing. This section will describe some of the characteristics of measured fuel flow, N1 and EGT (exhaust gas temperature) during the test. Although the main report and Appendix A describe the complete results, some emissions performance will be discussed here as it relates to the engine operational states defined in the test matrix.

A secondary goal of the project was to collect information on emissions performance during initial engine warm up. Those results are also discussed in this section.

The emission index for hydrocarbons (and by extension HAPs) is highly dependent on the specific fuel flow rate in the vicinity of idle. *A precise understanding of the dependence of the emission index on fuel flow rate is imperative for an acceptable description of the temperature dependence of hydrocarbon emission index.* Thus significant emphasis has been placed on a well defined "near-idle" test matrix for the measurements described in this work. This section will examine emission index and fuel flow trends in the ICAO databank and perform a comparison with the data collected here. Finally, some practical recommendations for using the test matrix described here are presented.

Background on Emissions Certification for Idle

The International Civil Aviation Organization (ICAO) recommends practices (ICAO 1981) for the emissions certification performance of CO, NOx, Smoke Number and unburned hydrocarbons (UHC). The results are tabulated in the Emissions Databank (ICAO 2006). The certification databank sheets are the legal benchmarks for engine emissions performance and are used in regulatory evaluations. They are also used in performing global modeling, air quality research and airport inventory assessments (Pison and Menut 2004; Unal et al. 2005).

Emissions of CO, NOx and UHC are compiled in units of grams per kilogram of fuel for the following named engine conditions: idle, approach, climb-out and take-off. NOx is expressed as "NO_2 equivalents" while UHC is expressed as "CH_4 equivalents." Fuel flow rates for each engine condition are also tabulated for the named conditions for each engine.

The Emissions Dispersion Modeling System (EDMS) uses the values tabulated in the ICAO databank in airport related inventory and modeling applications (Anderson et al. 2007; FAA 2006). Emissions inventory assessments could suffer bias due to uncertainties in the following:

1. time-in-mode
2. effect of ambient conditions on emissions, and
3. actual operational thrust levels or engine conditions.

In order to address the potential bias introduced in the assumed time(s)-in-mode, it is possible to analyze specific datasets to refine these values for case studies. For example, an analysis of tabulated "out-off-on-in" times for each airport can refine the time spent in the bulk "idle" mode for a specific airport. Though knowledge of the distribution of time(s) spent in on the ground would improve an inventory assessment, it does not directly evaluate the actual operational fuel flow values noted above as #3.

The effect of ambient conditions on HAP emissions near-idle engine states is the primary goal of this study. As discussed in the introduction and project motivation section, the idle phase of operations dominates the aircraft contribution to hydrocarbon emissions (Wood et al. 2008). Anecdotally, it is generally understood that most modern engines operationally idle on the ground at a fuel flow rate that is lower than the engine certification value (defined as 7% of rated thrust).

For pollutants whose emission indices increase with decreasing thrust, such as CO and UHC, the ICAO certification value named 'idle' generally underestimates total emissions because the emission index increase outweighs the fuel flow decrease. The relationship of the emission index, however with engine state can become complicated at "idle" because the engine is not performing in the optimized region of its design space.

On-wing emissions testing programs have characterized the difference between minimum ground idle (no bleed air demand) and the reference definition of idle (7%) (Spicer et al. 1994, Spicer et al. 1992, Timko et al. 2008, Yelvington et al. 2007). Observations of emissions from in-use aircraft suggest that, for a significant portion of the taxiway operational phase, the fuel flow rate is greater than minimum ground idle but less than the reference idle at 7% of rated thrust (Herndon et al. 2009). The test matrix developed for this project, and described in the next section, is intended to explore a practical airline/pilot operational definition of the engine states in addition to the minimum ground idle with no bleed and 7% thrust reference points. *This test matrix does not attempt to define a single point as representative of the idle phase of operation for inventory development purposes but rather attempts to measure the emissions characteristics at each of the defined points.*

Test Matrix Design Points

The aircraft engine states defined in this project were chosen based on settings using the cockpit control system. The engine states defined in this test were chosen to cover each of the following; typical operational procedures; atypical procedures; and the engine emissions certification reference condition. For the majority of the engines tested, the reference condition was set using the main fan speed (N1 = 25%). When the test was being conducted in weather where it was plausible that the pilots would use wing and/or inlet anti-ice systems, these states were investigated. The cockpit controls were used to enable the cabin climate control system. In order to investigate the no-bleed air engine state two different scenarios were employed. In one, the auxiliary power unit was operated to power other aircraft functions; in the other the entire bleed air demand was directed to the opposite engine. Whenever possible, the digital flight data recorder (DFDR) was used to correct and refine the engine sensor data (e.g., fan speeds, temperatures, fuel flows) recorded during the test.

For each of the ground idle operational states, the bleed air demand was modulated by alternately operating the cabin

Table B-1. Test matrix used during ACRP 02-03a winter testing.

Test Point	Time	Nominal Name	Instructions
	Mins.		
00		**Engine start**	Start engine and stabilize using no (or low) bleed on E1
	10		Hold for test team and apparent engine warm-up
01	**2**	**GI:nominal bleed**	Bleed balanced E1 <=> E2
02	**2**	**GI: w/de-ice (max bleed)**	Bleed balanced E1 <=> E2
03	**2**	**GI: w/de-ice (max all e1)**	Bleed shifted E1 <== E2
04	**5**	**Set N1=25%**	Nominal bleed, balanced E1 <=> E2
05	**1**	**GI: no bleed**	Bleed shifted E1 ==> E2
06	**3**	**GI: nominal bleed, without de-ice**	Nominal Bleed, balanced E1 <=> E2 *The truck moved downwind*
07	**1**	**Set N1=25%**	Nominal bleed, balanced E1 <=> E2
08	**5**	**GI: nominal bleed, without de-ice**	Nominal Bleed, balanced E1 <=> E2 *The truck creeps into position behind E2*
09	**2**	**GI:nominal bleed**	Bleed shifted E1 <== E2
10	**2**	**GI: w/de-ice (max bleed)**	Bleed balanced E1 <=> E2
11	**2**	**GI: w/de-ice (max all e2)**	Bleed shifted E1 ==> E2
12	**2**	**Set N1=25%**	Nominal bleed, balanced E1 <=> E2
13	**2**	**GI: no bleed on e2**	Bleed shifted E1 <== E2
14		**Shutdown**	Engine shutdown or 'safe to pull away'

"packs" and the aircraft wide de-ice system. When both engines were on, the bleed demand was either balanced between them or shunted to a single engine. The test matrix included ground idle states with zero bleed flow, nominal bleed flow, de-ice and maximum bleed flow on a single engine.

A summary of the winter time test matrix used is tabulated below. The times spent on each defined test point were variable depending on which experiments were being conducted. For example when running the gas chromatographic columns, additional time was spent on each condition. In order to obtain as many cold starts as possible, test point 0 was not always scripted. The fall test (DAL 2009) was similar, but the matrix dropped the states where additional deicing demand was placed on the engine because the ambient conditions did not warrant their use. Also, the DAL 2009 test was repeated three times in series due to the probe methodology experiments described in Appendix C.

Results

Fuel Flows Resulting from the Test Matrix

The fuel flow rate is depicted as a function of the category of test point condition during the MDW 2009 tests (with a CFM56-7 engine) in Figure B-1.

The categories in Figure B-1 are drawn from the nominal name given to each test point in the test matrix. The points have been horizontally offset (slightly) within each category in order to better depict points which are very close in fuel flow.

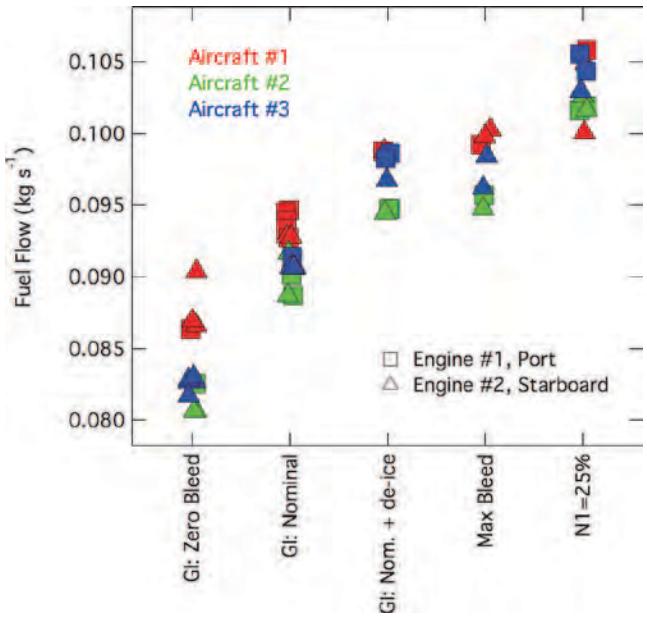

Figure B-1. Digital fight data recorded fuel flows by test condition category.

Fan Speed, Exhaust Gas Temperature, and the Relationship with Fuel Flow

In addition to fuel flow rate, two other engine characteristics, N1 and exhaust gas temperature (EGT) are indirectly modulated as a consequence of the test point conditions. N1 is related to the rotational speed of the fan in the turbofan engine. N1 is reported in units normalized by the maximum rotational speed for that engine and reported as a percent. N1 = 25% defines the 7%-idle condition for the CFM56 family of engines. Figure B2 depicts the relationship between N1, fuel flow and the effect of test conditions on exhaust gas temperature.

At first glance the figure suggests there are two disparate data groups that do not correlate well with fuel flow or EGT. Setting the data points with N1 greater than 23% aside for a moment, there is a general increase in EGT with fuel flow (dark reddish at lowest fuel flow, orange and yellow at higher fuel flow). Because the bleed air demand on the engine is responsible for increasing fuel flow rate and there is no concomitant increase in the engine intake fan speed, there is relatively more combustion heat available than at lower fuel flows and the exhaust gas temperature increases. When the engine is set to perform at a specified rotational speed, 25%, the outer fan speed is ensuring that the fuel to air ratio and the pressure in the combustor are scaling accordingly. The exhaust gas temperature is cooled with the increase in by-pass air flow induced by N1.

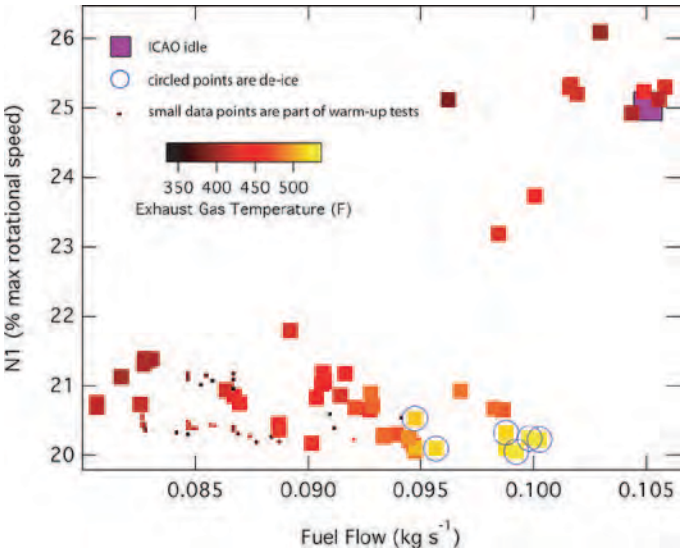

Figure B-2. N1 fan speed is depicted versus fuel flow rate. The data points are colored by exhaust gas temperature. The small data points were part of the warm up test points. The circled data in blue all represent the points where de-icing technologies were enabled.

This figure underscores the complexities in the near-idle regime for the on-wing engine between fuel flow, N1 and EGT. Similarly the combustor pressure and fuel-to-air ratio are not related linearly when bleed air demand is introduced. The overall CO_2 mixing ratio by volume at the engine exhaust plane is greater for the high bleed air demand condition than when N1 = 25%. Despite the complexity of accounting for bleed air demand in the engine conditions (between the lowest fuel flow rate—minimum engine idle, no bleed—and the greatest fuel flow rate—7% thrust or N1 = 25%), the emissions of VOCs are observed to be generally linear with absolute fuel flow rate.

Warm Up Emissions

During engine ground start there are three basic temporal regimes to consider: pre-ignition, post-ignition/pre-idle acceleration, and post-ignition at ground idle. The pre-ignition hydrocarbon emissions are represented by evaporated fuel. Surrounding the moment of ignition there will be a mixture of fuel like hydrocarbons and some partially burned hydrocarbons. The post-ignition period will be characterized by increasing combustion efficiency and any hydrocarbon emissions will be associated with concomitant carbon dioxide, CO_2, emissions. The examination of "warm-up" involves assessing the time constant of the phenomenon but also involves a consideration of what is influencing combustor performance during the dynamic post-ignition phase.

The figure depicting a turbofan engine from the main body of the report is repeated here as Figure B-3 in order to facilitate the discussion of combustor performance. The figure is has been adapted from Kerrebrock (Kerrebrock 1977).

The methodologies that predict emission combustor performance based on the pressure and temperature at the inlet to the combustor (P3 and T3 in Figure B-3) have been used to do an excellent job of predicting the gaseous emissions characteristics for turbofan engines at ground level and in flight altitudes (NEPAIR 2003, Sarli et al. 1975). Knowledge of the instantaneous combustion zone pressure and incoming pressure, along with fuel to air ratio can greatly improve the predictive skill of a model estimating combustor performance. The combustor efficiency will be related to P3 and T3. In an engine that has been off for a long enough time, the engine components will be in thermal equilibrium with ambient. When the engine is started, the core components, the turbine (approximately where EGT is measured) and the compressor stack will be relatively cold. While the EGT measurement is likely to be convolved with a time constant associated with the EGT harness hardware and the surrounding turbo-machinery, it nevertheless is a diagnostic of the warm-up time of the core components. Thus it may not be utterly implausible to use the EGT warm up time as a proxy of how long the compressor stack requires to "warm up" as well. The extent of heat transfer between the incoming air (at T2) and the air entering the combustor (T3) will be driven by the temperature gradient between T2 and the temperature of the compressor and the residence time in this region. In the condition of a cold start at idle speeds, the "warm-up" phenomenon (higher emissions of hydrocarbons and CO initially) is plausibly being influenced by the heat transfer occurring in the flow prior to entry into the combustor.

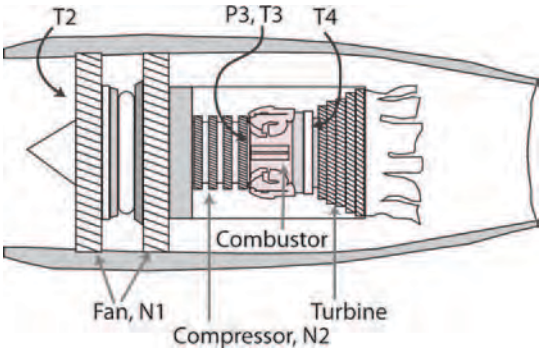

Figure B-3. Schematic of a turbofan engine.

In Figure B-4 a subset of the warm up data examines the time required to establish an equilibrium temperature within whatever time constant is associated with the EGT temperature measurement. The result depicted in Figure B-4 suggests that the exhaust gas temperature probably requires less than three minutes to reach ~90% of its steady state value.

In the MDW 2009 winter test, an effort was made to characterize the post-ignition emissions to empirically address the question of "warm-up." Whenever possible, the mobile laboratory was positioned ~40 m downwind of the engine during engine start. This was only done when the engines were known to be off for at least two hours prior to the start. The order of the test matrix initially precluded measurement of the engine starts for each of engine 1 and 2. We found we had sufficient flexibility with the sampling scheme, however, to attempt two additional near start observations.

The HCHO emission index as a function of time following ignition is depicted in Figure B-5. The time offset has been computed from the flight data recorder information and the time coded notes taken within the mobile laboratory. The chemical information in the emissions profile at other engine-state changes has been used to refine the estimate of the time offset between the flight data recorder and truck time. Conservatively, the absolute time since engine start is certain to five seconds.

Figure B-5 suggests that the CFM56-7B24 engines at the temperatures of this test (–7°C, –2°C) have two characteristic times. The first, initial rapid emissions change takes place within 20 to 60 seconds where the emission index drops considerably. The secondary change in emission index is

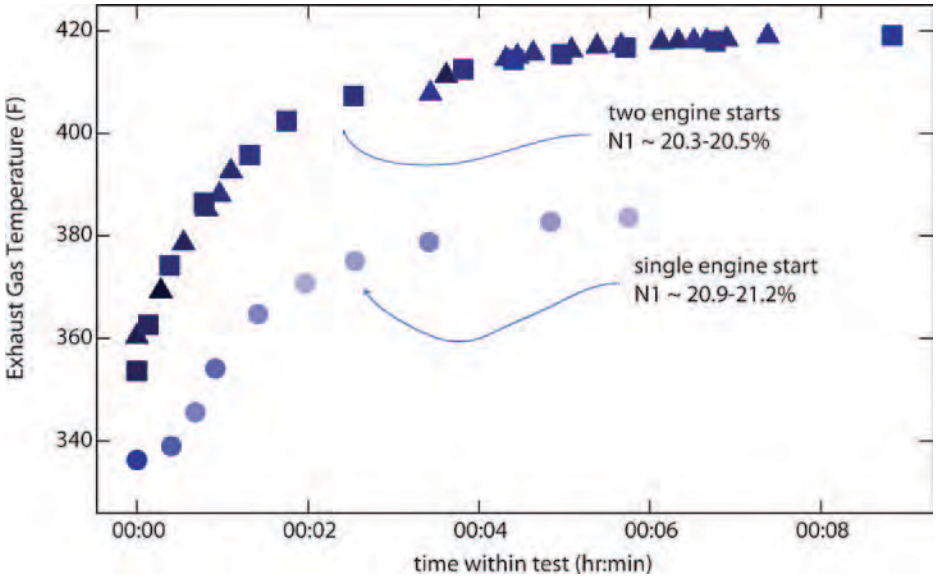

Figure B-4. This figure depicts the engine measured exhaust gas temperature as a function of the approximate elapsed time since engine start. The triangles, squares and circles denote different aircraft tests. The dark blue points reflect lower N1 rotational speeds for two of the starts than the lighter blue points.

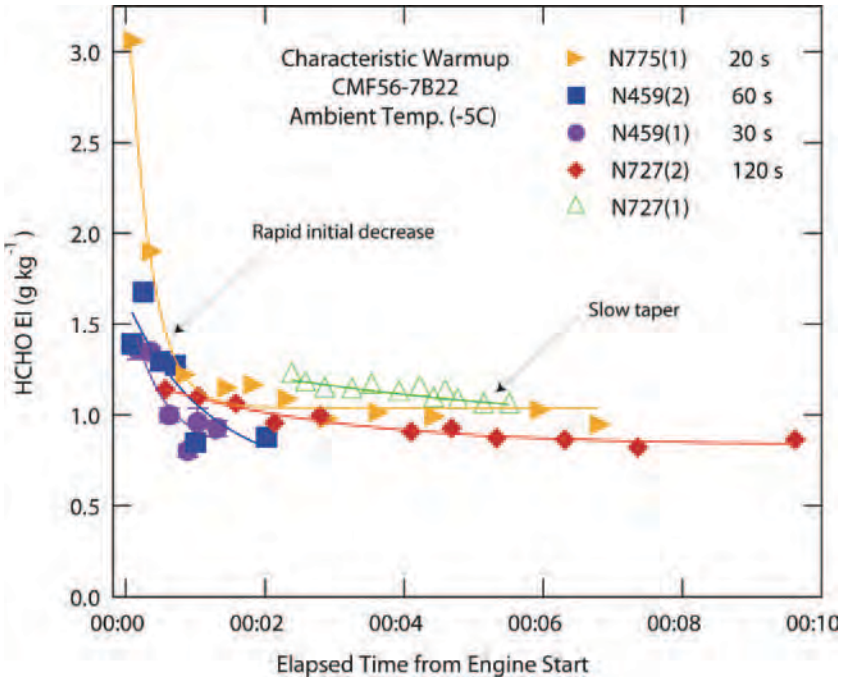

Figure B-5. The HCHO emission index is depicted as a function of the post-ignition warm up time. Although the relative times are precise, the absolute time following ignition for any of these curves is uncertain by five seconds. The solid lines represent fits of the data to a exponential decay. The approximate time constant associated with each curve is noted in the legend.

longer and characterized by a time constant of approximately 2 to 3 minutes.

The data suggests that following cold start, the emission index is approximately doubled compared to warm operation for less than a minute. A simplistic approach to gauge the effect this has on inventory modeling of a 13-minute idle time [engine-on; taxi-out] *is to add approximately one minute worth of additional idle emissions due to post-ignition warm up*.

The weaknesses in this argument are that no study has systematically looked at the reproducibility of this observation or the time needed to return to cold start conditions. Furthermore, the initial ten seconds following ignition are not well represented in this dataset. The warm up aspect of the study was secondary to the overall test goals, but these results could be used to further refine assessments of "warm-up" emissions as well as design better tests for future work.

Future Recommendation

The digital flight data recorder data (DFDR) when testing an on-wing aircraft is extremely useful when analyzing the emissions at the low fuel flows tested in this project. Although all effort is made to coordinate the test matrix between the research team and the in-cockpit engine drivers, the DFDR dataset can corroborate the actual conditions and generally explain emissions performance.

Data can be collected during the initial warm up period, however it should not be regarded as a stable engine condition. In these experiments, some effort was made to emulate a synthetic push-back, engine start, brief run up to achieve "break-away" thrust, followed by a wait at ground idle with a nominal bleed air demand typical of the taxi out phase per our airline partners standard procedures. In addition, the amount and variability of pre-ignition (fuel-like) hydrocarbon emissions is not well addressed by emission measurements. Such pre-ignition emissions might be better estimated using statistical analysis of the time between the start of fuel flow and the time of actual emission in concert with fuel analysis of the species emitted.

References Cited in Appendix B

Anderson, C., S. Augustine, D. Embt, T. Thrasher, and J. Plante. 2007. Federal Aviation Administration, Office of Environment and Energy. Emissions and Dispersion Modeling System (EDMS) User's Manual. FAA, AAE-07-01, Revision 3.

FAA. 2006. Emissions Dispersion Modeling System (EDMS). www.faa.gov/about/office_org/headquarters_offices/aep/models/edms_model/.

Herndon, S. C., E. C. Wood, M. J. Northway, R. C. Miake-Lye, L. Thornhill, A. Beyersdorf, B. E. Anderson, R. Dowlin, W. Dodds, and W. B. Knighton. 2009. Aircraft Hydrocarbon Emissions at Oakland International Airport. *Environ Sci. Technol.* 43: 1730–1736.

ICAO. 1981. *International standards and recommended practices, environmental protection. Annex 16 to the Convention on International Civil Aviation, Volume II, aircraft engine emissions.* 1st ed. Montreal, Canada: International Civil Aviation Organization.

ICAO. 2006. International Civil Aviation Organization Aircraft Engine Emissions Databank. www.caa.co.uk/docs/702/introduction-05102004.pdf.

Kerrebrock, J. L. 1977. *Aircraft Engines and Gas Turbines.* Cambridge, Massachusetts and London, England: The MIT Press.

NEPAIR. 2003. *Development of the technical basis for a New Emission Parameter covering the whole AIRcraft operation.* NEPAIR Final Technical Report, WP4/WPR/01 (G4RD-CT-2000-00182).

Pison, I., and L. Menut. 2004. Quantification of the impact of aircraft traffic emissions on tropospheric ozone over Paris area. *Atmos. Environ.* 38: 971–983.

Sarli, V. J., D. C. Eiler, and R. L. Marshall. 1975. *Effects of operating variables on gaseous emissions.* Paper presented at the Air Pollution Control Association Specialty Conference on Air Pollution Measurement Accuracy as it relates to Regulation Compliance, New Orleans.

Spicer, C. W., M. W. Holdren, R. M. Riggin, and T. F. Lyon. 1994. Chemical composition and photochemical reactivity of exhaust from aircraft turbine engines. *Ann. Geophysicae* 12: 944–955.

Spicer, C. W., M. W. Holdren, D. L. Smith, D. P. Hughes, and M. D. Smith. 1992. Chemical composition of exhaust from aircraft turbine engines. *Journal of Engineering for Gas Turbines and Power* 114 (1): 111–117.

Timko, M. T., S. C. Herndon, E. C. Wood, T. B. Onasch, M. J. Northway, J. T. Jayne, M. Canagaratna, R. C. Miake-Lye, and W. B. Knighton. 2008. Gas Turbine Emissions Part 1. Hydrocarbons and Nitrogen Oxides. *ASME J Eng Gas Turbines,* submitted.

Unal, A., Y. Hu, M. E. Chang, M. T. Odman, and A. G. Russel. 2005. Airport related emissions and impacts on air quality: Application to the Atlanta international Airport. *Atmospheric Environ.* 39: 5787–5798.

Wood, E., S. Herndon, R. C. Miake-Lye, D. D. Nelson Jr., and M. Seeley. 2008. *ACRP Report 7: Aircraft and Airport-Related Hazardous Air Pollutants: Research Needs and Analysis.* Washington, DC: Transportation Research Board.

Yelvington, P. E., S. C. Herndon, J. C. Wormhoudt, J. T. Jayne, R. C. Miake-Lye, W. B. Knighton, and C. C. Wey. 2007. Chemical Speciation of Hydrocarbon Emissions from a Commercial Aircraft Engine. *Journal of Propulsion and Power* 23: 912–918.

APPENDIX C

Exhaust Probe Sampling Techniques

This appendix discusses the probe sampling hardware used during the tests. It compares the results and documents the effect of the sampling method on hydrocarbon speciation.

Background Material

The SAE Aerospace Recommended Practice (ARP1256 revision B) describes the procedures for the continuous sampling and analysis of gaseous emissions from aircraft engines for carbon monoxide, carbon dioxide, nitric oxide, nitrogen dioxide and total hydrocarbons. At the Aircraft Particle Emissions Experiment (APEX—2004), a sampling system designed to preserve the magnitude and state of engine exhaust plane particulate emissions was developed (Wey et al. 2007). The fundamental premise of the sampling system was to use dry nitrogen gas to dilute and cool the extracted exhaust just after entry into the sampling probe tip. At that same experiment, measurements of speciated hydrocarbons were conducted (Knighton et al. 2007, Yelvington et al. 2007) using the probe with dilution gas at the probe tip and on a conventional gas-sampling probe using a heated transfer line without dilution. Differences in the hydrocarbon speciation profiles obtained with the two sampling methods were observed. A detailed comparison of the hydrocarbon profile measured from a similar but older engine using an undiluted, heated Teflon line (Spicer et al. 1994) with that determined at APEX (Knighton et al. 2007, Yelvington et al. 2007) showed good agreement in the relative abundance of hydrocarbon species. Subsequent experiments in 2008 using a new "chemical quick quench" (de la Rosa Blanco et al. 2010) probe and a traditional heated metal transfer line quantified differences in the hydrocarbon compounds and attributed them to the sampling line

In order to ensure that the HAP species measured in this work are indicative of the true exit plane and were not modified by the sampling method, the test protocol investigated the hydrocarbon profile using different sampling methods during the DAL 2009 test. This section describes the results of the comparison and makes some recommendations for preserving the hydrocarbon profile during sampling. The section is broken into four sections:

- Summary,
- Known issues in sampling,
- Sampling methods tested, and
- Comparison of sample methods.

Summary

The three field deployments (MDW 2009, DAL 2009, and MDW/ORD 2010) utilized two measuring distances as well as four sampling methodologies for measuring idle exhaust during controlled engine tests. Exhaust sampled from 1-meter behind the engine was sampled through either an undiluted "gas" probe, a dilution probe, or a chemical quick quench probe (CQQ). Sample was also collected using a "mobile probe" which utilized the ARI Mobile Laboratory (AML) as the "probe" as it moved in, out, and through the exhaust plume at distances between approximately 50 and 200 meters. Figure C-1 shows a quick overview of the sampling techniques used.

Emission index measurements for CO and larger hydrocarbons generally agree using the four sampling methods. Discrepancies exist between the CQQ, dilution probes and the gas probes for the smaller hydrocarbons, specifically formaldehyde and ethylene. It appears that the most successful method of sampling at 1-meter uses a dilution probe with a non-reactive (Teflon) sample line.

Known Issues in Sampling

Highly accurate measurements are an absolute necessity for evaluating the emissions performance of an aircraft engine [JP1]. During all tests, it is critical that the exhaust be sampled and delivered to the measurement instruments without changes to the exhaust components of interest. Changes in

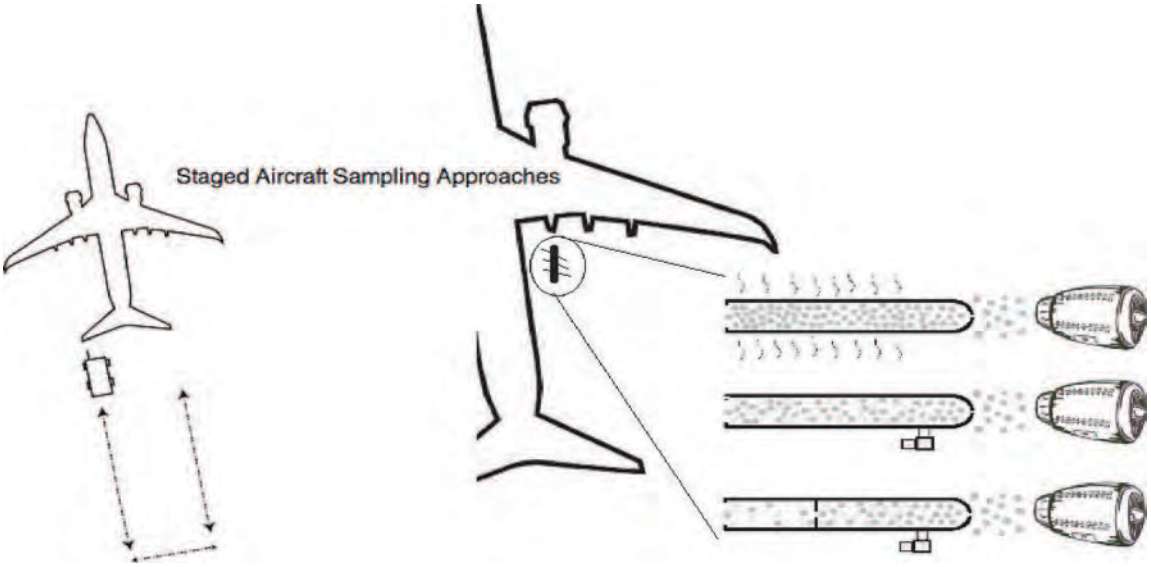

Figure C-1. Depiction of the four sampling methods used. The "mobile probe" is shown on the left. The three other sampling methods use probes placed one meter behind the engine. From top to bottom at the right are the standard gas probe, the dilution probe, and the CQQ probe.

CO and NO_x concentrations have been observed using different types of probes, different probe distances from the engine, and different methods of transportation of the sample from the probe to the analysis instrumentation. For example, at the JETS/APEX2 and APEX3 field campaigns a discrepancy existed in the emission indices of NO_2 when measured at a probe 1 m behind the engine compared to one that was 30 m from the engine. A lower emission index of NO_2 for the one meter probe was most likely caused by catalytic oxidation in the probe due to the temperature of the exhaust flow so close to the engine. When the probe was water cooled (at JETS/APEX2), the differences between 1 meter and 30 meter NO_2 emission indices were much

Table C-1. Sampling Summary, tabulates the number and types of engines and sampling methods used during the emissions tests conducted at MDW, DAL, and ORD.

Mobile Probe *Staged*			Stationary 1-meter Probe		
Test or *n*		engine	Test or *n*		Engine
MDW'09					
	1	CFM56-3			
	3	CFM56-7			
DAL '09			DAL '09		
	1	CFM56-7			CFM56-7
				1	Particle Probe (4)
					Gas Probe (2)
					CQQ Probe (3)
ORD-10			MDW '10		CFM56-7
	1	V2527		*4*	Probe (1) ARI
	1	PW4090			Probe (2) EPA

smaller and partially caused by "real" conversion of NO to NO_2 in the plume itself (rather than the probe or sampling lines) (Wood et al. 2008). Malte and Kramlich (Malte and Kramlich 1980) also reported a loss of CO and a shift between NO and NO_2 when sampling along a low pressure sample line. This shift is due to reactive species that would react with NO_2 and CO being eliminated from the mixture due to surface reactions rather than reaction in the gas flow (Malte and Kramlich 1980). Furthermore Kramlich and Malte (Kramlich and Malte 1978) reported that when the tip was hot, NO_2 is most likely reduced to NO via combination with O or H. The most widely used method of quenching chemical reactions in the transfer lines has been to dilute the sample with inert gas at the probe tip. This dilution lowers both the concentration and temperature of the reactive components of the exhaust.

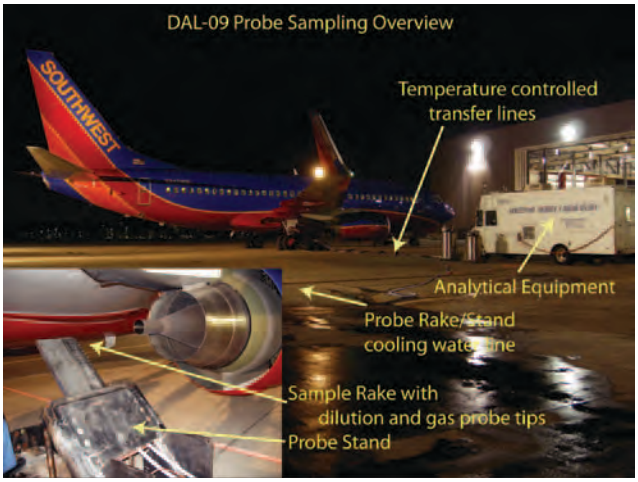

Figure C-3. Photograph depicting Staged 1-meter test setup at DAL 2009 test.

Sampling Methods Tested

Stationary 1-Meter Probe

Two main types of testing were conducted during the three mobile lab deployments (MDW 2009, DAL 2009, MDW/ORD 2010)—stationary probe measurements and mobile lab measurements. The stationary probe measurements involved a probe "rake," shown in Figure C-2, placed one meter directly behind engine 1 of the aircraft. Exhaust samples were then drawn along sample to the analytical instrumentation. The probe tip and rake system, shown on the right and below, were developed by AEDC and NASA and implemented in the stationary testing. The probe rake was integrated into the Missouri Science and Technology probe stand, which was placed directly behind engine 2 of the test aircraft and did not noticeably move when the engine was ramped up to 10% of the rated thrust. Minor modifications were required for the chemical quick quench probe tip, which previously had not been used for aircraft exhaust measurements. Sample lines, dilution lines, cooling hoses, and electrical control for the quick quench probe where then strung back via umbilical to the Aerodyne Mobile Lab, which was positioned just past the wingtip of the Aircraft being tested (Figure C-3).

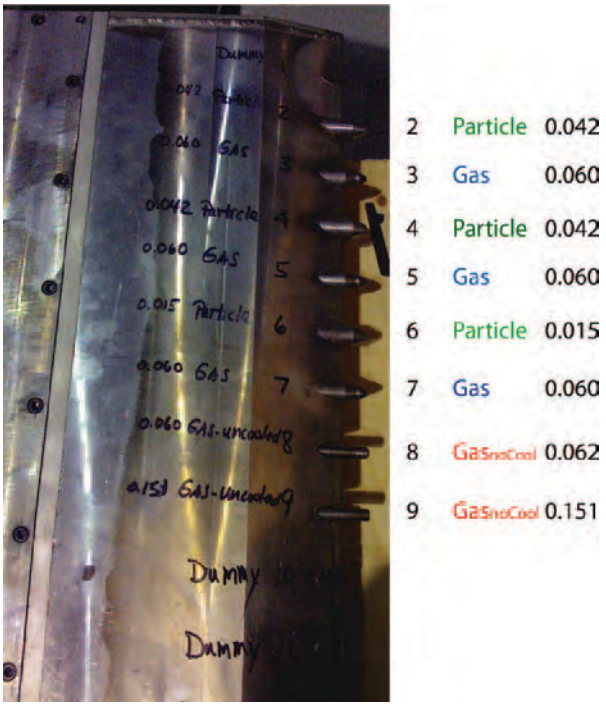

Figure C-2. The Probe Rake with various probe tips installed. The annotation to the right of the photo is the index, a description of the style of tip and the orifice diameter in inches.

Descriptions of the sampling methods:

i. Gas Probe

The gas probe is a conventional probe following the SAE 1256b recommendations and was used in the stationary 1 meter probe tests. The sample line consisted of 50 feet of ⅜″ outer diameter (OD) stainless steel tubing heated to 317°F. For the gas probe testing at DAL 2009 the exhaust was not diluted until just before being sampled by the analytical instrumentation inside the ARI mobile laboratory in order to bring the sample concentrations to within a range acceptable to the highly sensitive instruments.

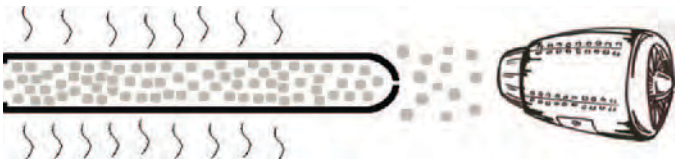

Gas Probe

ii. Dilution/Particle Probe

The dilution probe used in the stationary 1 meter probe tests consisted of 50 feet of either ⅜″ OD stainless steel tubing at ambient temperature (Particle probe at DAL 2009) or 50 feet of PFA (perfluoroalkoxy) Teflon tubing heated to 40°C (MDW 2010). For both of these tests, dry gaseous nitrogen (from liquid nitrogen dewars) was used as a diluent and mixed with the engine exhaust at the probe tip. The dilution probe used in MDW 2010 was heated to 40°C to prevent condensation of water on the walls of the transfer line due to the low ambient temperatures.

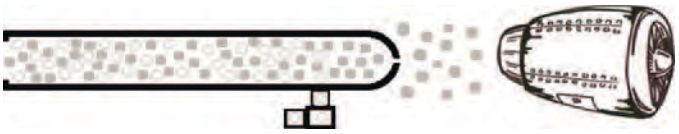

Dilution/Particle Probe

iii. Chemical Quick Quench Probe

The chemical quick quench involves nitrogen dilution at the probe tip as well as a seven fold pressure drop effected in order to minimize probe chemistry and to expedite the transfer of exhaust from the engine exhaust to the sampling instrumentation (the volumetric flow rate increased by a factor of seven following the pressure drop). The probe sample line consisted of 50 feet of ½″ OD PFA Teflon tubing.

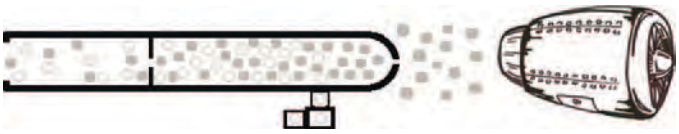

Chemical Quick Quench Probe

iv. Mobile Probe

In all three field deployments (MDW 2009, DAL 2009, and ORD 2010), for a portion of the emissions tests the Aerodyne mobile laboratory was driven behind stationary aircraft operating at varying idle engine conditions. Exhaust samples were naturally mixed with ambient air before being sampled by the inlet on the mobile lab. These tests proved to be valuable because not only could the fully evolved plume be sampled in a controlled scenario, but also did not require extended amounts of setup time that the stationary 1-meter probes need. There was also minimal contact between the exhaust and sampling tubing, since the only tubing involved was that inside the truck.

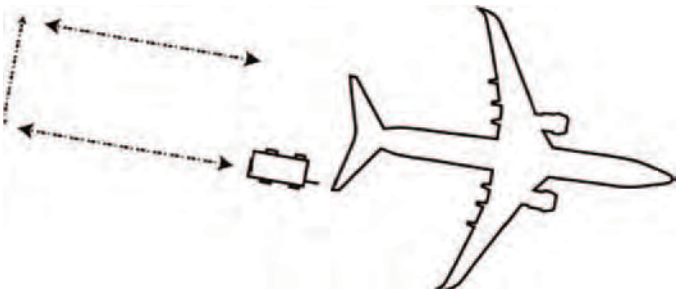

Mobile Probe

Comparison of Sample Methods

At DAL 2010 the stationary probe tests were conducted consecutively using the same aircraft (Boeing 737-700) and all tests were conducted on engine 2 (starboard). The same test matrix of near-idle engine conditions was used for each probe type. Engine conditions included the N1=25% fan speed, which corresponds to the ICAO 7% ground idle throttle setting, as well as ground idle throttle settings with varying amounts of bleed air demand which elevates the fuel flow.

For all four probe types tested in the DAL 2009 field mission, there was overall agreement for CO and most large hydrocarbons. Figure C-4 (top) depicts decreasing emission indices for CO as the fuel flow increases, using data from all probes. Figure C-4 (bottom) shows the relationship of CO emissions (measured by QCL spectroscopy) and benzene emissions (measured using the proton transfer mass spectrometer [PTR-MS]). Points in both plots marked with blue circles note points where the engine was still warming up and therefore had lower combustion efficiency. All these "warm-up" points were measured with the chemical quick quench probe. Note that as the test progressed the data became very similar to the other probe measurements. This same phenomena also occurred with the mobile probe testing where the first point recorded (ground idle with nominal bleed air) was significantly higher than the same fuel flow point at the end of the test. It is important to note that the high "warm-up" CO and benzene EI data points early in the tests are in fact variation in the engine exhaust, not instrument uncertainty because it is consistent through different analytical techniques.

While CO and the larger hydrocarbons show consistency through the three types of sample probes, formaldehyde and ethene emissions are slightly different when sampled through the gas probe (Figure-C5) compared to the other probes. Emission indices of HCHO were as much as 75% lower for the gas probe than other probes at low fuel flow rates, which is when the total emissions are greatest. The emission indices of formaldehyde are more or less constant for all gas probe points, suggesting chemistry occurring at some point in the sample process. The dilution probe points are also consistently lower than those of the chemical quick quench probe. In these tests, the dilution probe transfer line was stainless steel which might

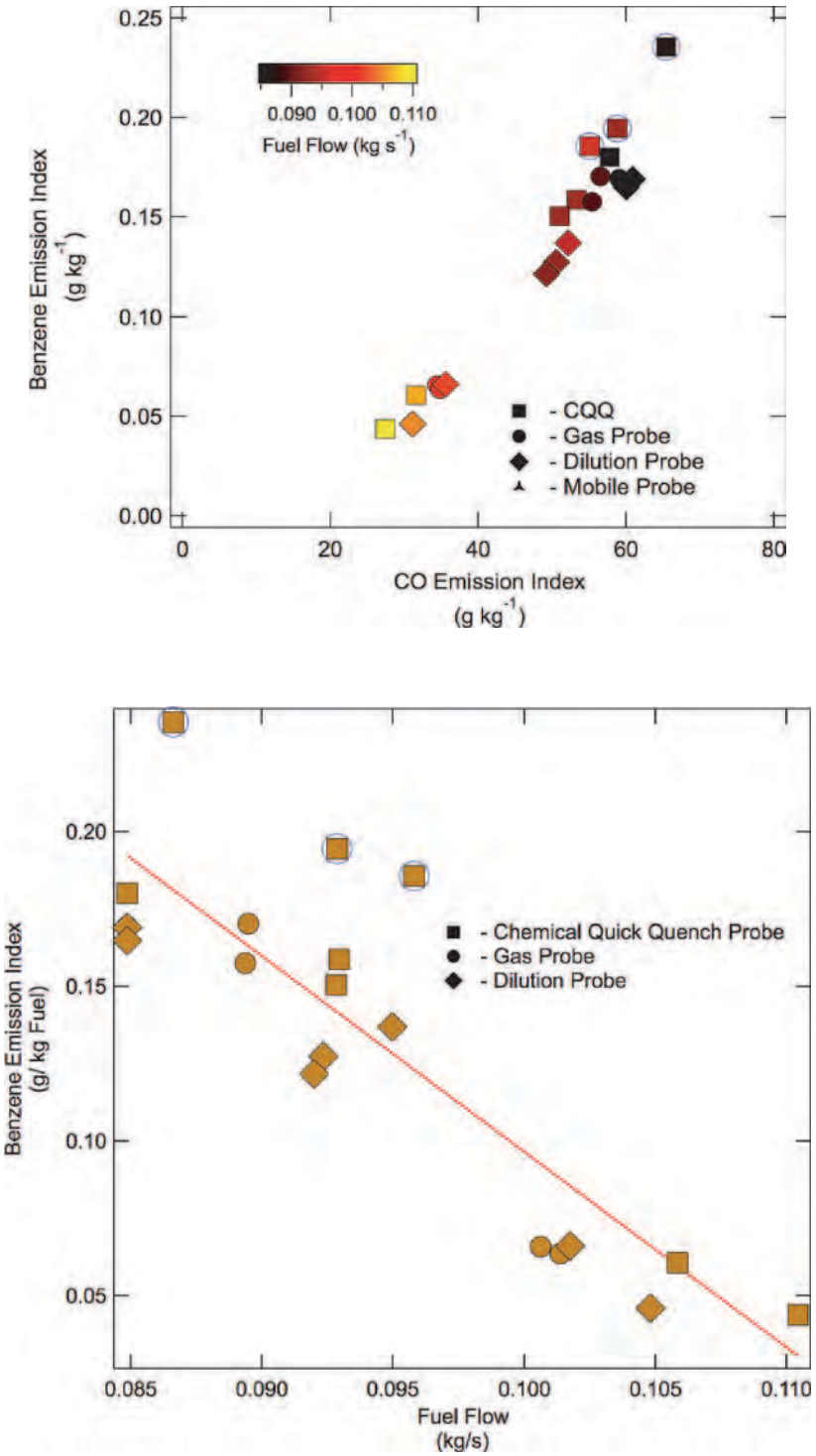

Figure C-4. CO versus Benzene Staged emission indices.

have been interacting with the sample flow similarly to the gas probe, but to a lesser extent because the sample was diluted and the walls were not being heated. CO_2, CO, and C_2H_4 concentrations are similar to those from the CQQ probe; however, the HCHO and NO_x numbers are lower.

The emission indices are actually approximately ⅓ of the values of those with nominal engine bleed during the CQQ test and are relatively static when compared to those of HCHO during the other tests. An independent measurement of HCHO provided by the PTR-MS corroborates the HCHO results shown in Figure C-5.

Figure C-6 shows three infrared spectra measured with the QC-TILDAS for a rotation-vibration set of lines for formaldehyde. Each spectra are 1 second averages collected

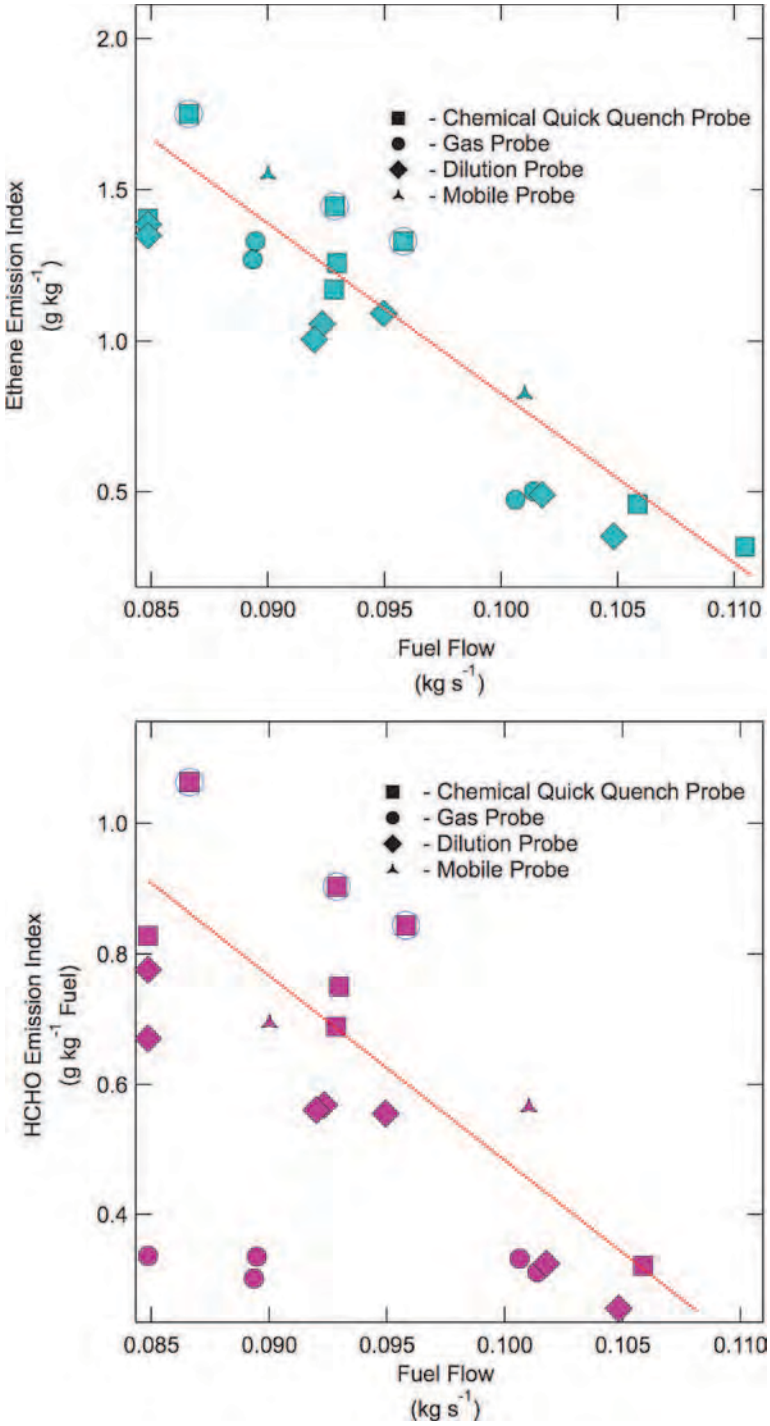

Figure C-5. Emission Indices vs. fuel flows for ethylene (top) and formaldehyde (bottom).

on three different probes. The data and fit line show the selectivity of this approach. The anomalous behavior of HCHO on the gas probe cannot be attributed to the presence of another carbonyl absorber.

Reliable sampling of semi-volatile material through long lengths of metal tubing is not achieved by either dilution on the particle probe or by heating as on the gas probe. Adsorption of the low vapor pressure compounds onto the sample line surface leads to retention of the sample within the lines. This retention leads to both a time delay and poor temporal response to rapidly changing events. The reduction in pressure employed via the quick quench probe more faithfully transports low vapor pressure compounds through the sampling lines. Assessment of reliable sampling is evaluated by examining the integrity of

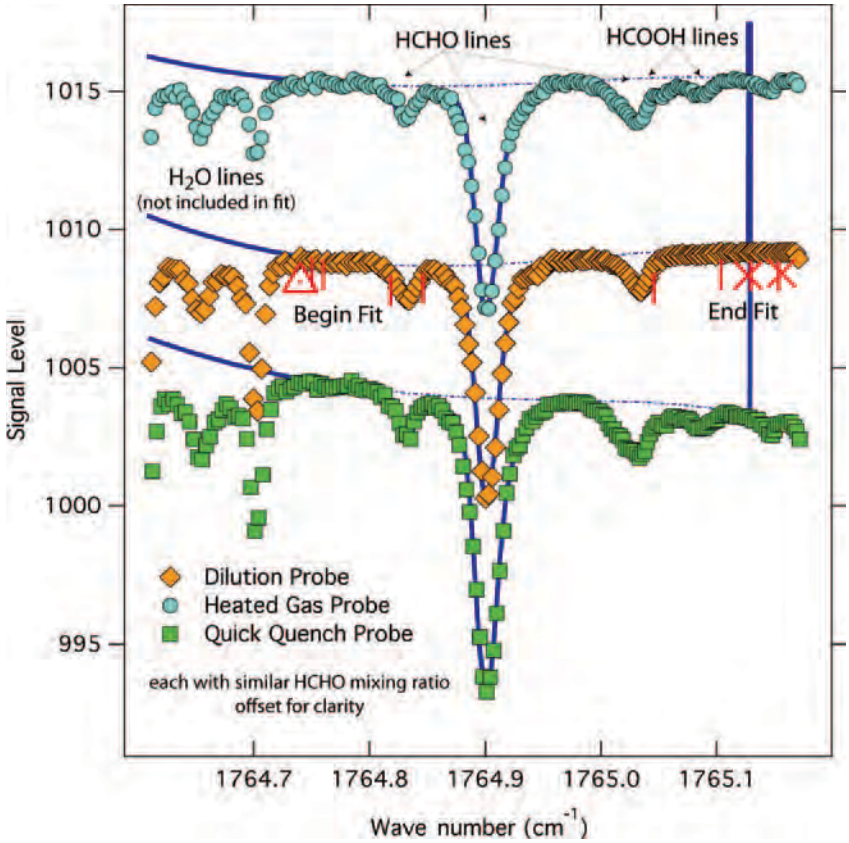

Figure C-6. Infrared absorption spectra from Aerodyne quantum cascade laser infrared spectrometer of the formaldehyde absorption line.

delivered sample from a composition and temporal perspective. To be considered reliable the sampling system must not alter the composition of the exhaust gas or perturb its temporal relationship with respect the CO_2, which serves as the dilution tracer or in the case of these figures, whose emission rate responds to the changing engine conditions.

The heated gas probe fails on both criteria set forth for reliable sampling. As discussed previously, the formaldehyde concentrations measured using this probe are altered substantially from that obtained by other sampling methods. Additionally, the temporal characteristics of semi-volatile compounds like naphthalene are not well preserved as seen in Figure-C7a.

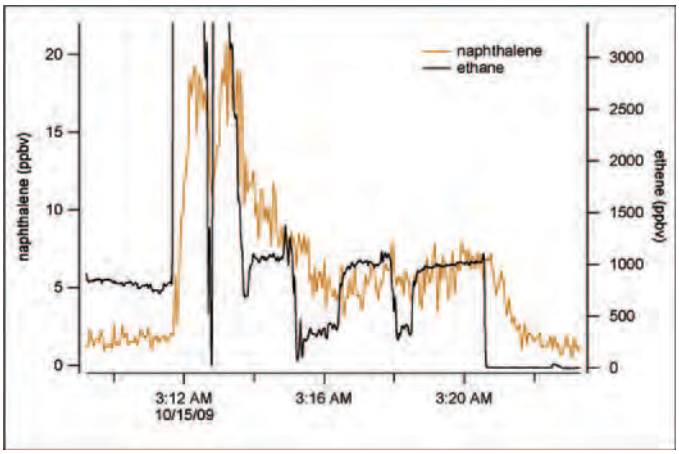

Figure C-7a. Time series of ethene (black) and naphthalene (tan) for the heated probe inlet.

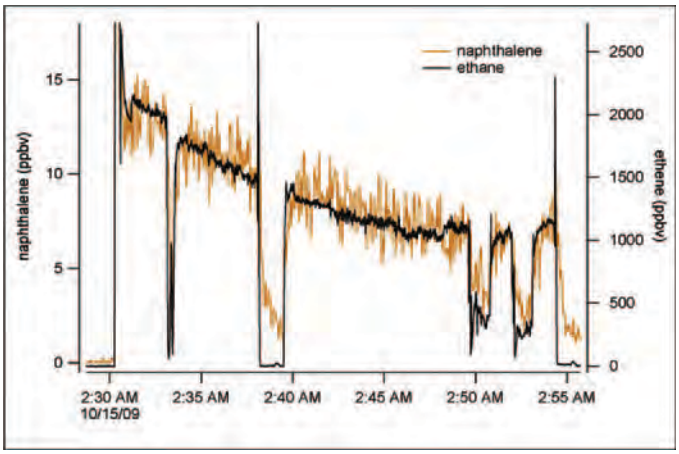

Figure C-7b. Time series of ethene (black) and naphthalene (tan) for the Quick quench probe.

The dilution probe and quick quench probes utilize dilution and dilution plus pressure reduction respectively to quench any chemical transformation from occurring within the sample lines. Both of these probes appear to limit these chemical transformations, as their results are similar. The temporal characteristics of the particle probe are similar to that observed for the heated gas probe. The quick quench probe provides much improved temporal response as can be seen in the accompanying figure. This figure shows that the naphthalene signal tracks the ethene response even during the rapid transitions in engine operation and sample line purges. The reduction in pressure employed via the quick quench probe more faithfully transports low vapor pressure compounds through the sampling lines.

Of the three stationary 1-meter probes tested during the DAL 2009 field campaign the chemical quick quench probe seemed to provide the best results for all the species of interest. It had the best time response for transferring sample from the probe to the instrumentation due to the seven fold pressure drop and appeared to maintain sample chemistry. The chemical quick quench probe might be somewhat excessive, however, for what is required. While doing staged testing at Chicago Midway airport in the winter of 2010, a dilution probe with a Teflon transfer line was implemented and seemed to minimize chemical reactions occurring in the sample line. It is the suggestion of this study not to rely on undiluted heated metal sampling for speciated hydrocarbons.

References Cited in Appendix C

de la Rosa Blanco, E., J. Peck, R. C. Miake-Lye, F. B. Hills, E. C. Wood, S. C. Herndon, P. E. Yelvington, and T. Leach. 2010. Minimizing sampling loss in trace gas emissions measurements for aircraft engines by using a chemical quick-quench probe, *Journal of Engineering for Gas Turbines and Power* 133 (7).

Knighton, W. B., T. Rogers, C. C. Wey, B. E. Anderson, S. C. Herndon, P. E. Yelvington, and R. C. Miake-Lye. 2007. Quantification of Aircraft Engine Hydrocarbon Emissions Using Proton Transfer Reaction Mass Spectrometry. *Journal of Propulsion and Power.* 23 (5): 949–958.

Kramlich, J. C., and P. C. Malte. 1978. Modeling and Measurement of Sample Probe Effects on Pollutant Gases Drawn from Flame Zones. *Combust. Sci. Technol.* 18: 91–104.

Malte, P. C., and J. C. Kramlich. 1980. Further Observations of the Effect of Sample Probes on Pollutant Gases Drawn from Flame Zones. *Combust. Sci. Technol.* 22: 263–269.

Spicer, C. W., M. W. Holdren, R. M. Riggin, and T. F. Lyon. 1994. Chemical composition and photochemical reactivity of exhaust from aircraft turbine engines, *Ann. Geophysicae* 12: 944–955.

Wey, C. C., B. E. Anderson, C. Wey, R. C. Miake-Lye, P. D. Whitefield, and R. Howard. 2007. Overview of the Aircraft Particle Emissions Experiment, *Journal of Propulsion and Power* 23: 898–905.

Wood, E. C., S. C. Herndon, M. T. Timko, P. E. Yelvington, and R. C. Miake-Lye. 2008. Speciation and Chemical Evolution of Nitrogen Oxides in Aircraft Exhaust near Airports. *Environ Sci. Technol.* 42: 1884–1891.

Yelvington, P. E., S. C. Herndon, J. C. Wormhoudt, J. T. Jayne, R. C. Miake-Lye, W. B. Knighton, and C. C. Wey. 2007. Chemical Speciation of Hydrocarbon Emissions from a Commercial Aircraft Engine. *Journal of Propulsion and Power* 23: 912–918.

APPENDIX D

Links Between Emissions and Air Quality in the Terminal and Fence Line

The focus of this project has been the quantification of HAP emissions from aircraft as a function of ambient conditions and engine type. The most immediate use of emission indices is for the generation of emission inventories, as required for environmental impact statements. Such emission inventories are also a crucial input for air quality models. Most air quality models, however, do not have the spatial resolution to predict differences in air quality between the airport ground and the airport fence line. Data collected as part of this project can partially elucidate the nature of air quality at these locations, as well as in downwind neighborhoods. Overall the emerging conclusion is that the air on airport grounds and near airports is usually not well mixed, and characterized by "background urban" air most of the time punctuated by occasional plumes of high concentrations that, depending on pollutant, can increase the average concentration considerably. Below we discuss examples at or near three airports: MDW (on the runway), ORD (on the runway and at the fence line), and OAK (2 km downwind).

Mixed Airport Emissions at ORD

After sampling the advected plumes at ORD and before the dedicated tests of the two united aircraft, the mobile lab was stationed for 25 minutes at the downwind perimeter of the airport grounds, approximately 100 m from the closest idling aircraft and over 200 m from the terminals where there was constant activity by GSE (ground support equipment) vehicles. Earlier on the airport grounds there was a clear distinction between the "background" concentrations of the various pollutants measured and the exhaust plumes from nearby aircraft and GSE vehicles, which appear as short "spikes" in the time series data (Figure D-1 between 5:45 and 6:00 pm.)

At the downwind location (6:25 pm onward in Figure D-1), the numerous exhaust plumes were more spread out in time (and therefore space) and the plumes had combined enough that the background concentrations observed earlier appeared elevated. For example, NO_x concentrations were usually between 12–14 ppb at the 1st location (5:45 pm to 6:07 in Figure D-1) and reached concentrations as high as 200 ppb for short durations, with an average concentration of 37 ppbv. At the 2nd location (after 6:20 pm in Figure D-1), [NO_x] was rarely below 22 ppbv and most spikes were less than 70 ppbv, but the average concentration was a very similar 36 ppbv. Similar results were observed for HCHO: the background (in-between-plume) concentration in the 1st position was 0.4 ppbv, with an average value of 2.6 ppb caused by a small number of short spikes that exceeded 50 ppbv. At the 2nd sampling location, [HCHO] was usually between 0.9 and 3.7 ppbv, with an average value of 1.8 ppbv.

Do the concentrations and ratios of concentrations of different species provide information that can be used to apportion the different emission sources (aircraft, GSE, etc)? Analysis of the data will surely contribute to an answer to this question. For example, a quick analysis of a one-minute section of data from 6:30 pm to 6:31 pm indicates a combined NO_x emission index of 6 g/kg fuel and an HCHO emission index of 0.3 g/kg. Comparison of these numbers to tabulated values for different emission sources may provide clues to the predominant sources. The NO_x emission index is within the (wide) range known for gasoline, diesel, and aircraft. The HCHO emission index, however, far exceeds that for gasoline and diesel vehicles, which are typically between 0.01 and 0.13 g/kg, but is lower than the values reported at these temperatures for CFM56-3x and CFM56-7x engines. This indicates a significant aircraft contribution. Further analysis of all species measured can provide more information.

Midway On-Runway Measurements

Similar measurements were recorded on February 17, 2010 on the MDW runway. Figure D-2 shows particle number density, formaldehyde, CO_2, and CO during a 30-minute time period. The air observed consisted of relatively

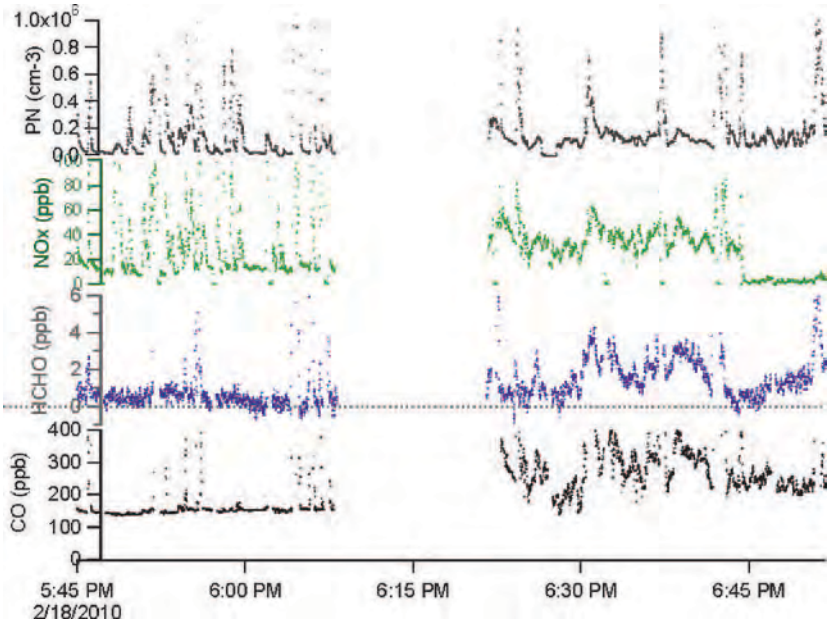

Figure D-1. Time series of four pollutants measured at ORD. Between 5:45 and 6:07, the mobile lab was positioned near the runways and observed short "spikes" of exhaust plumes. Between 6:20 and 6:50, the mobile lab was positioned several 100 meters downwind of aircraft and GSE activity, and observed an overall increase in the concentrations of all species, with "smoother" plumes that cannot always be individually identified.

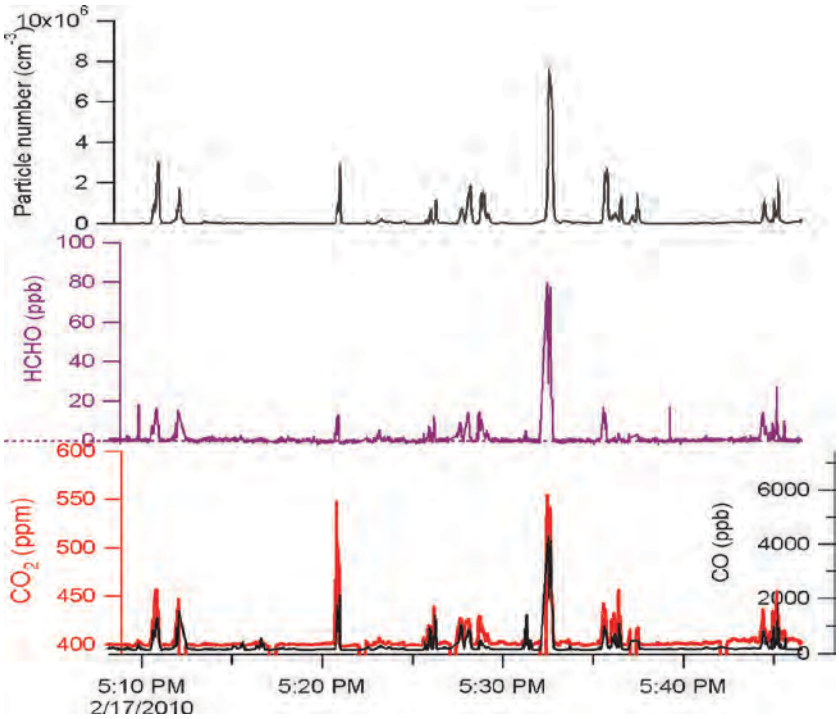

Figure D-2. Time series of data recorded on the MDW runway.

clean air most of the time punctuated by occasional short transients of very high concentrations of most pollutants measured. The average formaldehyde and particle number concentrations in between the occasional plumes were 0.2 ppbv and 10^3 particles/cm^3, respectively. As a result of the ~12 aircraft whose exhaust was sampled during this 35 minute time period, the average concentrations were increased to 1.4 ppbv and 187×10^3 particles/cm^3—results very similar to the ORD data shown above.

San Leandro Measurements

At the conclusion of the JETS-APEX2 study, the Aerodyne Mobile Laboratory spent two days at the San Leandro Marina (Figure D-3), which is ~2 km downwind of the OAK runway. Winds were consistently from the northwest. Although limited in duration, these measurements are unique in that they enabled observations of diluted airport emissions with no interferences from non-airport sources, since there is no land in between the emissions and the measurement site.

Figure D-3. San Leandro Marina and Oakland International Airport.

A 6-hour time-series of HCHO, CO, NO_x, CO_2, and PM number concentration is shown in Figure D-4. Individual aircraft exhaust plumes resulting from idle, take-off, and landing activity could be resolved. The average HCHO concentration in the time series shown is 1.3 ppb, while the interpolated background value is approximately 0.8 (similar to the background value observed on the airport grounds). More importantly, a dilution factor of ~5000 can be inferred for most of the observed plumes based on comparison of the observed CO_2 to known CO_2 concentrations at the exit of a high bypass turbine engine. Such a simplified source-receptor scheme would be an ideal scenario for testing dispersion models.

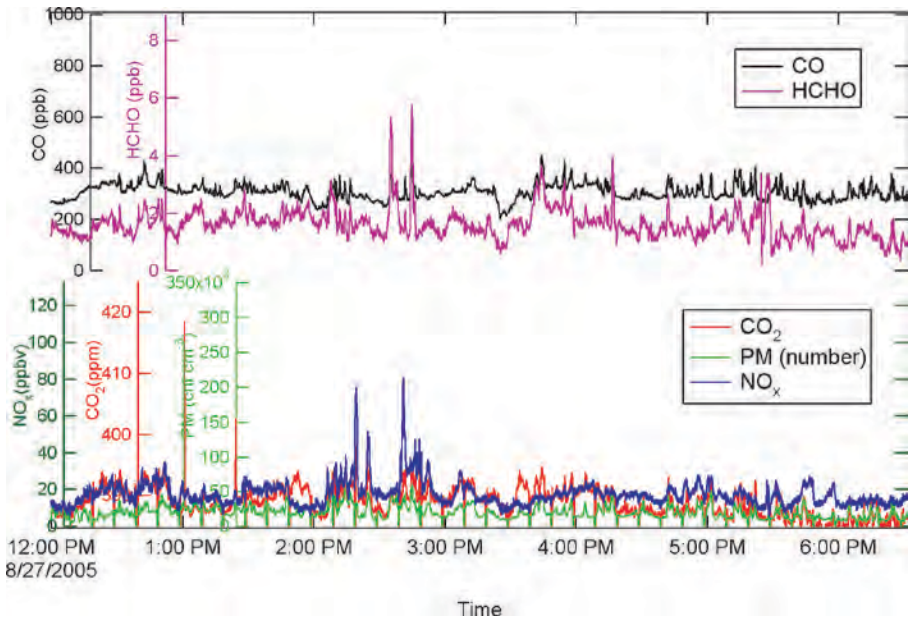

Figure D-4. Time series of measurements recorded 2 km downwind of OAK.

APPENDIX E

Quality Assurance Documentation for Analytical Methods

This section describes the results of the quality assurance procedures for the ACRP Project 02-03a that took place in February 2009, October 2009, and March 2010.

The key dilution tracer species appropriate to emission index characterization for aircraft engine is CO_2. The CO_2 emission index can be predicted quite accurately using fuel composition. If the combustor is lit, but operating away from its peak efficiency, CO is among the compounds that indicate inefficiency. Typically the CO_2 EI is 3160 g kg^{-1} fuel (Baniszewski et al. 2010). During these tests, the CO EI did not exceed 105 g kg^{-1} (or <5% of CO_2 in ppmC). This suggests that using CO_2 as the exclusive dilution tracer (or more formally the form that *all* fuel carbon is emitted in) for aircraft engine exhaust can bias the speciated hydrocarbon emission index by <5%.

This section begins by discussing analytical approach and calibration data for the principal dilution tracer and combustion product, CO_2. The subsequent section will describe the methodology and quality assurance procedures for the species measured using tunable infrared differential absorption (TILDAS). These include, CO, formaldehyde, ethane and for a subset of the work, NO_2 and methane. The majority of the HAP oxygenated and aromatic hydrocarbon compounds were measured using two related mass spectrometric methods: proton transfer reaction mass spectrometry (PTR-MS) and NO^+ mass spectrometry (NOMS). The validation of these measurement is described, both the independent calibration and when available the gas chromatographic comparison when sampling the aircraft exhaust matrix. In the final section the flame ionization detector (FID) operation and use is described in detail since this was the time the FID had been deployed on the truck sampling manifold.

Quality Assurance Description for Carbon Dioxide

This section includes a technical description of the different carbon dioxide measurement instruments deployed in ACRP 02-03a measurement campaigns at MDW 2009, DAL2010, and MDW 2010. Three different measurements of carbon dioxide were made with two employed on the sample line used for gas phase species characterization and one on the sample line used to characterize particulate characteristics.

The three different carbon dioxide instruments, a LiCor 820, and two LiCor 6262 were deployed. When the concentration range is in excess of 2500 ppmv, we use the Licor model 820 instrument equipped with the short absorption cell. When the concentration range is less than 2500 ppmv, we rely on two Licor model 6262 instruments. Occasionally, Licor model 840 are also used when the Licor 6262 is not available on a particular sampling line. The on-site calibration procedures are similar in principal for all of the units. The Licor 6262 have additional sorbent chemicals that are changed in the laboratory prior to deployment.

The LiCor instruments are non-dispersive infrared gas analyzers and have precisions under 1 ppm for the model 820 and under 600 ppb for the model 6262. Zeroes and spans were taken by overblowing the inlet to the instrument with either CO_2 free N_2 or calibration span gas. The instruments were calibrated to the span values after the readings were taken. All spans, subsequent to the initial setup calibration, were within 1% of the span value, which was gas taken from a tank certified to 1000 ± 20 ppm by the manufacturer (Scott Specialty Gases) and certified to 994 ppm by an absolute CO_2 measurement (accurate to 1%). Intercomparisons of this CO_2 standard with a second, independent 1% accuracy tank (Scott Marin gases) owned by University of California, Berkeley showed that both standards agreed within 0.7%.

The experience with these instruments suggests they typically hold their calibration very well when they are not subjected to caustic pressure changes and when particulate matter is filtered from the sample gas. The sample gas is moved through the instrument in two ways depending on the experiment. In the dedicated engine testing on the 1 meter probe (DAL 2009 and MDW 2010), there is little hope of having the manifold pressure be constant. To prevent the instrument from experiencing the pressure fluctuations in the manifold, we use a

sealed diaphragm pump to compress sample and "push" it through the instrument. The flow through the instrument is monitored with a venturi flow meter on the outlet to ensure that the instrument is always sampling continuously.

In the mode when sampling from atmosphere, when sampling from the front of the truck (exclusively at MDW 2009 and during the airport operations phases of all tests), we use the vacuum pump and a critical orifice to draw sample through the instrument. Generally, in this mode the QC-TILDAS instrument, described earlier, controls valving which periodically floods the inlet with zero air. This serves several functions. The licors are zeroed by this process, the time response is evaluated and any sample line temporal offset (1–2 seconds) is measured for all instruments on the manifold.

Quality Assurance: TILDAS Instruments

Measurements of CO, formaldehyde, ethane, NO_2 and methane

The instruments documented in this section employ Tunable Infrared Laser Differential Absorption Spectroscopy (TILDAS) as the fundamental analytical method for quantifying trace compounds. Although TILDAS methods using tunable diode lasers have been widely used for a variety of trace gas measurements (Sachse et al. 1987, Zahniser et al. 1995) the requirement for cryogenic cooling of lasers and detectors and the uneven quality of lead salt diode lasers has limited wider application of TILDAS methods. Improvements in engineering led to the development of the instrument deployed to the aircraft exhaust studies, robust and portable instrumentation that can operate without cryogenic cooling of the laser (Herndon et al. 2006, Jimenez et al. 2005, McManus et al. 2005, Nelson et al. 2002, Nelson et al. 2004)

During the ACRP 02-03a deployments the twin dual quantum cascade laser based instruments were configured to measure CO and formaldehyde (in the first chassis) and ethane and a second species (in the second chassis). The second species was NO_2 in the MDW 2009 and DAL 2010 but methane in the MDW 2010 test. An example spectrum depicting the spectrum and analysis software is depicted in the inset (Figure E-1).

The measurement of CO, though not specified by the research objective, is still fundamental to the overall approach of using fuel carbon content to arrive at mass per mass of fuel emission indices following the ICAO convention. CO was quantified using the singlet transition located at 2165.6 cm^{-1}. Formaldehyde (HCHO) was measured using a cluster of absorption lines at 1764.9 cm^{-1}. Ethene (C_2H_4) was measured using a pair of lines at 952.08 cm^{-1}. Nitrogen dioxide (NO_2)is also not specified by the program objective, however, we note that it has been extremely useful in prior measurements for helping rule out other potential emissions sources as well as been a keen diagnostic of the idling aircraft engine. It was measured using the absorption lines near 1599.9 cm^{-1}.

Although the QC-TILDAS method is fundamentally an absolute Beers-law absorption technique that does not require calibration, Aerodyne has found that the use of calibration procedures, either in the field or in the laboratory prior to deployment is a mandatory practice. The analysis

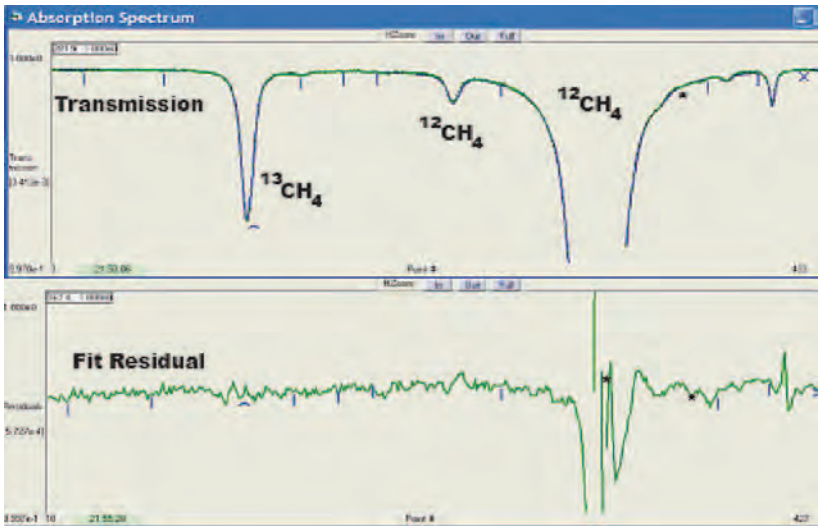

Figure E-1. Experimental spectrum with 210 m pathlength, 30 Torr, and CH4 mixing ratio of 1870 ppb with an averaging time of 30 s. The upper panel shows experimental spectrum (points) and fit (solid line) to the data using HITRAN spectral lines for 12CH4 (peak absorbance 0.07) and 13CH4 (peak absorbance 0.0022). The lower panel shows the residuals to the fit with a root-mean-square deviation of 10-5 absorbance units.

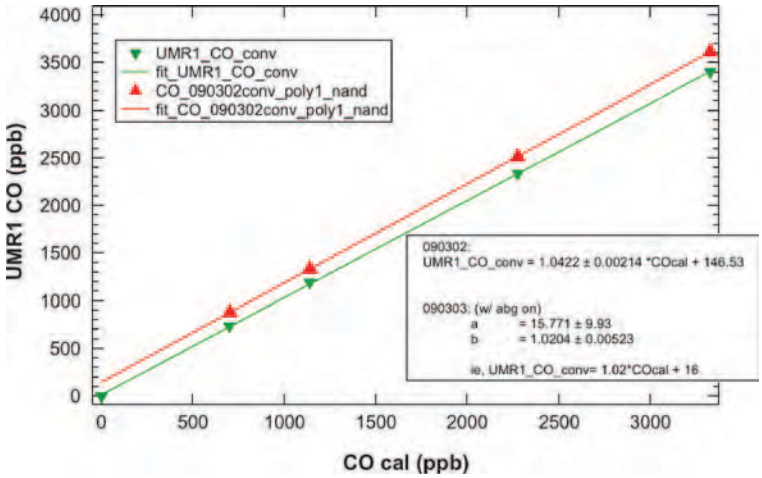

Figure E-2. In field calibration procedure used for CO.

software records all direct absorption spectra, which can facilitate archival re-analysis that retains substantial value if there are any future discoveries about the spectroscopy.

There are some fundamental sources of systematic error though that have to be checked and monitored that can foil this method. Typically the calibration is used to fix the source of the problem. The analytical method is an absolute number-density detection scheme, that is to say it counts the molecules along the beam path in the absorption cell. In order to convert this measurement to a mixing ratio, the cell pressure and temperature need to be accurately measured. The temperature measurement is known to be good to +/– 1K which is less than 1%. The pre-measurement checks for pressure are to compare the three manometers in the truck during stopped or very shallow flow to ensure they agree. Periodically the pressure heads are calibrated by the factory. They do require as much warm up time as the instrument itself for true readings.

The CO measurement was calibrated using a separate gas standard diluted in a dynamic calibration box. The result indicates the spectroscopic retrieval is within 4% of the imputed calibration concentration and the methodology has linearity over the range of CO encountered in this test (see Figure E-2).

A recent comparison of this instrument chassis and laser at a separate measurement campaign (not ACRP 02-03a related) of our calibration standard to one provided by collaborators from the University of California, Berkeley was excellent. They used a CO standard cylinder from Scott-Marin (a supplier) with a NIST-traceable uncertainty of 1%. QCL measurements (incorporating the correction indicated by calibrations with our CO source) of a sample of their 10.21 ppm calibration gas read 10.35 ppm—a difference of only 1%. This supports the accuracy of our calibrated CO measurements and implies the calibration procedure accounts for systematic biases in the components of the instrument including imperfections in our laser. The pulsed quantum cascade lasers in this instrument have a broader linewidth compared to the cw lasers, and the laser lineshape is not always symmetric. Any multi-mode character in the laser would also contribute to the QCL measurement being low. We conclude that the overall spectroscopic certainty in the analytical method of TILDAS applied to the detection of CO is accurate to 4%.

A new laser device that operates at a more favorable wavelength for the detection of C_2H_4 was acquired just prior to MDW 2009. The old laser was calibrated against gas chromatography during an eight week campaign and found to be within 3% of those measurements. The ethene measurement that will be done under this work has been calibrated against a standard cylinder of ethene, similar to the calibration of CO and NO. The same compressed gas cylinder contained the standards for methane, acetylene, and ethylene, thus calibrations for all three species were executed simultaneously. Figure E-3 shows the excellent agreement (1%) between the

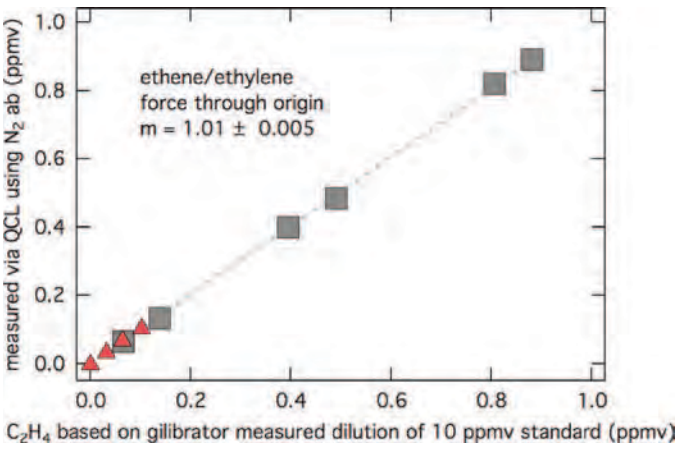

Figure E-3. The measured ethene mixing ratios are plotted vs the concentration of the diluted standard. The two sets of points represent two different dilution schemes (grey squares = dual gilibrator dilution; red triangles = automatic dilution calibration system)

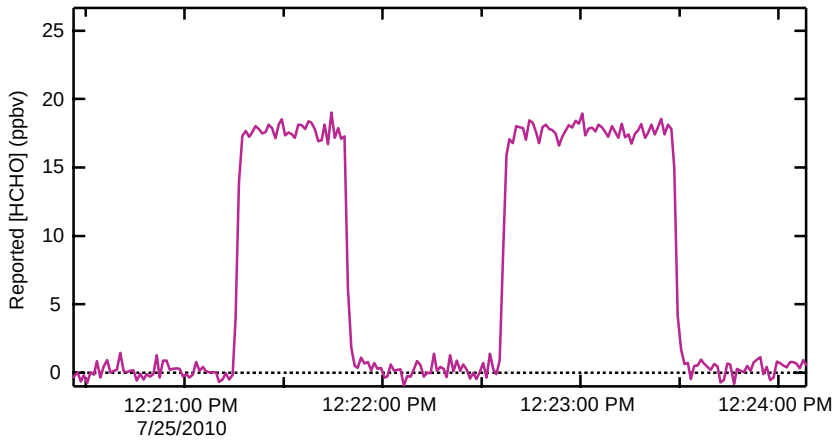

Figure E-4. The "top-hat" appearance of the time-series data shown in the figure above results from sudden introductions of the permeation tube flow (HCHO standard) into the total instrument flow.

QCL instrument's internal spectroscopic quantification of ethene and the calibration mixture prepared from the standard cylinder.

The accuracy of the HCHO measurement (using QC-TILDAS) is checked by sampling the output of a well-characterized permeation tube at a known dilution rate. The permeation flow stability requirement is high. As a result, these characterizations are typically performed when ample time is available to stabilize the output of the device. Because the on-wing aircraft testing involves being hosted by an airline, we often do not have time in the field to wait for stabilization. Thus the formaldehyde perm source characterization for the MDW 2009 test was performed prior to the test at Aerodyne. Similarly, the instrument was checked during and subsequent to the MDW 2010 sampling campaign. We have no evidence of any systematic drift in the verification of the formaldehyde instrument.

The procedure is described in the following example. The permeation flow was diluted into a total flow of 3.11 LPM as measured with a recently calibrated gilibrator flow meter. The reported concentration at cell pressures of both 26 Torr and 14 Torr was 17.73 ppbv. The calculated mixing ratio, based on a permeation rate of 62 ± 8 ng/min, atmospheric pressure of 735 Torr and ambient temperature of 298 K, is {1.24E15 molecules/min/3.11 liters/min}×{1 liter/1000 cm^3}/ 2.38E9 molecules/cm3 = 1.675E-8, or 16.75 ppb.

The difference of 0.98 ppbv out of 16.75 ppbv is 5.9%, well within the uncertainty of the HCHO permeation rate (12.9%). The overall accuracy of the HCHO measurement is 7%.

A second permeation rate using a different (lower range) HCHO device was also used to verify the spectroscopic certainty in the TILDAS/QCL approach. The result of this independent test is depicted in Figure E-5.

The data in Figure E-6 shows results of two calibrations performed after MDW 2010; the red triangles using the flow meter pair in the dilution box and the orange diamonds using two gilibrator measurements of flow to determine dilution levels. The agreement between both methods is excellent and values of methane measured with the spectrometer have not been adjusted by the factor 1.02 suggested by the calibration procedure. This provides a citable calibration based strictly on the well-researched and documented spectroscopy behind the HITRAN database (Rothman et al. 2008). The overall systematic uncertainty in the methane instrument is estimated to be 6%, based in part on the linestrength literature for these methane absorption lines and in part on the agreement with the independent calibration performance check documented here.

Proton Transfer Reaction and NO^+ Mass Spectrometry

Method Overview

Proton transfer reaction mass spectrometry (PTR-MS) is a chemical ionization mass spectrometry technique that utilizes H_3O^+ as the principal reagent ion. H_3O^+ reagent ions are generated in an external hollow cathode ion source through direct ionization of water vapor. These reagent ions are electrostatically injected into a drift tube reaction region where they merge with the gas to be sampled that has been reduced in pressure (~2 mbar). The drift tube reaction region is formed by a series of concentric stainless steel rings compressed between Viton or Teflon o-rings, which serve to electrically isolate the drift rings and provide a vacuum seal. The drift rings are electrically connected via a series of resistors. An electric potential applied to the top of the drift tube creates

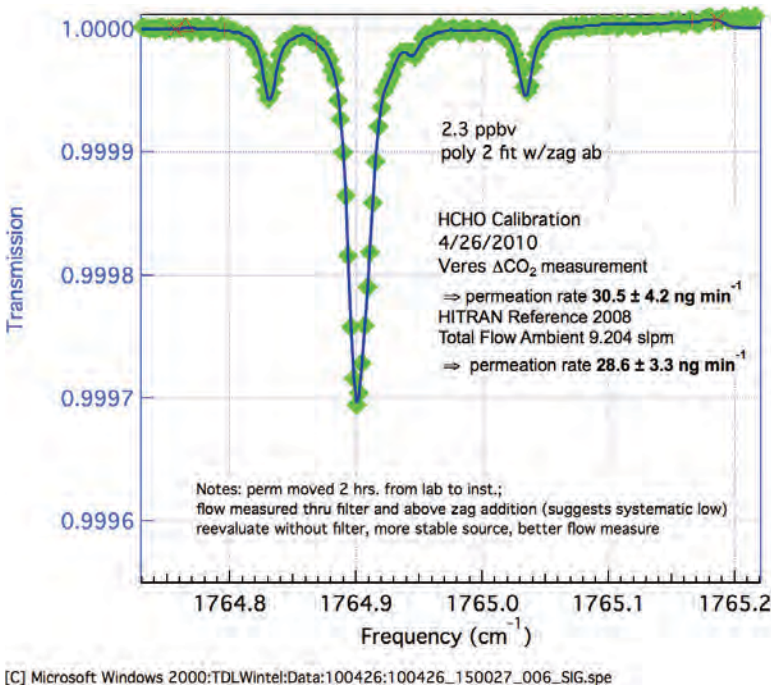

Figure E-5. Independent Calibration of HCHO Spectroscopy. The Figure depicts a spectrum collected during an independent check of the permeation rate of a second calibration device. The raw agreement between the catalytic conversion method and the online spectroscopic method is 6% for this trial. This verifies the quoted accuracy of the overall TILDAS-QCL approach.

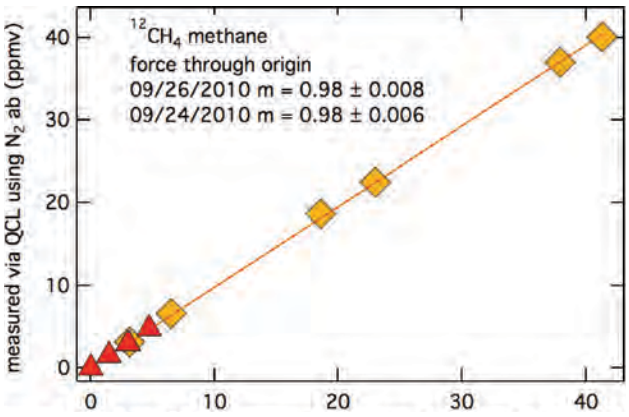

Figure E-6. The results from the QCL measurement of methane are plotted vs. the expected mixing ratio determined by dilution of the methane standard. The dilution levels for the points noted as orange diamonds were generated using two gilibrator based flow measurements. The dilution levels for the points noted by the red triangles were determined using the in-lab dilution and calibration system.

a uniform electric field which transports any positive ions through the drift tube. H_3O^+ reagent ions within the drift tube are pulled through the sample gas by the electric field where they will react upon collision with any molecule having a proton affinity greater than that of water. It is important to note that the primary components of air: N_2, O_2, Ar, CO_2, and the alkanes all have proton affinities less than water and thus do not react with H_3O^+. Most other organic substances except for acetylene and ethene react with H_3O^+ via a proton transfer reaction, reaction 1.

$$H_3O^+ + R \xrightarrow{k} RH^+ + H_2O \qquad \text{(R1)}$$

The proton transfer reaction forms the protonated molecule RH^+, which is a stable reaction product in many cases. The drift tube reaction region is terminated by a plate that contains a small aperture through which a fraction of the unreacted reagent ions and product ions are extracted, focused into a quadrupole mass spectrometer and detected using a secondary electron multiplier. The resulting mass spectrum contains quantitative information regarding the composition of the gas sample, providing that the composition of the sample is known or can be deduced.

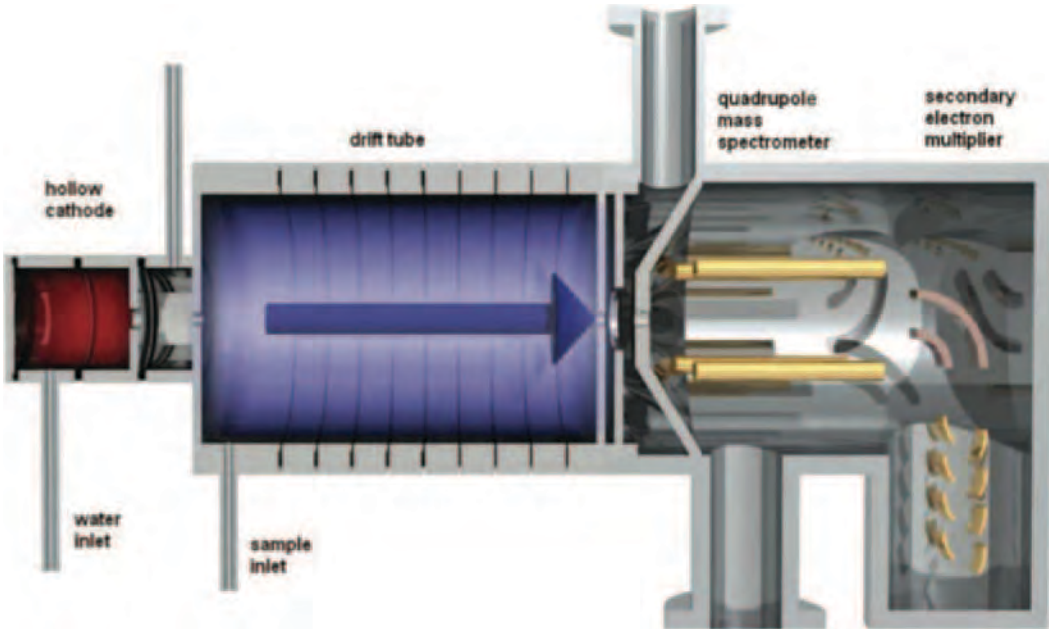

Figure E-7. Schematic of the PTR-MS.

The PTR-MS can be adapted to employ NO^+ as the reagent ion by switching the hollow cathode source gas from water vapor to dry air. NO^+ reacts via a charge transfer reaction, reaction 2, with compounds having ionization energies lower than 9.26 eV:

$$NO^+ + R \xrightarrow{k} R^+ + NO \qquad \text{(R2)}$$

NO^+ provides greater measurement specificity as only the dienes and the aromatic hydrocarbon exhaust components fit this criterion. This technique was developed specifically for the measurement of 1,3-butadiene.

Quantification

Quantification of the PTR-MS ion signals is possible directly from first principles, but is most reliably done via calibration with certified gas standards. In this test the concentrations reported were evaluated from calibrated response factors, except for naphthalene for which a calibration standard was not available. Naphthalene was quantified using a sensitivity factor based on a surrogate (discussed below).

The standard equation for quantifying a target compound, designated generically as (R) is shown in equation PTR-1.

$$[R] = \left(\frac{I_{RH^+}}{I_{H_3O^+} + X_R I_{H_3O^+(H_2O)}}\right)\left(\frac{10^6}{S_R}\right)\left(\frac{T}{300}\right)^2\left(\frac{2}{P}\right)^2 \qquad \text{(PTR-1)}$$

The term [R] represents the concentration of R in ppbv. S_R is the sensitivity factor expressed as normalized counts per second (ncps) per ppbv T and P represent the drift tube temperature and pressure respectively that are referenced to a standard condition. The term $\left(\frac{I_{RH^+} \bullet 10^6}{I_{H_3O^+} + X_R I_{H_3O^+(H_2O)}}\right)$ represents the product ion response expressed in ncps, which is the mass spectral intensity of RH^+ measured in cps per 1 million reagent ions. This normalization step accounts for any variation in the product ion intensity resulting from changes in the reagent ion intensity. The intensity of H_3O^+ is too large to measure directly and its intensity is determined by measurement of the O-18 isotope of this ion detected at m/z 21, which is then multiplied by 500 to correct for the isotopic dilution. Measurement of the intensity of $H_3O^+(H_2O)$ is measured directly at m/z 37. Some components react with both H_3O^+ and $H_3O^+(H_2O)$ while others do not. The X_R term is a factor between 0-1 that accounts for the reactivity difference between $H_3O^+(H_2O)$ and H_3O^+ towards R.

Quantification with the NO-MS is accomplished in an analogous fashion as shown in equation NOMS-2.

$$[R] = \left(\frac{I_{R^+}}{I_{NO^+}}\right)\left(\frac{10^6}{S_R}\right)\left(\frac{T}{300}\right)^2\left(\frac{2.1}{P}\right)^2 \qquad \text{(NOMS-2)}$$

The term [R] represents the concentration of R in ppbv. S_R is the sensitivity factor expressed as normalized counts per second (ncps) per ppbv T and P represent the drift tube temperature and pressure respectively that are referenced to a standard condition.

Table E-1. Gas standards employed in the calibration of the PTR-MS and GC/FID during ACRP 02-03a.

Gas Standard Identifier	Components	Concentration
Scott Specialty Gas	1,3-butadiene in N_2	10.1 ppmv
MSU-multicomponent	methanol in N_2	520 ppbv
	acetonitrile in N_2	520 ppbv
	propene in N_2	480 ppbv
	acetaldehyde in N_2	490 ppbv
	acetone in N_2	500 ppbv
	isoprene in N_2	440 ppbv
	methacrolein in N_2	410 ppbv
	benzene in N_2	510 ppbv
	toluene in N_2	500 ppbv
	styrene in N_2	480 ppbv
	p-xylene in N_2	480 ppbv
	1,2,4-trimethylbenzene in N_2	480 ppbv
	alpha pinene in N_2	410 ppbv

Calibration

Calibrations were performed by dynamically diluting certified gas standards with dry compressed air or VOC free air generated by passing ambient air through a heated Pt catalyst. Several gas standards were employed. The 1,3-butadiene calibrations were performed using single component standard, Scott Specialty Gases. Sensitivity factors for all other components were evaluated using a multi-component standard (Apel-Reimer) owned by MSU. The stated accuracy of standards is +/– 5%. Table E-1 provides composition information on the gas standards used.

Flows of the gas standards and the dilution gas were controlled using mass flow controllers. The outflow from the mass flow controllers was mixed together and delivered to the sample inlets of the two PTR-MS instruments and GC/FID. In all cases, the PTR-MS instruments and the GC/FID were all calibrated using the same gas mixtures.

Calibration checks were performed daily. Day to day variations were within +/–10% and attributed to statistical variability of the method and an average sensitivity factor was employed to compute the reported concentrations. The calibration factors employed in this study are summarized in Table E-2.

Table E-2. Compound response factors for the PTR-MS and NO-MS instruments during ACRP 02-03a. The PNL PTR-MS was deployed at MDW 2009 and MDW 2010. The MSU PTR-MS instrument was deployed as the NO-MS at MDW 2009 and MDW 2010 and as a PTR-MS at DAL 2009.

	MDW 2009			DAL 2009		MDW 2010		
Compound	NO-MS	PTR-MS		PTR-MS		NO-MS	PTR-MS	
	S_R	S_R	X_R	S_R	X_R	S_R	S_R	X_R
acetaldehyde	---	24.2	1	27.7	0.34		10.3	1
1,3-butadiene	14.2	---		---		12.0	---	
benzene	15.2	14.7	1	22.2	-0.21	13.0	6.3	1
toluene	20.6	15.7	1	29.2	0.045	17.6	6.2	1
styrene	25.2	---		27.4	0.35	21.0	6.1	1
p-xylene	27.4	---		31.1	0.33	22.3	5.5	1
naphthalene	25.5	---		32.0	0.37	20.7	4.5	1

Estimation of Uncertainty

The PTR-MS technique does not have any official adopted protocol for evaluation of measurement uncertainty. Measurement uncertainty arises from two main sources: 1) the purity of the ion signal (i.e., does all of the signal arise from a singular compound or from multiple compounds) and 2) uncertainties in the measured ion intensities and the calibration response factors S_R and X_R. With respect to 1, it must be recognized that the interpretation of the mass spectrum of the PTR-MS or the NO-MS is critically dependent on the sample matrix. The ions used to monitor the compounds reported in this study have been evaluated extensively for the PTR-MS (Knighton et al. 2007; Wey et al. 2006) and to a lesser extent for NO-MS (Knighton et al. 2009), which is a newer technique. Except for naphthalene, a GC coupled to the PTR-MS (Timko et al. 2011) or the NO-MS (Anderson et al. 2010) has been used to verify the ion assignments in the jet engine exhaust matrix. The sample introduction system for our GC does not efficiently transfer semivolatile compounds (i.e., naphthalene) to the GC column. The cumulative body of our work on jet engine exhaust supports that acetaldehyde, 1,3-butadiene, benzene, toluene, and styrene can be reliably measured within the aircraft exhaust matrix and no additional discussion of these compounds is warranted.

The determination of the C2-benzenes (sum of ethylbenzene and xylene isomers) and naphthalene requires additional discussion. The PTR-MS measurement at m/z 107 actually reflects the sum of the C2-benzenes plus benzaldehyde (C_7H_6O), because the quadrupole mass spectrometer lacks the resolution to separate these compounds. This result is illustrated in the accompanying Figure E-8, which shows the GC/PTR-MS trace of m/z 107 taken from a jet aircraft engine burning JP8 fuel. The peaks have been annotated to identify the C2-benzene isomers and benzaldehyde. The distribution (relative peaks areas) of these species has been consistently observed in other GC/PTR-MS measurements and agrees well with the exhaust profile reported in SPECIATE. This result in concert with our observation of near-idle VOC emissions scaling has been used to adjust the PTR-MS measurements made in DAL 2009 to reflect only the C2-benzenes. The PTR-MS measurements in DAL 2009 were scaled based on the SPECIATE distribution that the C2-benzenes represent 57% of the measured m/z 107 signal. This has been done so that the PTR-MS results can be compared directly to the measurements made with the NO-MS. NO^+ does not react with benzaldehyde and the NO-MS instrument provides a direct measure of only the C2-benzenes.

The attribution of naphthalene to the m/z 129 (PTR-MS) and m/z 128 (NO-MS) measurements comes with greater uncertainty, as these results have not been confirmed by independent GC evaluation. Furthermore, the lack of calibration standard for naphthalene increases the uncertainty in the absolute quantification. There are no known or anticipated interferences to the determination of naphthalene with the PTR-MS (Knighton et al. 2007). The NO^+ determination is less certain as it is known that this ion can react with 1-heptene by an association reaction and with the larger alkenes (>C7) via an insertion mechanism to produce ions at m/z 128 (Diskin et al. 2002). The electric field employed in PTR-MS and NO-MS techniques strongly discriminates against association reactions so the interference from 1-heptene is expected to be minimal. Less is known about how the electric field will affect the insertion reaction channels. Quantification of naphthalene is based off the calibrated response factor of 1,2,4-trimethylbenzene. 1,2,4-trimethylbenzene is chosen as surrogate for naphthalene because it is similar in molecular weight, has comparable

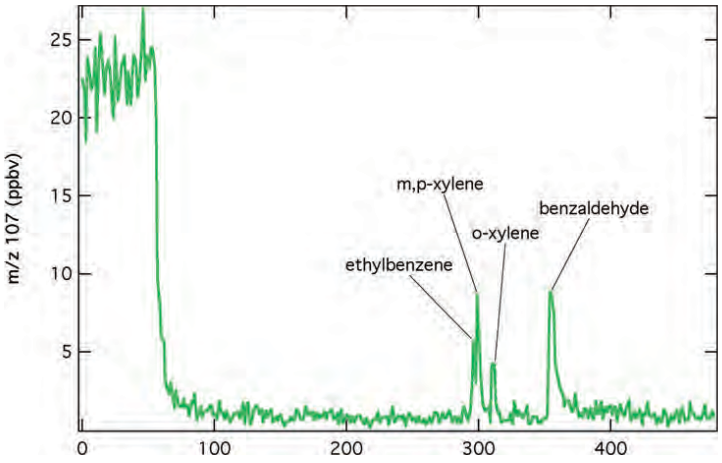

Figure E-8. GC/PTR-MS trace of m/z 107 for a jet engine burning JP8 fuel.

reaction rate constants and is present in calibration gas. It is recognized that the naphthalene determination is heavily caveated and that these measurements should not be over interpreted. We believe the naphthalene measurement is sufficiently valuable to justify its inclusion in this data set. Naphthalene is the only semivolatile compound present in jet engine exhaust at sufficient levels to be assessable by either the PTR-MS and NO-MS. As a semivolatile it will be the first to condense onto the sample lines or existing particles and thus serves as a valuable marker for evaluating the integrity of the extraction probes and the associated sample lines.

The precision of the sensitivity factors derived from the individual calibration experiments generally falls within the +/−10% level. Evaluation of the uncertainty in the ion intensity measurements requires defining a specific time base. A single 1-second measurement will have a greater uncertainty than a time averaged series or ensemble of data points. Rather than specifically deriving an uncertainty value it is more appropriate to provide an estimate. Since Poisson statistics governs the variability in the ion intensity measurements the noise in the ion signal scales in proportion to the magnitude of the response. This means the relative uncertainly remains essentially constant and independent of sample concentration. Assuming a 10% uncertainty to both the ion intensity measurements and the calibration factors leads to an overall uncertainty of approximately 15%. The uncertainty will be greater for the determination of the C2-benzenes since this determination is for a collection of isomers. The p-xylene calibration factor has been applied for the quantification of the C2-benzenes. Naphthalene has the greatest uncertainty since it employs a surrogate sensitivity factor. The uncertainty is naphthalene measurement is estimated to be 30%.

Comparison of the PTR-MS and NO-MS measurements at MDW 2010

Four compounds—benzene, toluene, styrene, and naphthalene—were monitored and quantified by both the PTR-MS and NO-MS techniques during the MDW 2010 dedicated engine tests. Figure E-9 depicts the results of side-by-side comparison and illustrates that both instruments provided reproducible results. All of the measurements appear to be well correlated, but show poorer quantitative agreement than was anticipated. The PTR-MS data are ~30% higher than the corresponding NO-MS measurements

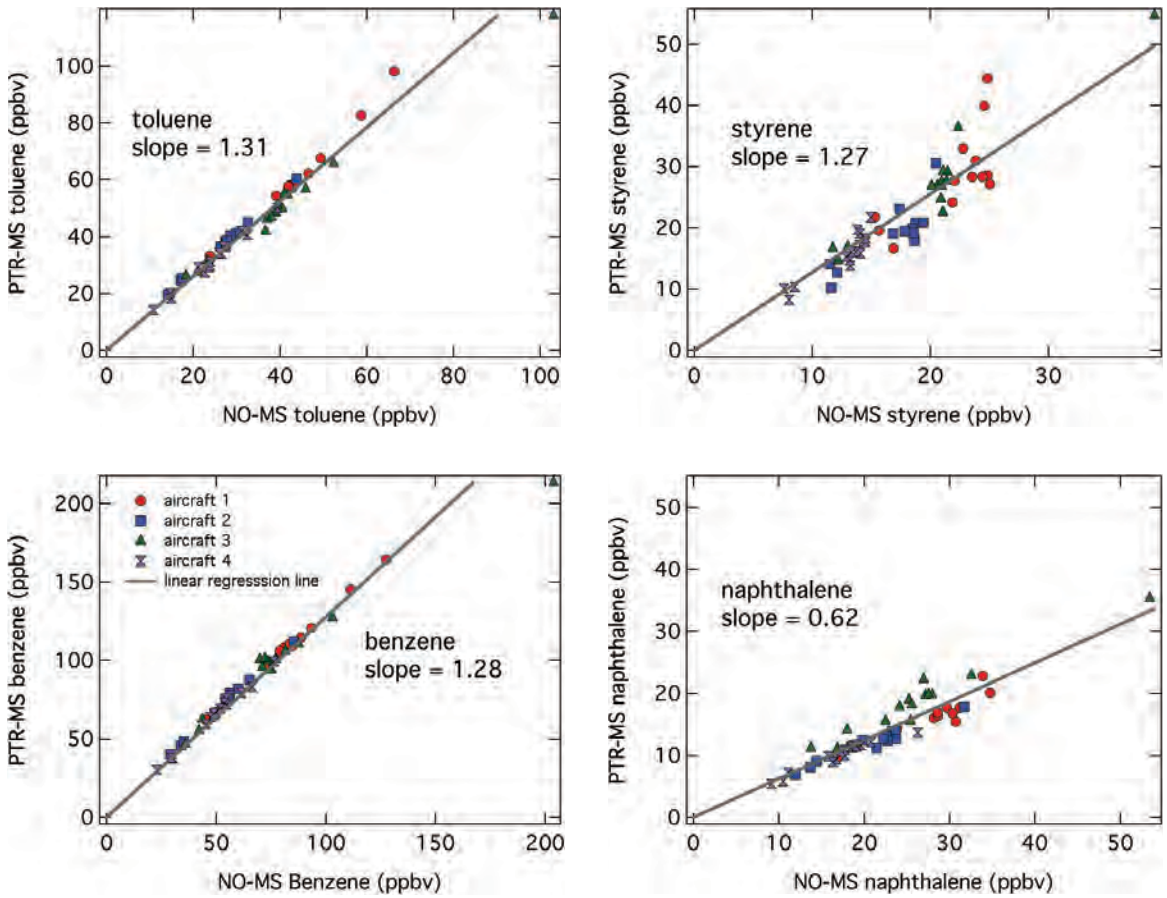

Figure E-9. Comparison of PTR-MS and NO-MS measurements at DAL 2010.

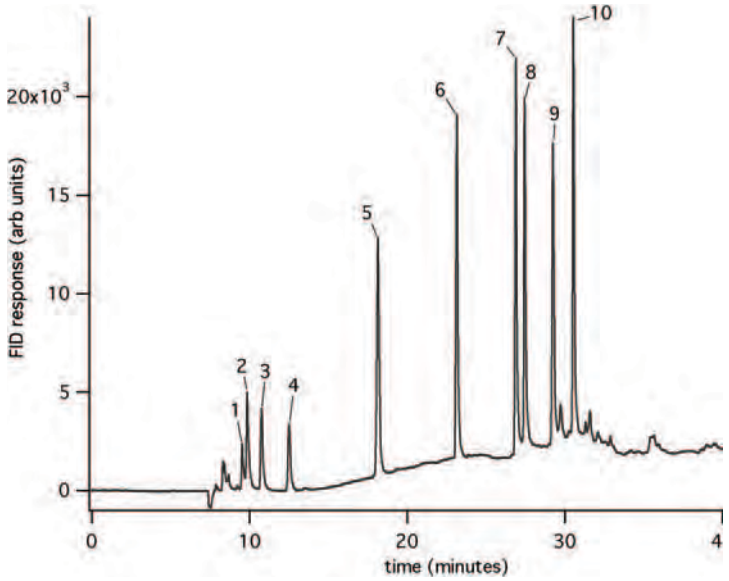

Figure E-10. Chromatogram of PTR-MS calibration gas mixture.

for benzene, toluene and styrene. The naphthalene measurement shows a different result where the PTR-MS measurement is ~40% lower than that of NO-MS. This latter result is suggestive that the NO-MS determination may suffer from interferences due to the presence of the 1-heptene and longer chain alkenes as described above. The consistent offset between the PTR-MS and the NO-MS for benzene, toluene and styrene is suggestive of a calibration problem rather than a measurement difference. While a calibration difference would be an easy explanation, this seems unlikely as both instruments were calibrated in concert using the same calibration gas and delivery system. There is no clear objective resolution to why the methods differ or to which data is the more accurate. In many venues agreement at this level is considered to be excellent.

Comparison of the PTR-MS and the GC/FID at DAL 2009

A SRI model 8610C gas chromatograph (GC) using a flame ionization detector (FID) was deployed for the analysis of hydrocarbon exhaust gas emissions. Exhaust gas samples are trapped and pre-concentrated on a solid adsorbent (TENAX). A vacuum pump is used to pull the gas sample through the trap (~100 ml/min) for 2 minutes. At the conclusion of the trapping period, the adsorbent trap is heated and the contents of the trap are injected onto the head of the chromatographic column using a 10-way multiport valve. The chromatographic column, Restex MXT-1, utilizes a temperature program where the temperature is held at 50°C for 4 minutes, ramped at 10°C per minute to 200°C and then held for 4 minutes.

Calibration of the detector response, adsorbent trapping characteristic and column retention characteristics of the GC/FID were evaluated by analyzing a diluted mixture of the certified gas standard used to calibrate the PTR-MS. Figure E-10 shows a chromatogram obtained for the analysis of the PTR-MS calibration gas mixture. The components present in PTR-MS calibration gas mixture are tabulated in Table E-3. The peaks that are labeled in Figure E-10 are identified in Table E-3. Separation on the MST-1 column is

Table E-3. Calibration standard component list. Boiling point and concentration in the calibration gas standard.

Compound	Boiling point (°C)	Concentration (ppbV)	Peak number
propene	-48	480	-
acetaldehyde	21	490	1
isoprene	34	440	2
acetone	56	500	3
methanol	65	520	-
methacrolein	69	410	4
benzene	80	510	5
acetonitrile	82	520	-
toluene	111	500	6
p-xylene	138	480	7
styrene	146	480	8
alpha-pinene	157	440	9
1,2,4-trimethylbenzene	169	480	10

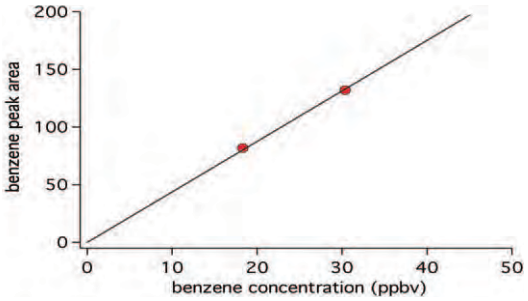

Figure E-11. FID response curve for benzene.

Table E-4. FID response factors.

compound	peak area/ppbV	peak area/ppbC
benzene	4.38	0.73
toluene	5.12	0.73
p-xylene	5.30	0.66
styrene	4.78	0.60
1,2,4-trimethylbenzene	5.74	0.64

essentially determined by compound boiling point and the elution order was determined on this basis. Note that not all of the compounds present in the calibration mixture are observed in the chromatogram. The FID response to compounds containing heteroatoms is diminished relative to their carbon numbers and is essentially absent for 1-carbon compounds such as methanol and acetonitrile. Propene does not appear to be retained on TENAX and its peak could not be identified.

Standard curves were produced for each of the five aromatic compounds by plotting peak area response versus sample concentration. The standard curve for benzene is shown in Figure E-11. The slope of these plots provides response per unit concentration. The magnitude of the slopes should vary in proportion the number of carbons in the compounds. Table E-4 is a summary of the compound responses for the aromatic compounds. Benzene and toluene show a constant per carbon response as expected. The higher molecular weight compounds exhibit smaller per carbon responses. This result is not expected and may be the result of retention of these less volatile compounds in the sample lines. Quantification of exhaust samples assumes that the peak area/ppbC response factor of 0.73 expressed by benzene and toluene is correct.

Two engine exhaust gas samples were analyzed by the GC/FID. One sample was taken during the initial engine warm-up period while the second sample was obtained during test point 16 (ground idle, zero bleed). The resulting chromatograms from these samples are shown in Figure E-12. The two chromatograms are very similar and show essentially

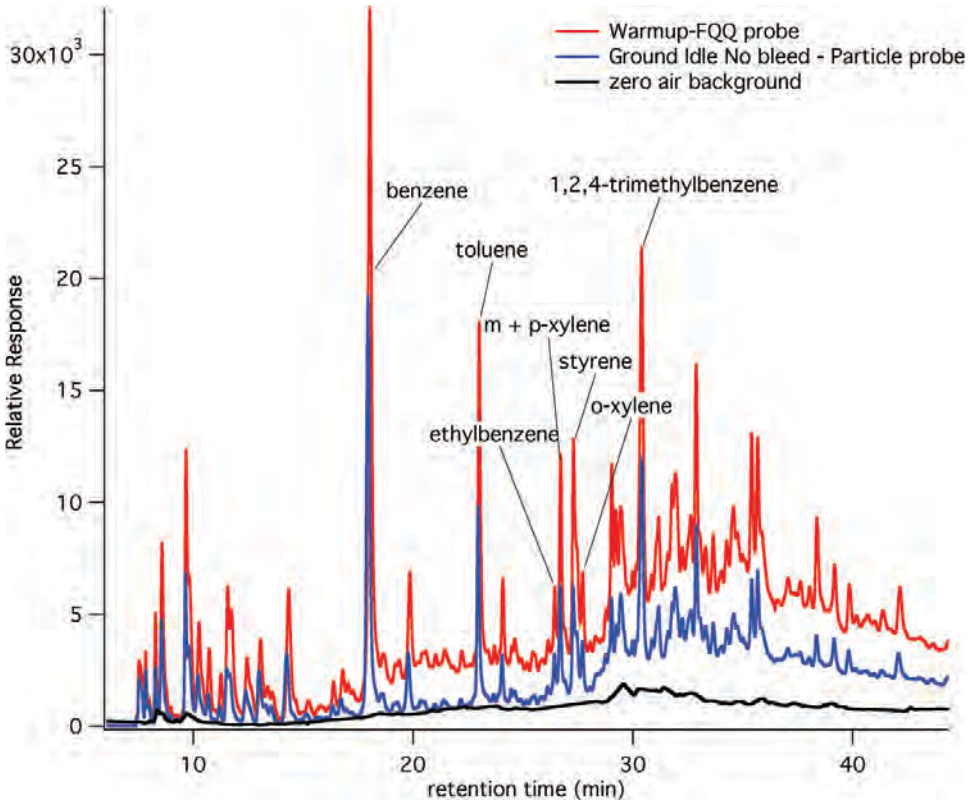

Figure E-12. GC analysis of diluted engine exhaust.

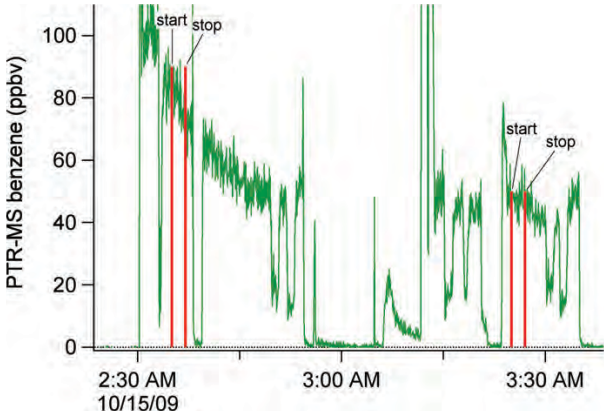

Figure E-13. Time series of PTR-MS benzene and GC-FID benzene. Green continuous trace is the benzene from the PTR-MS and the red bars are the GC-FID quantified benzene where height is indicative of mixing ratio.

the same peaks in the same relative proportions. The benzene peaks are the largest single peaks in both chromatograms. Other identifiable peaks in these chromatograms have been labeled. The integrated peak areas in Figure E-12 can be used to assess the average concentration present in the exhaust stream during the sample period. These results can then be compared to the PTR-MS measurements that were being made simultaneously. The PTR-MS benzene measurements are shown in Figure E-13 and indicate the beginning and end times for the GC sample acquisition. The warm-up sample was taken at approximately 2:35 while test point 16 corresponds to the sample taken at approximately 3:25. Table E-5 is a summary of the inter-comparison of the GC/FID and PTR-MS measurements. The PTR-MS measurements reflect the average of the concentrations recorded while the GC sample was being taken. The C2-benzenes represent the sum of ethyl benzene and the three xylene isomers. For the GC/FID measurements the individual peak areas of these compounds have been summed together. The PTR-MS cannot provide a direct measure of the C2-benzenes because benzaldehyde, a prominent component in aviation exhaust is also detected at the same mass-to-charge ratio. The SPECIATE profile

Table E-5. Inter-comparison of GC/FID and PTR-MS measurements.

compound	Warm-up		Test point 16	
	PTR-MS	FID	PTR-MS	FID
benzene	79.4	79.9	47.6	48.6
toluene	28.9	24.9	17.0	13.5

indicates that 57% of measured intensity originates from the C2-benzenes with the remaining 43% coming from benzaldehyde. The concentration reported in the PTR-MS column has been adjusted accordingly. Inspection of the results in Table E-5 indicates that for this limited set of compounds that the two methods are in excellent agreement.

Summary of PTR-MS and NO-MS Measurements

The ACRP Project 02-03a involved the deployment of two PTR-MS instruments, MSU PTR-MS and the EMSL PTR-MS, at MDW 2009 and MDW 2010 and one PTR-MS (MSU) at DAL 2009. At MDW the MSU PTR-MS was operated in alternate reagent NO+ mode. These instruments were challenged to operate under a wide range of environmental conditions over three campaigns spanning a period 13 months. Overall the level of agreement between the PTR-MS and NO-MS is considered to be excellent. The comparison of the PTR-MS and GC/FID demonstrated excellent agreement. Any study that challenges different instruments risks the possibility that the instruments will deliver different results. Many of these inter-comparison studies reveal that while instruments appear identical certain instrument/operator pairs often succeed where others don't. It is not without some bias, but we favor the MSU measurements, except for naphthalene, for inclusion in the final data archive. This decision is based in part on intimate knowledge of the MSU instrument and its performance as well as a demonstrated consistency over a period of many year and campaigns. Table E-6 summarizes the compounds measured and the instrumental method used for the data submitted to the final archive.

Table E-6. Summary of compounds measured and instrument technique employed.

Compound	MDW 2009	DAL 2009	MDW 2010
acetaldehyde	PTR-MS	PTR-MS	PTR-MS
1,3-butadiene	NO-MS	----	NO-MS
benzene	NO-MS	PTR-MS	NO-MS
toluene	NO-MS	PTR-MS	NO-MS
C2-benzenes	NO-MS	PTR-MS	NO-MS
naphthalene	NO-MS	PTR-MS	PTR-MS

Flame Ionization Detector Deployment at MDW 2009

Some special remarks are required on the flame ionization detector (FID) instrument. The FID instrument was operated during the first day in its rack using manual calibration protocols recommended in the manual. This instrument operated at its highest gain setting and experienced frequent drifts in the zero signal level, sometimes beyond the scale of the digitization range. We found that the switching from sample to calibrate did not always reproduce pressures in the detector. This prompted us to devise a new method that would perform zeroes and calibration without using the internal valves. For the second day of testing, we developed a new zero and calibration mode for the instrument. We operated it in sampling mode only with the potentiometers set at middle scale. We over blew the inlet with zero air every five minutes during the test on an automatic timer. Following each zero we over blew the inlet with the propane standard (2.4 ppmC). The frequent "zero" data was used to correct the data in the intervening sampling periods. Each subsequent span was used to scale the intervening sampling period.

A time series resulting from this procedure is depicted in Figure E-14.

The FID data for the second day of testing is adequate for analysis. For future tests we will improve the instrument in the laboratory and provide more temperature and vibration isolation when installed in the truck. Qualitatively, a portion of the noise of this instrument was due to people walking in the truck, which suggests it can be fixed with internal improvements.

Despite its widespread use, there are several limitation of the FID instrument measurement approach when characterizing a complex mixture of hydrocarbons. For example, the FID instrument does not employ any chromatographic separation of compounds. The instrument has unknown response factors to compounds containing heteroatoms and no response to formaldehyde. Essentially, for each oxygen in the molecule, the instrumental response to one carbon is removed. This means the instrument does not really count all of the carbon in a partially oxidized hydrocarbon. Furthermore, the signal level can only be calibrated in units of carbon atoms. In order to express the output from this instrument as mass, frequently the mass of methane is used; or it reports methane equivalent emissions.

This campaign represented the first opportunity to compare the FID response to that of the spectroscopic HCHO measurement when the sample was diluted into ambient air. The correlation of HCHO with FID response has been used to relate the results of several tests to the ICAO databank measurements. For example in Herndon et al. (2006), the range of 0.21–0.26 g HCHO per FID g methane was used to estimate the relationship between taxiway operational measurements and the ICAO databank. An alternative method using the

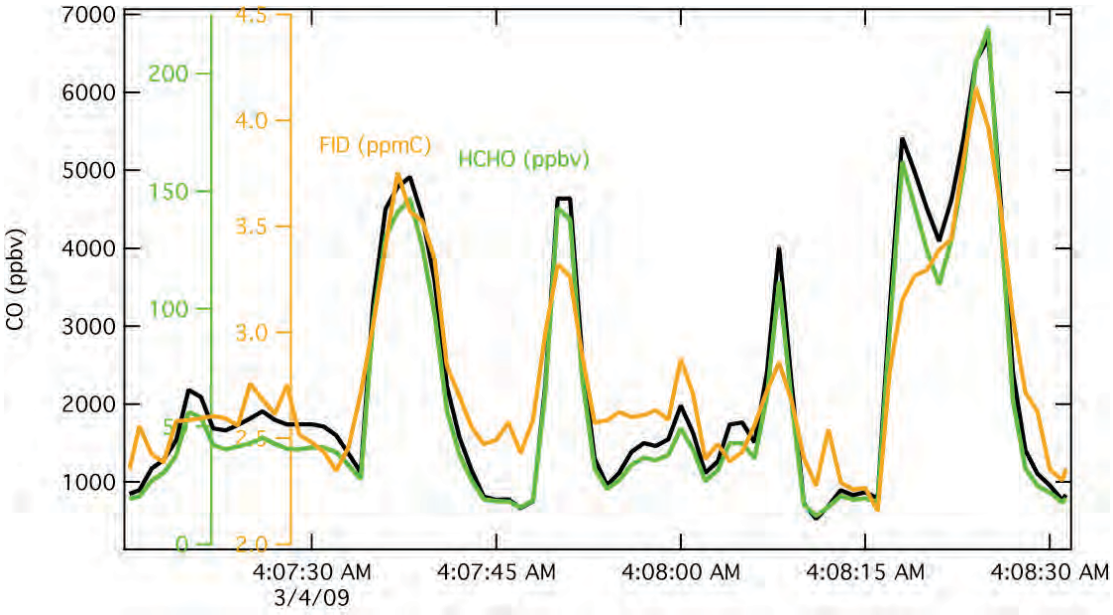

Figure E-14. Segment of time series data collected on the second day with the FID zero and span procedure engaged (not shown). Note that the CO (black) and the HCHO (green) are highly correlated. The FID data is also correlated (orange/yellow) but is noisier and is offset due to atmospheric methane and the sum of other urban area hydrocarbons. The time response of the FID is also slightly longer (slower) than the HCHO and CO instruments.

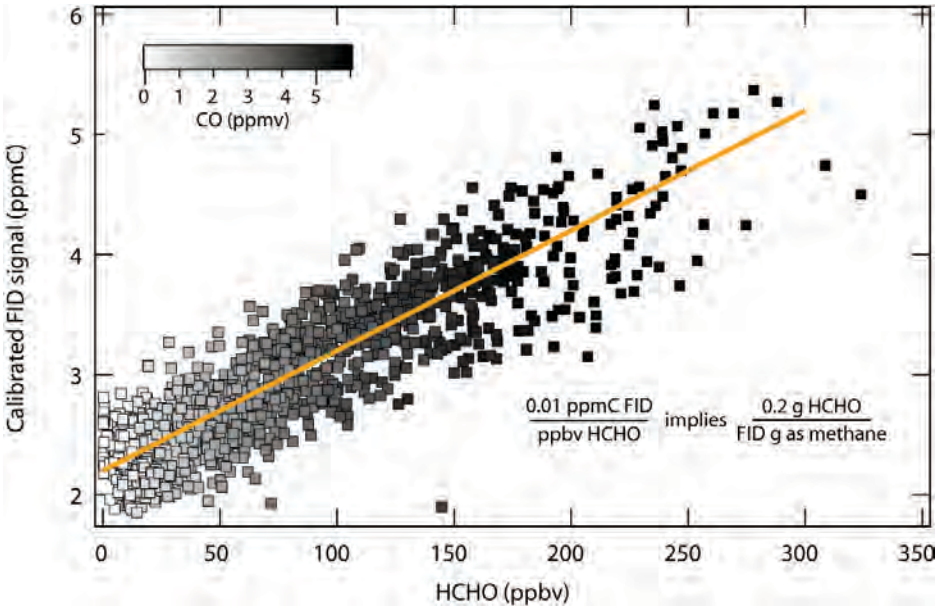

Figure E-15.

hydrocarbon profile of Spicer et al. (1992, 1994) and a synthetic estimate of the FID response to various hydrocarbons suggests a value of 0.22 g HCHO per FID gram as methane. The comparison derived from the measurements in this test suggests this ratio is 0.2 g HCHO per FID gram as methane, which agrees very well with the previous estimates.

References

Anderson, B. E., et al. 2010. Alternative Aviation Fuel Experiment (AAFEX) *Rep.*

Baniszewski, D., D. Martin, and J. DeLeon. 2010. Petroleum Quality Information System 2009 Annual Report *Rep.*

Diskin, A. M., T. S. Wang, D. Smith, and P. Spanel. 2002. A selected ion flow tube (SIFT), study of the reactions of $H3O^+$, NO^+ and $O2^+$ ions with a series of Alkenes; in support of SIFT-MS. *International Journal of Mass Spectrometry* 218: 87–101.

Herndon, S. C., M. S. Zahniser, D. D. Nelson, Jr., J. H. Shorter, J. B. McManus, R. Jimenez, C. Warneke, and J. A. de Gouw. 2006. Airborne measurements of HCHO and HCOOH using a pulsed quantum cascade laser system. *Accepted J. Geophys. Res.*

Jimenez, R., S. Herndon, J. H. Shorter, D. D. Nelson, J. B. McManus, and M. S. Zahniser. 2005. Atmospheric trace gas measurements using a dual-quantum cascade laser mid-infrared absorption spectrometer. *SPIE Proceedings* 5738(37): 318–331.

Knighton, W. B., E. C. Fortner, S. C. Herndon, E. C. Wood, and R. C. Miake-Lye. 2009. Adaptation of a proton transfer reaction mass spectrometer instrument to employ NO^+ as reagent ion for the detection of 1, 3-butadiene in the ambient atmosphere. *Rapid Comm. in Mass Spec.* 23(20): 3301–3308.

Knighton, W. B., T. Rogers, C. C. Wey, B. E. Anderson, S. C. Herndon, P. E. Yelvington, and R. C. Miake-Lye. 2007. Quantification of Aircraft Engine Hydrocarbon Emissions Using Proton Transfer Reaction Mass Spectrometry. *Journal of Propulsion and Power* 23(5): 949–958.

McManus, J. B., D. D. Nelson, J. H. Shorter, R. Jimenez, S. Herndon, S. Saleska, and M. Zahniser. 2005. A high precision pulsed quantum cascade laser spectrometer for measurements of stable isotopes of carbon dioxide. *J. Modern Optics* 52: 2309–2321.

Nelson, D. D., J. S. Shorter, J. B. McManus, and M. S. Zahniser. 2002. Sub-part-per-billion detection of nitric oxide in air using a thermoelectrically cooled mid-infrared quantum cascade laser spectrometer. *Applied Physics B* 75: 343–350.

Nelson, D. D., J. B. McManus, S. Urbanski, S. Herndon, and M. S. Zahniser. 2004. High precision measurements of atmospheric nitrous oxide and methane using thermoelectrically cooled mid-infrared quantum cascade lasers and detectors. *Spectrochimica Acta A* 60: 3325–3335.

Sachse, G. W., G. F. Hill, L. O. Wade, and N. Y. Chou. 1987. Airborne tunable diode laser system for rapid CO and CH_4 measurement (A). *J. Opt. Soc. Am. A* 4: 54.

Timko, M. T., S. Herndon, E. de la Rosa Blanco, E. Wood, Z. Yu, R. C. Miake-Lye, W. B. Knighton, L. Shafer, M. DeWitt, and E. Corporan. 2011. Combustion Products of Petroleum Jet Fuel, a Fischer Tropsch Synthetic Fuel, and a Biomass Fatty Acid Methyl Ester Fuel for a Gas Turbine Engine. *Combust. Sci. Technol.* in press.

Wey, C. C., et al. 2006. *Aircraft Particle Emissions Experiment (APEX).* NASA/TM-2006-214382, ARL-TR-3903.

Zahniser, M. S., D. D. Nelson, Jr., J. B. McManus, and P. L. Kebabian (1995), Measurement of trace gas fluxes using tunable diode laser spectroscopy, *Phil. Trans. R. Soc. Lond. A, 351,* 357–369.

Abbreviations and acronyms used without definitions in TRB publications:

AAAE	American Association of Airport Executives
AASHO	American Association of State Highway Officials
AASHTO	American Association of State Highway and Transportation Officials
ACI–NA	Airports Council International–North America
ACRP	Airport Cooperative Research Program
ADA	Americans with Disabilities Act
APTA	American Public Transportation Association
ASCE	American Society of Civil Engineers
ASME	American Society of Mechanical Engineers
ASTM	American Society for Testing and Materials
ATA	American Trucking Associations
CTAA	Community Transportation Association of America
CTBSSP	Commercial Truck and Bus Safety Synthesis Program
DHS	Department of Homeland Security
DOE	Department of Energy
EPA	Environmental Protection Agency
FAA	Federal Aviation Administration
FHWA	Federal Highway Administration
FMCSA	Federal Motor Carrier Safety Administration
FRA	Federal Railroad Administration
FTA	Federal Transit Administration
HMCRP	Hazardous Materials Cooperative Research Program
IEEE	Institute of Electrical and Electronics Engineers
ISTEA	Intermodal Surface Transportation Efficiency Act of 1991
ITE	Institute of Transportation Engineers
NASA	National Aeronautics and Space Administration
NASAO	National Association of State Aviation Officials
NCFRP	National Cooperative Freight Research Program
NCHRP	National Cooperative Highway Research Program
NHTSA	National Highway Traffic Safety Administration
NTSB	National Transportation Safety Board
PHMSA	Pipeline and Hazardous Materials Safety Administration
RITA	Research and Innovative Technology Administration
SAE	Society of Automotive Engineers
SAFETEA-LU	Safe, Accountable, Flexible, Efficient Transportation Equity Act: A Legacy for Users (2005)
TCRP	Transit Cooperative Research Program
TEA-21	Transportation Equity Act for the 21st Century (1998)
TRB	Transportation Research Board
TSA	Transportation Security Administration
U.S.DOT	United States Department of Transportation